PERFORMANCE CHARACTERISTICS OF LIQUID METAL MHD POWER GENERATOR USING SINGLE- AND TWO-PHASE FLOW

Nobuhiro Tanatsugu

Preface

This monograph is the dissertation submitted by the author in fulfillment of the dgree of Doctor of Engineering in the University of Osaka, and is founded on the studies made under the supervision of Professor Tokuo Suita in the postgraduate course of Osaka University. All the experimental investigations were performed with the blow-down apparatus using both mercury and NaK as the working fluid, situated in the Department of Nuclear Engineering, Faculty of Engineering, Osaka University.

March 6, 1973

Nobuhiro Tanatsugu

Contents

Chapter 1 Introduction 1

1-1 Status of Liquid Metal Magnetohydrodynamic Energy Conversion Systems 1

1-2 Problems Treated in the Present Thesis 6

Part I

Power Generation Using the Single-Phase Flow as the Working Fluid

Introduction 10

Chapter 2 Decrease in Power Density due to Finite Electrode Conductivity in D.C. Liquid Metal MHD Generator 13

2-1 Introduction 13

2-2 Non-Perfect Conductor Analysis 14

2-3 Comparison with End Loss 18

2-4 Numerical Computation with Both End Loss and Non-Perfect Conductor Effect Taken into Consideration 20

2-5 Experimental Verification 23

2-6 Validity of One-Dimensional Flow Approximation 24

2-7 Discussions and Concluding Remarks 25

References 28

Figures and Tables 29

Chapter 3 Energy Loss in Liquid Metal MHD Induction Converter due to Discrete Tooth-Slot Arrangements 39

3-1 Introduction 39

3-2 Formulation of the Problem 40

3-2-a Constant Current Mode 40
3-2-b Constant Voltage Mode 46
3-2-c Validity of Slit-Channel Approximation
(Skin Effect and Leakage of Magnetic Flux) 52
3-3 Experimental Apparatus 53
3-4 Experimental Results and Discussions 55
3-5 Concluding Remarks 57
References 60
Figures 61

Part II
Power Generation Using the Two-Phase Flow
as the Working Fluid
Introduction 72

Chapter 4 Frictional Pressure Drop for NaK-N_2 Two-Phase Flow
in Rectangular Cross Section Channel
of Large Aspect Ratio 74
4-1 Introduction 74
4-2 Frictional Pressure Drop in Two-Phase Flow 75
4-2-a Treatment of Two-Phase Mixture as a Continuous
Medium 76
4-2-b Expression of the Frictional Pressure Drop
for Two-Phase Flow in Comparison with That
for Single-Phase Flow 76
4-3 Experimental Apparatus 79
4-4 Experimental Results and Discussions 80
4-4-a Pressure Drop due to the Momentum Change 80

4-4-b Friction Factor for NaK-N_2 Two-Phase Flow 81
4-4-c Empirical Correlation of Frictional Pressure Drop for NaK-N_2 Two-Phase Flow 83
4-5 Concluding Remarks 84
Appendix: The Ratio of Frictional Pressure Drop between That in Two-Phase Flow and That in a Single-Phase Liquid Flow of the Same Velocity as That of the Liquid in the Two-Phase Flow Modified from; 87
(1) Martinelli's Empirical Analysis 87
(2) Bankoff's Variable Density Single-Fluid Model 88
References 89
Figures 90

Chapter 5 Apparent Electrical Conductivity of Liquid Metal-Gas Two-Phase Mixture 95
5-1 Introduction 95
5-2 Previous Results Obtained by Other Authors 96
5-3 Experimental Procedure 97
5-4 Experimental Results and Discussions 98
5-4-a Relation of the Electrical Conductivity to the Flow Pattern 99
5-5 Concluding Remarks 100
References 101
Figure 102

Chapter 6 Performance Characteristics of MHD Induction Generator Using the Two-Phase Flow 103
6-1 Introduction 103

6-2 Experiment 104

6-3 Experimental Results 104

6-3-a Performance Characteristics of the Experimental Converter Operated with NaK Flow in Single-Phase as Working Fluid 104

6-3-b Performance Characteristics of the Experimental Converter Operated with NaK-N_2 Two-Phase Flow in Comparison with Those with NaK Single-Phase Flow 105

6-4 Analysis of Induction Converter with Two-Phase Mixture as Working Fluid 107

6-4-a Power Law Distribution for Both Velocity and Void Fraction Proposed by Bankoff 110

6-4-b Performance Characteristics of Induction Converter Numerically Obtained with Power Law Distribution for Both Velocity and Void Fraction 112

6-5 Discussions and Concluding Remarks 113

Appendix: The Relation between the Average Void Fraction with a Power Law Distribution and the Bulk Void Fraction Determined Experimentally by the Gamma-Ray Attenuation Technique, 116

The Relation between the Average Velocity and the Bulk Velocity Obtained Experimentally from the Liquid Mass Flow Rate 117

References 118

Figures 119

Chapter 7 Summary 124

Acnowledgements 131

List of Papers by the Author 132

List of Lectures by the Author 133

Chapter 1
Introduction

1-1 Status of Liquid Metal Magnetohydrodynamic Energy Conversion Systems

The efforts towards the achievement of Magnetohydrodynamic (MHD) power generation had been inaugurated in 1831 when Faraday attempted to demonstrate MHD power generation by measuring a potential induced from the interaction of the tidal currents in the River Thames with the terrestrial magnetic field.

Although his attempt came to be a failure, he set forth the basic principles which are applicable to MHD power generation.

From that time on, the progress has been made slowly but steadily in this field, and then has been enhanced rapidly by five International Symposia on Magnetohydrodynamic Electrical Power Generation held every second year since 1962 and thirteen Symposia on Engineering Aspects of Magnetohydrodynamics held in USA.

The basic attraction of MHD power generation is that a fluid can serve both as the thermodynamic working substance and as the moving component of the generator. The consequent elimination of rotating parts is potentially advantageous, particularly for high-temperature systems.

There are three approaches in MHD power generation.

(1) Open cycle, combustion-gas plasma MHD power generation.

(2) Brayton cycle, inert-gas plasma MHD power generation.

(3) Rankine or quasi-Ericson cycle, liquid metal MHD power

generation.

The first approach was developed to use an MHD generator as a topping cycle for fossil-fuel central power stations to increase the overall thermal efficiency. In this case, the combustion gas flows directly through a generator channel and is released to the atmosphere after seeded substance for conductivity-enhancement is removed from it. At present this approach proceeds to the construction of both large-scale and long-lifetime generator.

The second and third approaches have been extended by the interest in use of MHD generations with nuclear heat sources.

The prospects for developing high-temperature gas-cooled reactor, sodium-cooled fast breeder reactor and future fusion reactor back up these two approaches. In contrast to the first approach, a closed cycle is clearly required and therefore there is some freedom in the selection of a working fluid.

The second approach is to employ a gas-cooled reactor with helium as the working fluid in Brayton cycle. Since it is difficult to obtain an adequate equilibrium electrical conductivity due to the temperature limitations imposed by nuclear heat sources, any conductivity-enhancement scheme is required such as nonequilibrium ionozation, in which the electric field produced by motional induction is used to heat electrons preferentially.

From the studies performed in this approach, it has, however, become evident that the attainment of adequate electrical conductivity of the plasma within the temperature limits of the

reactor to be possible in near future is unrealizable in spite of many efforts in the various conductivity-enhancement attempts.

The tird approach is to generate electric power in an MHD generator operated with the liquid phase or the liquid-vapor or gas two-phase.

Interest in liquid metal MHD power generation has arisen because of the high power density, which makes operation with modest magnetic fields possible, the large magnetic Reynolds number sufficient to make direct a.c. power generation possible, and the possibility of operating these systems at lower operating temperature than with plasmas.

In addition to the application in the central power station, the liquid metal MHD power generation except for the quasi-Ericson cycle proposed by Petrick appears to be adaptable as a power supply for space application, because of the attractive specific weights, the high-temperature system, which keeps the radiator area (and weight) to an acceptable level in space where heat is rejected by radiation, and the greater reliability for long-duration operation in space-vehicle missions by having no rotating parts in the system.

In contrast to an usual Rankine (or Bryton) cycle which uses the vapor (or gas) phase as the working fluid, the liquid metal MHD cycles must transfer the thermal energy of a vapor phase into kinetic energy or stagnation pressure of a fluid (liquid or two-phase mixture) of sufficient electrical conductivity to adequately interact with the magnetic field in the MHD generator.

Consistent with this constraint, there have been proposed to date four basic cycles for the conversion system, i.e. Separator (proposed by Elliott in 1961), Injector-condenser (Jackson and Brown,1962), Emulsion (Petrick and Lee, 1964) and Slug flow cycles (Bjerklie and Powell, 1968). The first two cycles involve a two-step conversion in which the MHD generator operates on kinetic energy that is derived from the conversion of thermal energy prior to entering the generator.

A vapor is used to accelerate a liquid metal and then the vapor is either separated or condensed. The extraction of electrical energy from the liquid metal is the second conversion step.

In the last two cycles the working fluid may be either a homogeneous (emulsion) or an inhomogeneous (slug) two-phase flow mixture, and the conversion of thermal to electrical energy is accomplished without an intermediate separation or condensation step. That is, the accelerated two-phase mixture passes directly through the generator. In all four cycles the acceleration of the liquid is achieved by the vapor or gaseous phase while the conductivity is attributed to the liquid.

Although both the Injector-condenser and Separator cycles have been studied since the liquid metal MHD energy conversion concept was introduced at the first International Symposium on MHD Electrical Power Generation in 1962 and is the most developed cycles, it has become evident from the analytical and experimental studies that they have lower efficiencies than the cycles with two-phase flow in the generator. This is due to the large

losses, e.g. friction and shock losses, in the separator and injector units.

For this reason, interest in the Emulsion and Slug flow cycles has increased since the fifth International Symposium in 1971.

The liquid metal MHD energy conversion systems adopt generally the induction generator as a converter for the conversion of kinetic energy to electrical energy by making use of the large Reynolds number inherent in liquid metal.

The MHD induction generator has several advantages over d.c. MHD generators in that there is no need for d.c.-a.c. inverters, the stator windings serve as a step-up transformer to increase the terminal voltage and reduce the armature current, and there is no need for electrodes and connections for heavy direct current.

An MHD induction machine was first proposed as pump by Chubb in 1915 to pump a liquid metal by means of a rotating magnetic field in a spiral-channel induction pump. From that time on, several significant experimental studies have been undertaken and then Delany et al. first operated in 1963 a flat channel constant-velocity induction generator using a plasma as the working fluid.

Reid and Jackson performed in 1963 the first experiment of liquid metal MHD induction generator using NaK-78 (78 w/o K, 22 w/o Na) as the working fluid although the machine was not self-excited. The first generator to operate with self-excitation using only capacitors to provide the reactive power was constracted by Glukhikh and Kirillov in 1966 and yielded

a maximum net output power of 1160 watts with an electical efficiency of 29.5 percent at 20 Hz.

In 1971, Cerini and Elliott carryied out simultaneously the power generation by means of MHD induction generator and the acceleration of liquid metal with NaK-78 as the electrically conducting liquid and N_2 as the accelerating gas in the converter consisting of a nozzle, separator, generator and diffuser.

They obtained a net output power of 1.0 kw, which was less than half of the expected value due either to high void fraction or error in the previous correlation of conductivity versus void fraction.

Taking it into consideration that the cycles using two-phase flow is more efficient as mentioned previously, more experimental studies are required with respect to the effect of the vapor phase on generator performance (especially induction generator performance).

1-2 Problems Treated in the Present Thesis

Liquid metal MHD power generation is treated analytically and experimentally in the present thesis which consists of two parts.

The performance characteristics of d.c. Faraday generator using liquid metal mercury and flat liner induction generator using liquid metal eutectic NaK-78 (78 w/o potassium, 22 w/o sodium) as the electrically conducting working fluid are discussed in Part I, and the properties of two-phase mixture and the performance characteristics of induction generator in which the two-phase mixture flows are discussed in Part II using NaK-N_2

wo-phase flow system.

In the liquid metal MHD d.c. power generator, the electrical conductivity of working fluid is so large as to be comparable with that of the electrode. Under such circumstances the perfect conductor approximation no longer holds for the electrode, because the electric potential loses its constancy and acquires a certain pattern of distribution in the electrode as well as in the fluid.

The power density becomes non-uniform, and furthermore the average power density becomes smaller than in the case of a generator with the perfect conductor electrode.

In Chapter 2, this problem is solved both analytically based on the simple approximations and numerically taking the end loss into account. The results obtained is verified with the experimental generator using mercury flow as the working fluid.

In Chapter 3, the performance characteristics of a flat liner channel MHD induction generator operated in both constant current and constant voltage mode are obtained analytically, appling the slit channel approximation but taking account of variations in the travering magnetic field intensity in the direction of the fluid flow according to differences in the disposition of the teeth and slots in the stators.

The analytically obtained solutions were verified with the experimental generator operated in constant voltage mode using NaK-78 as the working fluid.

The details of the liquid metal-vapor or gas two-phase flow in the magnetic field (especially the traveling magnetic field)

remain not to be made clear.

A large number of analytical and experimental studies with respect to the frictional pressure drop for the two-phase flow have been performed for the most part using water as a liquid phase. It is in such field as the sodium cooled fast breeder reactor and the liquid metal MHD power generation that the liquid metal-vapor or gas two-phase flow has begun to be treated.

Since the frictional pressure drop for the two-phase flow has been discussed usually in such flow system, e.g. liquid-vapor mixture in boiler tubes or in various refrigeration systems, that is affected by mass flow rate, it has been compared with the superficial single-phase pressure drop, obtained by assuming that only single-phase flow rate is flowing alone in the channel, or the actual single-phase pressure drop, obtained by assuming that the total flow rate is flowing in the channel as a single-phase.

On the other hand, in such flow system, e.g. liquid metal-vapor or gas mixture in the MHD power generator, that is affected by the velocity of liquid, the frictional pressure drop for the two-phase flow should be discussed comparing with that for the liquid flow with the same velocity as that of the liquid in the two-phase mixture.

This problem is discussed in Chapter 4 and the expression of the frictional pressure drop for the two-phase flow is obtained empirically based on the experiment using NaK-N_2 two-phase flow.

In Chapter 6 is discussed the correlation of apparent electrical conductivity of two-phase mixture versus void fraction, which is

one of the most impotant values in the liquid metal MHD power generation using the two-phase flow as the working fluid.

This value has been given theoretically by Maxwell and Grossman, and obtained experimentally by Petrick, Elliott and several other investigators but the results obtained by them does not consist satisfactory with each other due to the difference in the fluid, the flow condition and the method of measurement.

Water-nitrogen gas, mercury-water and NaK-nitrogen gas mixtures in the static electric, static magnetic and traveling magnetic field are treated here.

In Chapter 6, the performance characteristics of the induction converter using the two-phase mixture flow are treated experimentally and analytically in comparison with those using the single-phase liquid flow as a working fluid.

The experiments have been performed with the flat-linear channel induction converter, through which NaK-N_2 two-phase mixture flowed at a velocity in the range of 5~30 m/sec.

Coupling the electro-magnetic equations with the power law distribution for both velocity and void fraction proposed by Bankoff, the author has solved numerically the performance characteristics of the induction converter using two-phase flow and explained well the results obtained experimentally.

The results obtained in this chapter is one of a few contribution to the progress in the MHD induction power generation using the two-phase flow.

The summary conclusions are described in Chapter 7.

Part I

Power Generation Using the Single-Phase Flow as the Working Fluid

Introduction

A lot of studies for the MHD power generation using a liquid metal single-phase flow as a working fluid have been performed analytically and experimentally imagining Separator and Injector-condenser cycles which were proposed early in the researches of this field.

The a.c. induction generator and the d.c. Faraday generator are feasible as a converter of kinetic energy to electrical energy. The former has been studied mainly, for it has several advantages over the latter as mentioned in the previous section.

For the most part of the analytical and experimental studies with respect to both these generators, the flat liner channel has been adopted for its simplicity and a few studies using the spiral or annular channel (for induction generator only) have been performed.

One of the problems in the flat liner channel generator is the end loss due to the eddy currents in the fluid upstream and downstream of generator.

Another problem in the d.c. Faraday generator arises as a result of the performance characteristics inherent in it, i.e. low output voltage and hevy current. That is, the electric conductivity of working fluid is so large as to be compara-

ble with that of the electrode and therefore the perfect conductor approximation no longer holds for the electrode, because the electric potential loses its constancy and acquires a certain pattern of distribution in the electrode as well as in the fluid.

The power density becomes non-uniform in the generator, and furthermore the average power density becomes smaller than in case of a generator with the perfect conductor electrode.

In Chapter 2, this problem is treated analytically and experimentally and discussed comparing with the end loss.

In MHD induction generators, the channel through which the working fluid flows is set in the air gap of the magnet and therefore this air gap should be much larger than that of usual induction machines.

On account of this large air gap, all of the magnetic flux does not traverse the air gap and there is inevitably some leakage in the direction of working fluid flow.

Besides, the magnet, which generates the traveling magnetic wave, consists of a finite number of teeth and slots, and thus the effective value of the magnetic field intensity generated in the air gap varies in the direction of fluid flow according to the disposition of these teeth and slots.

The liquid metal MHD induction generator possesses another serious problem, which is associated with the fluid channel which protects the polyphase windings and laminated stators and other structural parts of the generator from the liquid metal working fluid which flows at high velocity and temperature,

and furthermore under high pressure in the particular case of the constant cross-sectional area generator. Since the traveling magnetic field is applied over a metallic channel, eddy currents are induced in the channel wall, which cause power loss. Details of these problems are discussed analytically and experimentally in Chapter 3.

Chapter 2

Decrease in Power Density due to Finite Electrode Conductivity in Liquid Metal MHD D.C. Generator

2-1 Introduction

In the liquid metal MHD power generator, the electric conductivity of the working fluid is so large as to be comparable with that of the electrode. Since the current density in the electrode as well as in the working fluid is large, the perfect conductor approximation can not always be applied to the electrode.

Since the electrode conductivity is finite, a potential gradient is created in the electrode. This distortion of the electric potential distribution in the working fluid causes non-uniformity in the power density, and furthermore the average power density is thereby lowered in comparison with the case of perfect conductor approximation. The joule loss in the electrode as well as the power density in the working fluid become non-uniform, and consequently the electrode resistance can no longer be treated as part of the bus-bar resistance.

On the other hand, an analysis performed by Sutton et al.[1] has revealed that the end loss is decreased by reducing the load factor K and by increasing the aspect ratio, i.e. the ratio of electrode length to channel width.

According to the analysis treated here, however, the loss due to the non-perfect conductor, shows a behavior contrary to the end loss with both the load factor and the aspect ratio as

parameters.

In this chaper, the performance characteristics of the generator with non-perfect conductor electrodes is analyzed under certain simplified assumptions, and also the numerical analysis is performed taking the end loss into account.

Furthermore, a description is given of experiments performed with a mercury blow-down facility which have verified the results obtained analytically and numerically.

2-2 Non-Perfect Conductor Analysis

When the working fluid flow is steady under a static field, Maxwell's second law becomes

$$\nabla \times E = 0. \tag{2-1}$$

Since there are no change densities in the medium, with

$$\nabla \cdot E = 0 \tag{2-2}$$

and Eq. (1), the Laplacian field equation formulates the behavior of the potential:

$$\nabla^2 \Phi = 0 \tag{2-3}$$

The electric current density is given from Ohm's law:

$$J = \sigma (-\nabla \Phi + U \times B) \tag{2-4}$$

If the perfect conductor approximation is adopted, Eq.(3) can be analytically treated under simple boundary conditions using conformal mapping[1] or Fourier series[2][3]. However, considering the conductivity of the electrode to be finite, Eqs.(2-3) and (2-4) are solved numerically or analytically, based on the following assumptions:

(1) Constant cross section in MHD channel

(2) One-dimensional single-phase flow in X direction

(3) Induced magnetic field is neglected

(4) Electric current flows in Y direction in working fluid and in X direction in electrode

The assumption (4) will be now verified using the results of numerical calculation. In Fig.2-1, constant pitch of load terminal position is further assumed, and taking advantage of the symmetry acquired by neglect of the induced magnetic field, the analysis is made only over the zone bounded by the parallel dashed lines.

The electric potential on the electrode is expressed by

$$\Phi(x)=aUB-aj_y(x)/\sigma_f \qquad 0\leq x\leq L \qquad (2\text{-}5)$$

and the potential gradient at x by

$$\frac{d\Phi}{dx}=\int_x^L \frac{j_y(x)}{\sigma_e t}\,dx \qquad (2\text{-}6)$$

From Eqs.(2-5) and (2-6),

$$\frac{d^2\Phi}{dx^2}-\kappa^2\Phi=-\kappa^2 aUB \qquad (2\text{-}7)$$

where

$$\kappa^2=\frac{\sigma_f}{\sigma_e at} \qquad (2\text{-}8)$$

Equation (2-7) can be solved analytically under the boundary conditions

$$(1)\quad \frac{d\Phi}{dx}=0 \qquad x=L \qquad (2\text{-}9)$$

$$(2)\quad \Phi=KaUB \qquad x=0 \qquad (2\text{-}10)$$

and the solution becomes

$$\Phi(x) = aUB\left[1-(1-K)\cdot\frac{\exp\{\kappa(L-x)\}+\exp\{-\kappa(L-x)\}}{\exp(\kappa L)+\exp(-\kappa L)}\right] \quad (2\text{-}11)$$

From Eqs.(2-4) and (2-11), the electric current density in the fluid and the output current are given by

$$j_y(x) = \sigma_f(1-K)UB\cdot\frac{\exp\{\kappa(L-x)\}+\exp\{-\kappa(L-x)\}}{\exp(\kappa L)+\exp(-\kappa L)} \quad (2\text{-}12)$$

$$I = 2b\int_0^L j_y dx$$

$$= \sigma_f(1-K)UB2bL\frac{\tanh\chi}{\chi} \quad (2\text{-}13)$$

where $\chi=\kappa L$ (2-14)

The effective internal resistance R_{ieff} of the generator can be determined with use of the load resistance R_o:

$$R_o I = K2aUB \quad (2\text{-}15)$$

where $$K = \frac{R_o}{R_o+R_{ieff}} \quad (2\text{-}16)$$

From Eqs.(2-13), (2-15) and (2-16),

$$R_{ieff} = \frac{a\kappa}{\sigma_f b}\coth\chi \quad (2\text{-}17)$$

When perfect conductor approximation is made, the internal resistance can be given by

$$R_i = \frac{a}{\sigma_f bL} \quad (2\text{-}18)$$

The performance characteristics of a generator under perfect conductor approximation, for instance, the output power, the electro-mechanical power extracted from the fluid, the joule

loss in the fluid, the pressure drop across the generator channel due to the electric retarding force, are expressed respectively as follows:

$$\overline{P_o} = 4abL(1-K)K\sigma_f U^2B^2 \tag{2-19}$$

$$\overline{P_f} = 4abL(1-K)\,\sigma_f U^2B^2 \tag{2-20}$$

$$\overline{P_{floss}} = 4abL(1-K)^2\sigma_f U^2B^2 \tag{2-21}$$

$$\overline{\Delta P} = L\sigma_f(1-K)UB^2 \tag{2-22}$$

Using these expressions, in a generator with non-perfect conductor electrode, the pressure drop across the generator channel and the electro-mechanical power of the fluid become

$$\Delta P = \int_x^L j_y B dx = \overline{\Delta P}\cdot\lambda_0 \tag{2-23}$$

$$P_f = 4abU\Delta P = \overline{P_f}\cdot\lambda_0 \tag{2-24}$$

and the output power

$$P_o = 2I\Phi(0) = \overline{P_o}\cdot\lambda_0 \tag{2-25}$$

where

$$\lambda_0 = \frac{R_i}{Rieff} = \frac{\tanh\chi}{\chi} \tag{2-26}$$

The joule loss in the fluid and in the electrode are respectively

$$P_{floss} = \frac{4ab}{\sigma_f}\int_0^L j_y^2\,dx$$

$$= \overline{P_{floss}}\,\{\lambda_0/2+2(\exp\chi+\exp(-\chi))^2\} \tag{2-27}$$

$$P_{eloss} = \frac{4b}{\sigma_e t}\int_0^L\left\{\int_x^L j_y\,dx\right\}^2 dx$$

$$= \overline{P_{floss}}\,\{\lambda_0/2-2(\exp\chi+\exp(-\chi))^2\} \tag{2-28}$$

The resistance ratio λ_0, which determines the performance characteristics of the generator with finite conductivity electrode, is presented graphically in Fig.2-2. As is evident from Fig.2-2, λ_0 approaches unity with decreasing χ, which depends on the ratio of conductivity between fluid and electrode, and on the generator configuration.

This means that decreasing χ approaches the performance characteristics of the generator to the ideal. The reader should refer to Table 1 in which the conductivity ratios of various metals are shown.

2-3 Comparison with End Loss

Provided the magnetic field terminates abruptly at the end of the electrodes, the resistance ratio λ_{end} which was referred to in the previous section can also be defined as the ratio between the effective internal resistance of the end loss and the internal resistance of the ideal generator:

$$\lambda_{end} = \frac{R_i}{R_{ieff}} = 1 - \frac{K}{1-K}\frac{2\ln 2}{C\pi} \tag{2-29}$$

The ratio of power density between that of a generator with end loss and that of the ideal generator can be defined as

$$\frac{\text{Actual power density}}{\text{Ideal power density}} = \lambda_{end} \tag{2-30}$$

If only the non-perfect conductor effect is taken into consideration, the ratio of power density is given from Eq.(25):

$$\frac{\text{Actual power density}}{\text{Ideal power density}} = \lambda_0 \tag{2-31}$$

The ratio between the end loss and the electro-mechanical power of fluid is

$$\frac{\text{End loss}}{\text{Electro-mechanical power of fluid}} = \frac{K^2}{1-K}\frac{2\ln 2}{C\pi} \qquad 0 \leqq K \leqq K_{max} \tag{2-32}$$

where

$$K_{max} = \left(1+\frac{2\ln 2}{C\pi}\right)^{-1} \tag{2-33}$$

The ratio of the joule loss in the electrodes and the electro-mechanical power of fluid in the non-perfect conductor treatment is given by

$$\frac{\text{Joule loss in electrodes}}{\text{Electro-mechanical power of fluid}} = (1-K)\left\{\frac{1}{2} - \frac{2\chi}{\exp(2\chi)-\exp(-2\chi)}\right\} \qquad 0 \leqq K \leqq 1 \tag{2-34}$$

Rewriting Eq.(2-14), the "electrode configuration decision factor G" is defined as follows:

$$\chi = GC_{\sigma}^{1/2}\, C^{1/2} \tag{2-35}$$

where

$$G = \frac{1}{\sqrt{2}\,(m-1)}\left(\frac{TL}{t}\right)^{1/2} \tag{2-36}$$

From Eqs.(2-30),(2-31),(2-32) and (2-34), it can be made clear that the end loss effect is reduced as the aspect ratio C is increased, while the same changes would increase the non-perfect conductor effect.

As is evident from Eqs.(2-35) and (2-36), when we select an electrode with small C, the G value can be made large, which permits reducing the dimensions of the electrode and the number of load terminals.

The sum of the end loss factor and the electrode loss factor individually determined is given by

$$\lambda' = \frac{\tanh \chi}{\chi} - \frac{K}{1-K}\frac{2\ln 2}{C\pi} \tag{2-37}$$

In the case where both loss factors have the same order of magnitude, it is necessary to treat the Laplace equation numerically.

2-4 Numerical Computation with Both End Loss and Non-perfect Conductor Effect Taken into Consideration

In the non-perfect conductor analysis, the analytical solutions are made under the assumptions described before, while the perfect conductor approximation is adopted for the end loss calculation.

However, treating the end loss and the electrode loss simultaneously makes it impossible to solve the Laplacian field equation analytically. Besides, we must verify the validity of the approximate solutions which are given under the principal assumption that the distributions of the electric line of force and the electric equipotential line embody no distortion.

For these purposes, a numerical computation using high speed digital computer is performed to determine the electric equipotential lines[2][4]. Equation (2-3) is solved numerically for the generator configuration shown in Fig.2-3 with the following boundary conditions:

$$\Phi(x,a+t)=KaUB \qquad L-P\leq x\leq L+p \qquad 3L-p\leq x\leq 3L \tag{2-38}$$

$$\Phi(x,0)=0 \qquad 0\leq x\leq E \tag{2-39}$$

$$j_x(x,y) = \sigma_f\left(-\frac{\partial\Phi}{\partial x}\right)=0 \qquad 0\leqq y\leqq a \qquad x=0 \qquad x=E \qquad (2\text{-}40)$$

$$j_y(x,y) = \sigma_f\left(-\frac{\partial\Phi}{\partial y}\right)=0 \qquad 3L\leqq x\leqq E \qquad y=a \qquad (2\text{-}41)$$

$$j_x(x,y) = \sigma_e\left(-\frac{\partial\Phi}{\partial x}\right)=0 \qquad x=0 \quad x=3L \quad a\leqq y\leqq a+t \qquad (2\text{-}42)$$

$$j_y(x,y) = \sigma_e\left(-\frac{\partial\Phi}{\partial y}\right)=0 \qquad 0\leqq x\leqq L-p \quad L+p\leqq x\leqq 3L-p \quad y=a+t \qquad (2\text{-}43)$$

$$j_y(x,y) = \sigma_f\left(-\frac{\partial\Phi}{\partial y} + UB\right) = \sigma_e\left(-\frac{\partial\Phi}{\partial y}\right) \qquad 0\leqq x\leqq 3L \qquad y=a \qquad (2\text{-}44)$$

The numerical computation is performed with the finite difference method.

Figure 2-4 shows the ratios between the effective internal ciency are shown in Fig.2-6, and the power density in Fig.2-7. losses.

The curves (1) and (2) represent $\lambda(1)$ and $\lambda(2)$, the ratios viewed from the 2nd load terminal and from the outermost load terminal.

The dotted curve (3) shows the results analytically obtained with Eq.(2-26). Figure 2-5 shows $\lambda(1)$ and $\lambda(2)$ as functions of the load factor K.

The ratios of the electrode loss and the end loss to the electro-mechanical power extracted from the fluid and the efficiency are shown in Fig.2-6, and the power density in Fig.2-7.

From Fig.2-4, it is clear that $\lambda(1)$ and $\lambda(2)$ are both lower than λ_0, and that between the first two curves, $\lambda(2)$ is appreciably lower than $\lambda(1)$. This order can be explained first from the

end loss and second from the distortion suffered by the electric line of force and the electric equipotential line which rise to higher levels with increasing χ. Furthermore, the end loss is considered to affect $\lambda(2)$ much more than $\lambda(1)$.

Figure 2-4 reveals the fact that the differences of $\lambda(1)$ and $\lambda(2)$ from λ_0 increase with χ. This is considered to result from accentuation of the distortions with increasing χ.

Since the end loss becomes small for an actual generator whose aspect ratio might be much larger than that of the generator treated here, e.g., C=3, $\lambda(1)$ and $\lambda(2)$ should approach λ_0 unless large distortions appear.

For an actual generator, the end loss will also be reduced by increasing vanes placed in the flow upstream and downstream of the electrodes and/or by magnetic field extensions beyond the ends of the electrodes which decrease the gradients in the magnetic field at the inlet and outlet and suppress the eddy currents in the fluid[1][6][7].

It is to be noted in Fig.2-5 that $\lambda(1)$ and $\lambda(2)$ fall far below λ_0 at large load factors where the end loss becomes more marked: $\lambda(2)$ reduces to zero at K=0.82 instead of at 0.87 as given by Sutton, and no output power is obtained from the outermost load terminal at values of K above this value.

It is seen from Fig.2-6 that the electrode and end losses show a contrary behaviours in respect of K. Though the generator efficiency equals K for an ideal generator, in our case it decreases abruptly at large K due to the end loss, as shown in Fig.2-6, and also as pointed out by Sutton.

The power density in this case has its maximum value, not at K=0.5 as in an ideal generator, but at less than 0.5. (see Fig.2-7)

Figure 2-8 shows typical distributions of electric lines of force and equipotential lines in a quarter section of generator.

It is seen that for χ=2.14, the distortions do not appear distinctly in the fluid except in the extremities, whereas in the electrode distortions appear, and this is one of the reasons why $\lambda(1)$ and $\lambda(2)$ are lower than λ_0, as seen in Fig.2-4.

2-5 Experimental Verification

Experiments were performed using a mercury blow-down facility, with the generator shown Table 2. The apparatus had a relatively large aspect ratio and magnetic field extensions, for the purpose of reducing the end loss. The range of fluid velocity through the generator channel was 2~6 m/sec.

Since the end loss increases with the load factor and reaches maximum at K=1, the open circuit voltages were measured to determine the end loss. The open circuit voltages obtained for case (1) agreed with that of the ideal generator shown by the solid line in Fig.2-9, indicating that the end loss was negligibly small.

Figs.2-10 and 2-11 show the experimentally determined power densities for the case where copper electrodes were used, and the curves (1) represent the theoretical power density in the case of a perfect conductor. The curves (2) represent the theoretical power density obtained from Eq.(2-25) and the

dotted curves the numerically computed power density.

Figure 2-12 correspond to Figs.2-10 and 2-11 in the case where stainless steel electrode are used.

In these figures the experimental results are lower than the power densities obtained from Eq.(2-25). This is due to the contact resistance between the electrode and mercury[5] as well as on account of the distortions of lines of electric force and of equipotential.

Similar results were obtained with copper electrode while mercury amalgamation had not proceeded, but with increasing amalgamation the power density improved. With stainless steel electrode, however, no amalgamation could occur to reduce the contact resistance. The experimentally determined potential difference along the electrodes for case (3) is presented in Fig.2-13, together with the theoretical curve analytically obtained from Eq.(2-11).

2-6 Validity of One-Dimensional Flow Approximation

One-dimensional flow is assumed in the present treatment.

It should be necessary to ascertain the validity of the approximation for a realistic liquid MHD condition as well as for the present generator conditions as analyzed and experimented.

It may be possible to reduce the question to a Hartmann problem where laminar flow is assumed[8]. The velocity profile of flow yields the boundary layer in which the electromotive force becomes smaller than the output voltage and the electric current flows in the direction opposite to that of the electric

current in the main region of flow.

The ratio between the boundary layer depth and the generator channel height is given by

$$\frac{\text{Boundary layer depth}}{\text{Generator channel height}} = \frac{\ln(1-K)^{-1}}{H_a} \qquad H_a >> 1 \qquad (2\text{-}45)$$

Then the ratio might be smaller for a turbulent flow with 1/7-power flow profile.

Table 3 shows the parameters necessary to calculate the ratio.

In our experiment the Hartmann number falls within the range 12-40, and the flow is turbulent because the Reynolds number becomes 10^5 in order, so that the ratio determined from Eq.(2-45) becomes so small as to permit the boundary layer to be neglected. For an actual generator with a fluid velocity of 50 m/sec, the generator channel height of 0.05 and the magnetic field of 1 Tesla, the Reynolds number takes the order of 10^6, and the Hartmann number $10^3 \sim 3\times10^3$.

This indicates that the treatment adopted here should be a good approximation.

2-7 Discussions and Concluding Remarks

It may be qualitatively stated that, with increasing load factor, the electrode loss decreases whereas the end loss increases, as is clear from Eqs.(2-32) and (2-34). The sum of the two losses, as expressed by Eq.(2-37) cannot be considered to represent accurately the losses incurred in an actual generator, where the two kinds of loss are interrelated and not independent of each other.

Since the experiments were performed under such condition as to minimize the end loss, the experimental results agreed very well with the value calculated from Eq.(2-25). The small difference that remained between computation and experiment can be interpreted to be due to the fact that magnetic field extensions are applied in the experiment to reduce the end loss whereas in the computation the field extensions are not taken into account.

Nomenclature

a: Half width of fluid channel

b: Half height of fluid channel

TL: Length of fluid channel

L: Half length between terminals

C: Aspect ratio (=TL/2a)

m: Number of terminals

p: Terminal width

B: Magnetic field

U: Fluid velocity

σ_f: Electrical conductivity of fluid

σ_e: Electrical conductivity of electrode

C_σ: Ratio of conductivity between fluid and electrode

K: Load factor

R_o: Load resistance

R_i: Internal resistance with perfect conductor approximation

R_{ieff}: Internal resistance with non-perfect conductor or end loss

H_a: Hartmann number=Bb(electrical conductivity/viscosity)$^{1/2}$

Superscript

$(\bar{\ })$: Performance characteristics of the ideal generator

References

1) Sutton, G.W., Horwits, H.,Jr., Poritsky, H.: Trans. AIEE, Communication and Electronics, 58[1], 687-695 (1962).

2) Weh, H., Waltke, G., Appun, P.: Energy Conversion, 9, 31-38 (1969).

3) Hughes, W.F., Young, F.J.: "The Electro-magnetodynamics of Fluids", p.167 (1967), John Wiley & Sons, Inc., New York.

4) Roberts, J.J., Wessel, W.R., Petrick, M.: 10th Symp. on Engineering Aspects of Magnetohydrodynamics, March, 1969.

5) Elrod, H.G., Jr., Fouse, R.R., et al.: Trans. ASME, 589-594 (May, 1952).

6) Petrick, M., Roberts, J.J.: Proc. Symp. Magnetohydrodynamic Electrical Power Generation, Warsaw, 1968, SM-107/20, 1968.

7) Moszynski, J.R.: ANL-7188, (1967).

8) Petric, M., Lee, K.Y.: ANL-6870, (1964).

The contents of this chapter are presented in Journal of Nuclear Science and Technology, Vol. 8, No. 10, pp. 588～596, October 1971.

Table 1 Conductivity ratio

Fluid \ Electrode	Cu	Stainless steel (AISI-347)	Temp. (°C)
Na	0.15	2.3	800
	0.18	4.4	400
	0.20	6.6	200
NaK-78*	0.065	1.0	800
	0.061	1.5	400
	0.053	1.7	200
	0.043	2.0	20
Hg	0.026	0.73	300
	0.018	0.84	20

* NaK-78 Na 22w/o, K 78 w/o

Table 3 Properties of liquid metal in reference to the Hartmann and Reynolds numbers

	Ratio between electric conductivity and viscosity (sec/kg-Ω)	Kinematic viscosity (m^2/sec)	Temp. (°C)
Na	1.21×10^{10}	2.36×10^{-7}	800
	1.64×10^{10}	3.25×10^{-7}	400
	1.64×10^{10}	4.98×10^{-7}	200
NaK-78	6.60×10^{9}	2.13×10^{-7}	800
	7.32×10^{9}	2.68×10^{-7}	400
	6.11×10^{9}	3.87×10^{-7}	200
Hg	6.78×10^{8}	1.14×10^{-7}	20

Table 2 Generator configuration adopted in experiment

Case	Channel width (m)	Channel height (m)	Channel length (m)	Electrode width (m)	Magnetic field region (m)	Aspect ratio	Electrode	Number of terminals
(1)	0.0164	0.003	0.50	0.0035	0.50	30	SUS-27	4
(2)	0.0200	0.003	0.24	0.0035	0.50	12	Cu	3
(3)	0.0200	0.003	0.24	0.010	0.50	12	Cu	3

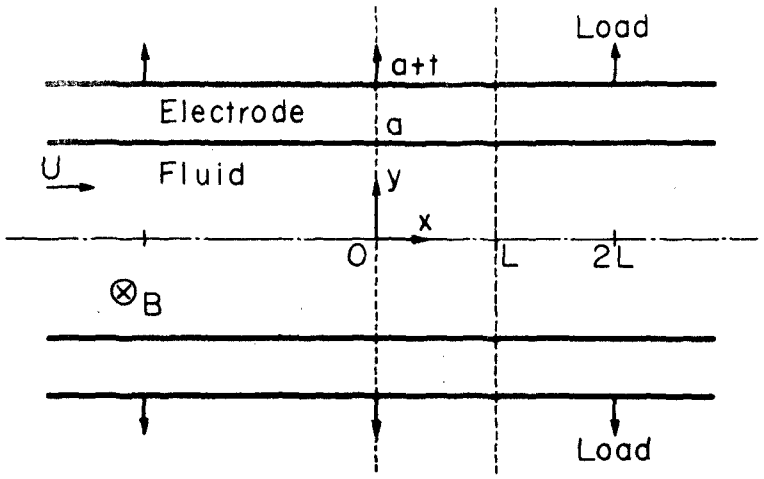

Fig. 2-1 Generator geometry for analysis

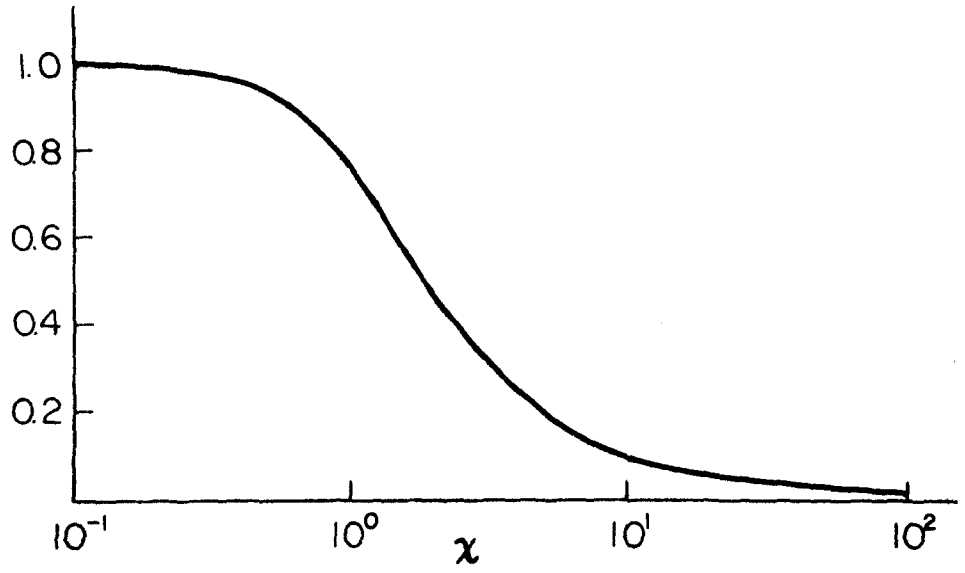

Fig. 2-2 Ratio λ_0 between R_i and R_{ieff} for generator with non-perfect conductor electrode

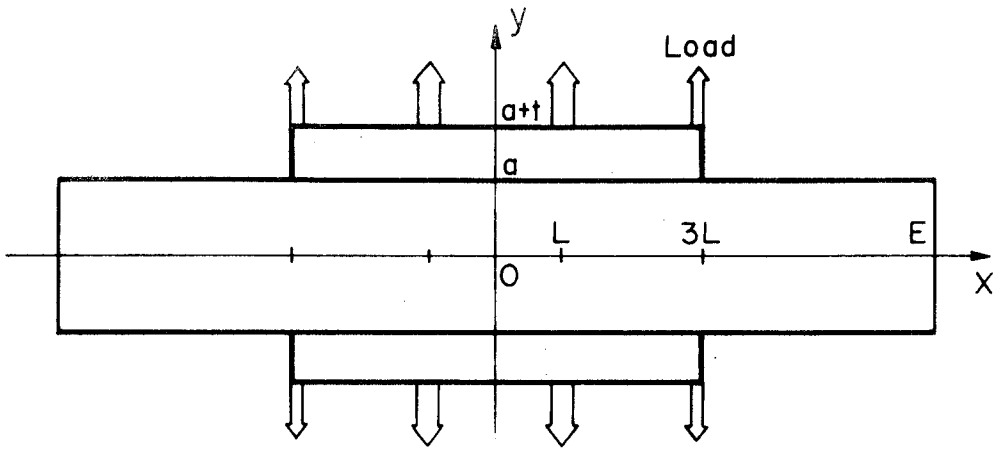

Fig. 2-3 Generator geometry for numerical computation

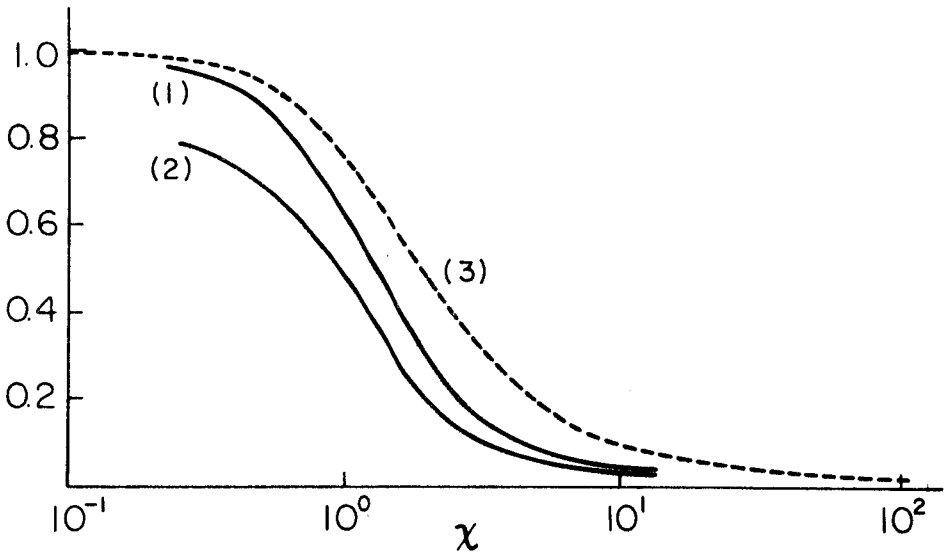

(1) λ(1), (2) λ(2), (3) λ_0, K=0.5, C=3

Fig. 2-4 Ratio between R_i and R_{ieff} obtained by numerical computation

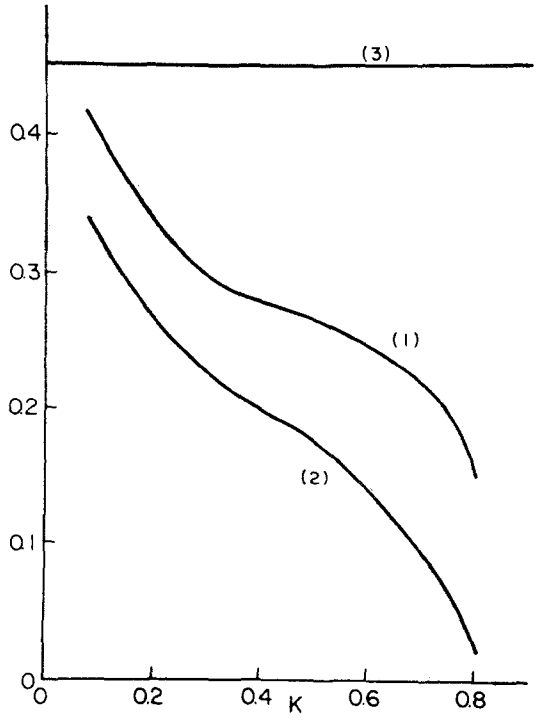

(1) $\lambda(1)$, (2) $\lambda(2)$, (3) λ_0, χ=2.14, C=3

Fig. 2-5 Ratio between R_i and R_{ieff} obtained by numerical computation

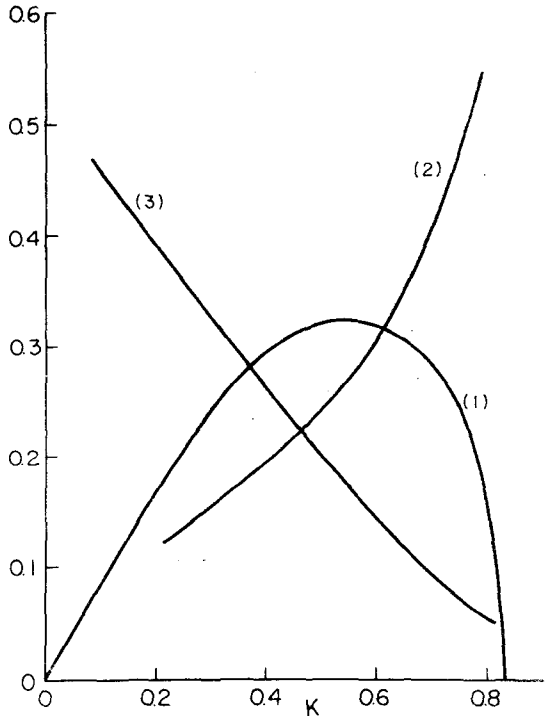

(1) Efficiency, (2) End loss, (3) Electrode loss, χ=2.14, C=3

Fig. 2-6 Generator efficiency and ratios of end and electrode losses in reference to electromechanical power extracted from fluid

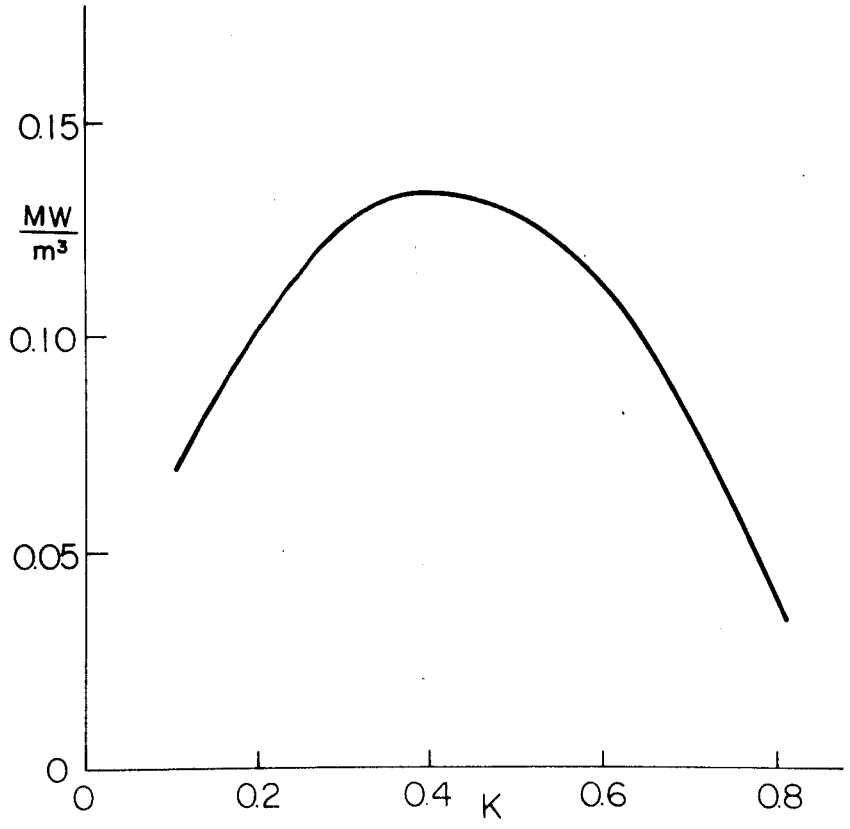

Electrode: Stainless steel (AISI-347), Fluid Sodium, Temp.: 800°C

Fluid velocity: 1 m/sec, Applied magnetic field: 1 Tesla

Dimensions

Generator length: 0.6 m, Electrode width: 0.05 m, Channel height: 0.01 m, Channel width: 0.2 m, Channel length upstream and downstream of generator: 0.075 m

Number of terminals: 4, χ=2.14, C=3

Fig. 2-7 Power density

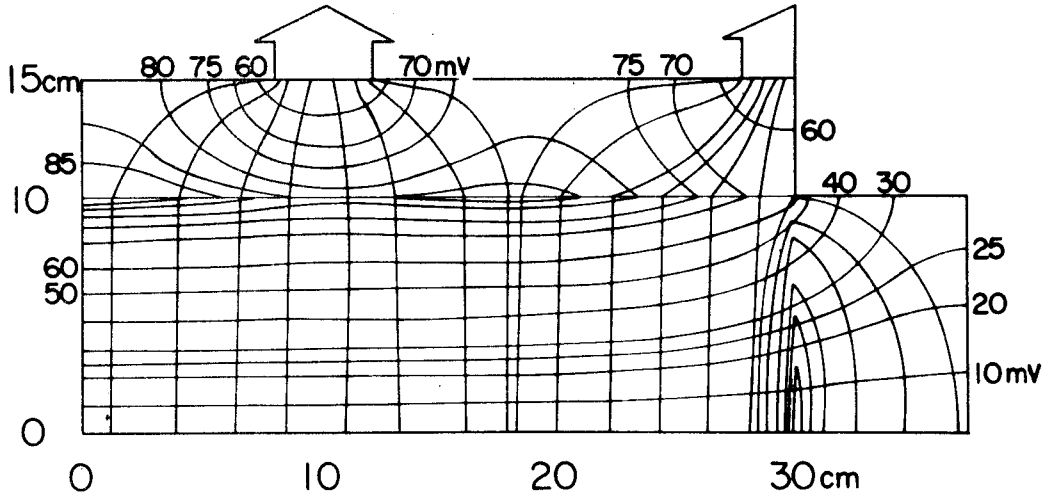

Electrode: Stainless steel (AISI-347), Fluid : Sodium, Temp.: 800°C, Fluid velocity: 1 m/sec, Applied magnetic field: 1 Tesla

Dimensions

Generator length: 0.6 m, Electrode width: 0.05 m, Channel height: 0.01 m, Channel width: 0.2 m, Channel length upstream and downstream of generator: 0.075 m

Number of terminals: 4, χ=2.14, C=3

Fig. 2-8 Distribution of current lines and equipotential lines

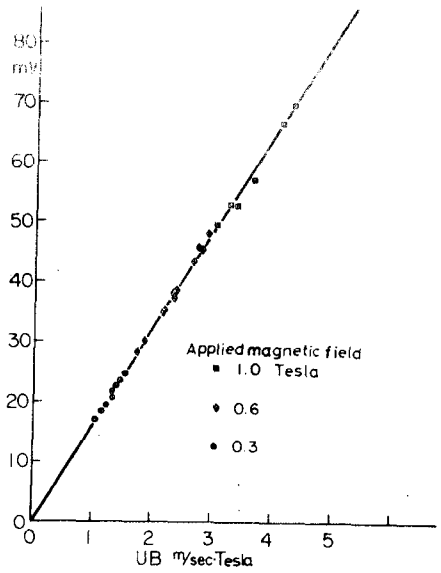

Fig. 2-9 Output voltage for K=1

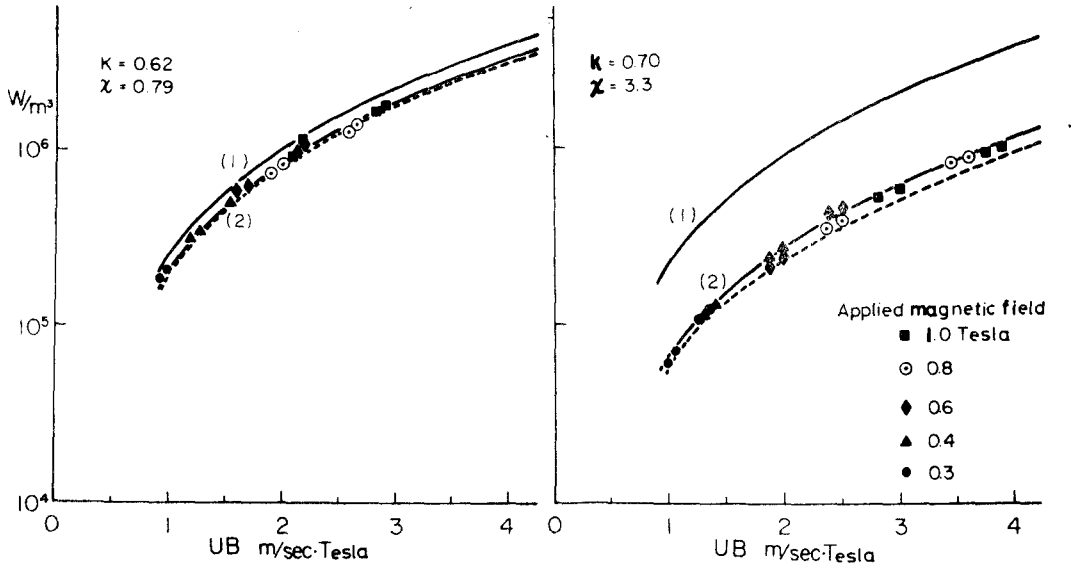

(1) Theoretical power density with perfect conductor

(2) Theoretical power density obtained with Eq.(25)

Dotted curve: Numerical computation

Fig. 2-10 Experimental power densities for case (3)

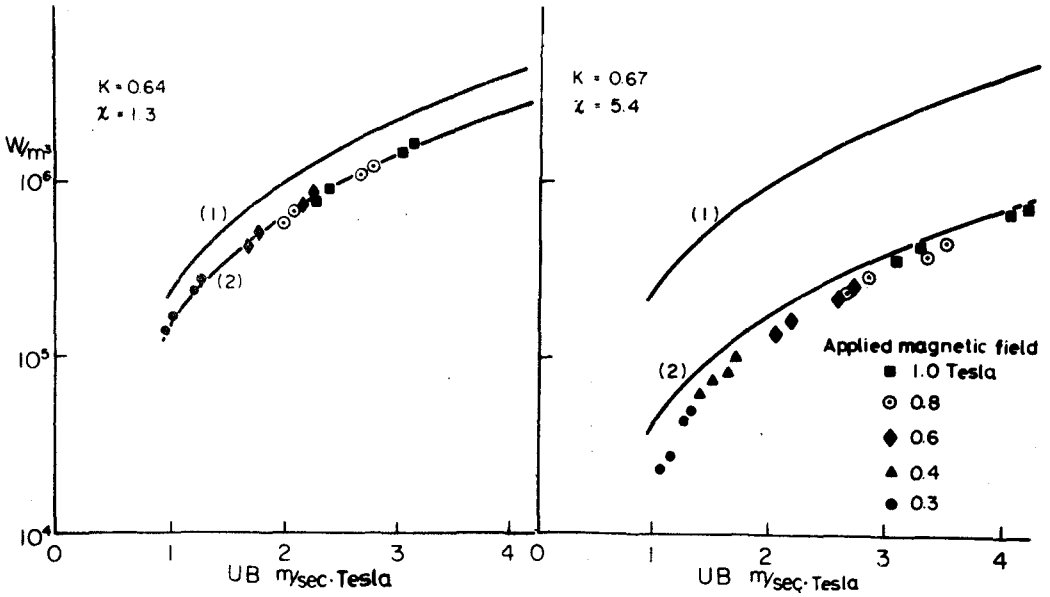

Fig. 2-11 Experimental power densities for case (2)

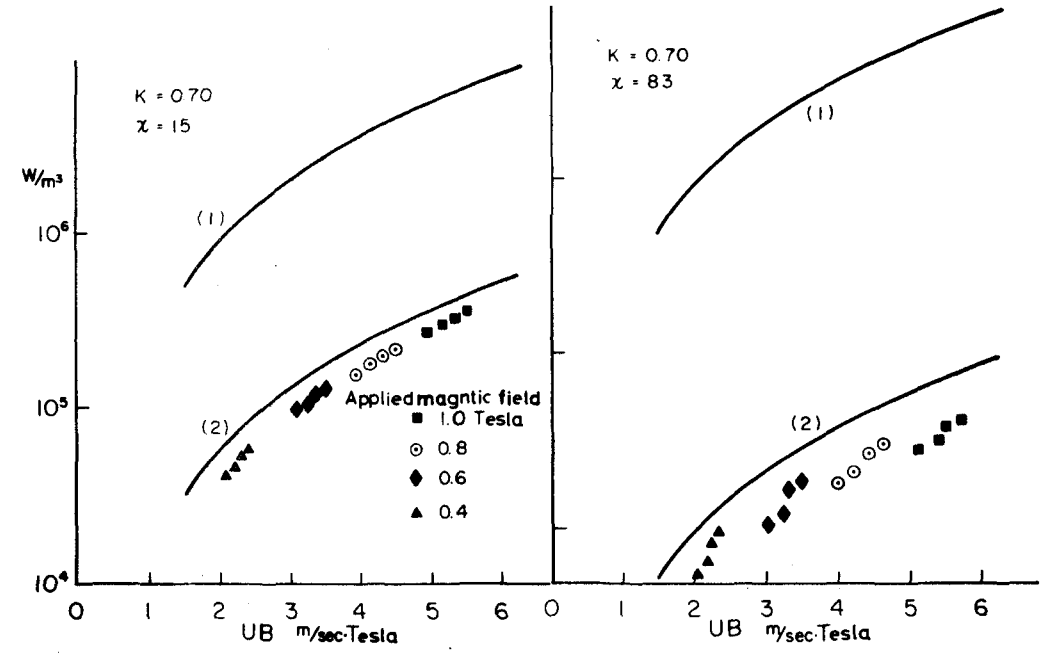

Fig. 2-12 Experimental power densities for case (1)

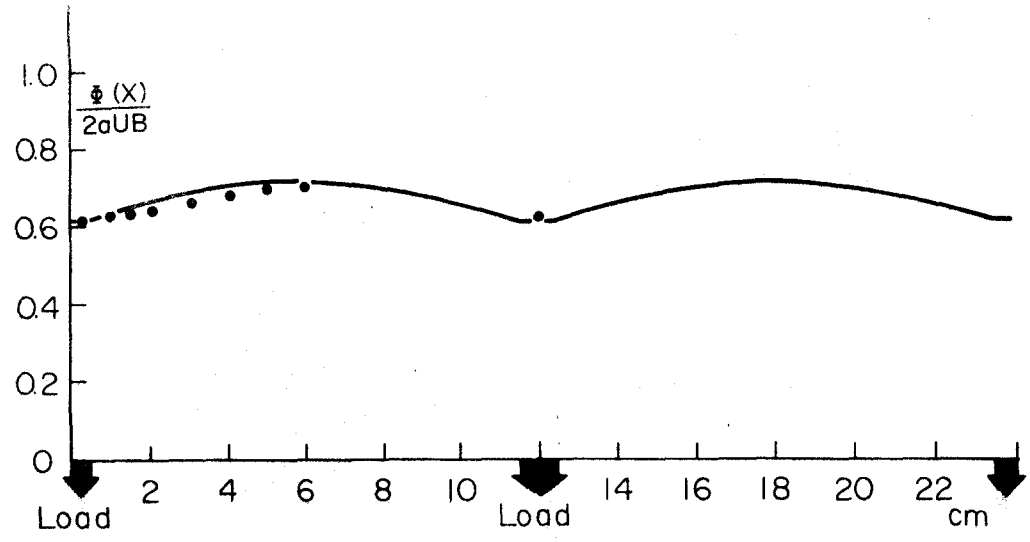

Fig. 2-13 Potential difference along electrode for case (3)

Chapter 3

Energy Loss in Liquid Metal MHD Induction Generator due to Discrete Tooth-Slot Arrangements

3-1 Introduction

In the present chapter, an analysis is made of the performance characteristics of liquid metal MHD induction generators taking into consideration the variation of the effective value of the magnetic field intensity of the traveling magnetic wave due to the disposition of teeth and slots as well as the ohmic loss in the metallic channel wall. In this analysis, the author adopts the "slit channel approximation" which assumes that the magnetic flux traverses the air gap of the magnet without attenuation. The validity of this approximation is verified in Section 3-2-c using the analyses performed by Wang and Dudzinsky[1][3], Pierson and Jackson[2], who have assumed that the effective intensity of the magnetic field is constant in the direction of fluid flow but decreases toward the center of the air gap in the direction parallel to the magnetic field due both to the flux leakage and to the skin effect.

The author treats the induction generator under both constant current mode and constant voltage mode operation in the theoretical analysis.

Furthermore, in order to verify the analytical solutions, experiments have been undertaken with an experimental induction generator using NaK-78 as the electrically conducting working fluid, which is accelerated through the generator channel by

compressed N_2 gas.

3-2 Formulation of the Problem

3-2-a Constant Current Mode

The configuration of the MHD induction generator to be analyzed is shown in Fig.3-1. The working fluid flows in the x-direction with velocity V between two parallel channel walls of infinite extent in the x- and z-directions spaced a distance b apart. The fluid is assumed to be incompressible, homogeneous, isotropic, and electrically neutral with conductivity σ_f and permeability μ_0, which is the same as that of free space.

The channel walls have a thickness of w/2 and a permeability of μ_0, and may be either electrical insulators or conductors with conductivity σ_w.

The electromagnet iron has a permeability of $\mu_c >> \mu_0$ and is laminated in the x-direction to minimize eddy current losses.

The exciting plates are assumed to be thin so that they can be replaced by current sheets in which the electric current flows in the z-direction. Insulators of infinitesimal thickness are required between the different regions to prevent current flow in the y-direction.

In order to decouple the electro-magnetic equations from the fluid mechanical equations, the author assumes further that the fluid velocity is constant both across the channel and in the direction of flow.

In the rationalized MKS system, neglecting the displacement current, Maxwell's equations are

$$\nabla \cdot B = 0 \tag{3-1}$$

$$\nabla \times B = \mu_0 J \tag{3-2}$$

$$\nabla \times E = -\frac{\partial B}{\partial t} \tag{3-3}$$

$$\nabla \cdot E = 0 \tag{3-4}$$

and Ohm's law

$$J = \sigma (E + V \times B) \tag{3-5}$$

Furthermore, the author assumes that the magnetic field in the air gap of the magnet is transverse to the flow, i.e. y-directed and independent of y ("Slit channel approximation")[2].

This approximation is discussed later using the analytical solution given by Wang and Dudzinsky. The differential form of Maxwell's equations cannot be used because of the neglected y-dependence of B[2]. Instead, B is determined from the integral form of Eq.(3-2), which is

$$\oint B \cdot dl = \mu_0 \int J \cdot n \, da \tag{3-6}$$

and this equation is applied to the dashed contour of Fig.3-1, where 1 is the dashed line, a the area bounded by the dashed line, n the unit vetcor perpendicular to the x-y plane, and J the sum of the exciting electric current and the electric currents in fluid and wall. From Eq.(3-6), the author the relation between the total magnetic field intensity and the electric current densities in the three regions, in the form

$$\frac{\partial B_y(x,t)}{\partial x} = \frac{\mu_0}{b+w} \{J_f(x,t)b + J_w(x,t)w + J_0(x,t)\}, \tag{3-7}$$

where J_0 is the exciting electric current density per unit

length and J_f is the electric current density in the fluid and J_w that in the channel wall.

From Eq.(3-5), the electric current density in the fluid and in the wall are given respectively by

$$J_f(x,t) = \sigma_f\{E_z(x,t) + VB_y(x,t)\} \tag{3-8}$$

$$J_w(x,t) = \sigma_w E_z(x,t) \tag{3-9}$$

The disposition of the teeth and slots in the electromagnet stator determines the variation of the effective value of the exciting magnetic field.

The author approximates this variation by a sinusoidal wave as shown in Fig.3-2 and then the exciting magnetic field $B_0(x,t)$ is expressed by

$$B_0(x,t)=B_{0m}\{(1-\gamma)+\gamma/2(\exp(jn\kappa x)+\exp(-jn\kappa x))\} \times\exp\{j(\omega t-\kappa x)\} \tag{3-10}$$

where n is the number of teeth per wave length, κ the wave number, ω the angular frequency, $j=(-1)^{1/2}$, and γ expresses the rate of variation ($=B_p/B_t$) and $B_{0m}=\sqrt{2}B_t$.

We can suppose that the exciting magnetic field expressed by Eq.(3-10) is created by the current sheet whose electric current per unit length is given from Eqs.(3-6) and (3-10):

$$J_0(x,t) = \frac{b+w}{\mu_0} B_{0m} j\kappa[(\gamma-1)+\gamma/2\{(n-1)\exp(jn\kappa x) -(n+1)\exp(-jn\kappa x)\}] \exp\{j(\omega t-\kappa x)\} \tag{3-11}$$

Since the magnetic field is in the y-direction, and is independent of y, while the electric field is in the z-direction and independent of z, Eqs.(3-1) and (3-4) are always satisfied.

Assuming the magnetic field and the electric field to be a time harmonic function, they become

$$B_y(x,t) = B_{yx}(x)\exp(j\omega t), \tag{3-12}$$

$$E_z(x,t) = E_{zx}(x)\exp(j\omega t), \tag{3-13}$$

and then Eq.(3-3) becomes

$$B_{yx}(x) = \frac{1}{j\omega}\frac{dE_{zx}(x)}{dx} \tag{3-14}$$

Substituting Eqs.(3-8), (3-9), (3-11) and (3-14) into Eq.(3-7), we obtain the second order linear differential equation in respect of the electric field intensity:

$$\frac{d^2E_{zx}}{dx^2} - Q_1\frac{dE_{zx}}{dx} - Q_2E_{zx} = F(x), \tag{3-15}$$

where

$$Q_1 = \frac{R_{mf}}{1+\varepsilon_2}\kappa(1-s), \tag{3-16}$$

$$Q_2 = j\frac{R_{mf}}{1+\varepsilon_2}\kappa^2(1+\varepsilon_1\varepsilon_2), \tag{3-17}$$

$$F(x) = \kappa^2V_sB_{0m}[(1-\gamma)+\gamma/2\{(1-n)\exp(jn\kappa x) + (1+n)\exp(-jn\kappa x)\}]\exp(-j\kappa x), \tag{3-18}$$

$$R_{mf} = \mu_0\sigma_fV_s/\kappa \quad \text{(Magnetic Reynolds number)}, \tag{3-19}$$

$$V_s = \omega/\kappa \quad \text{(wave velocity)}, \tag{3-20}$$

$$s = (V_s-V)/V_s \quad \text{(slip)}, \tag{3-21}$$

$$\varepsilon_1 = \sigma_w/\sigma_f, \tag{3-22}$$

$$\varepsilon_2 = w/b. \tag{3-23}$$

The general solution of this differential equation becomes

$$E_{zx}(x) = C_1\exp(l_1 x)+C_2\exp(l_2 x) + [E_1+1/2\{E_2\exp(jn\kappa x) + E_3\exp(-jn\kappa x)\}]\exp(-j\kappa x), \quad (3\text{-}24)$$

where

$$l_{1,2} = \frac{Q_1 \pm \sqrt{Q_2^2+4Q_2}}{2} \quad (3\text{-}25)$$

$$E_1 = \frac{(\gamma-1)V_s B_{0m}}{1+jR_{mf}(s+\varepsilon_1\varepsilon_2)/(1+\varepsilon_2)} \quad (3\text{-}26)$$

$$E_2 = \frac{-(1-n)\gamma V_s B_{0m}}{(1-n)^2+jR_{mf}\{(1-n)s+n+\varepsilon_1\varepsilon_2\}/(1+\varepsilon_2)} \quad (3\text{-}27)$$

$$E_3 = \frac{-(1+n)\gamma V_s B_{0m}}{(1+n)^2+jR_{mf}\{(1+n)s+\varepsilon_1\varepsilon_2-n\}/(1+\varepsilon_2)} \quad (3\text{-}28)$$

Applying the periodical boundary condition, i.e., $E_{zx}(x=m\lambda) = E_{zx}(x=(m+1)\lambda)$ at $m=0, \pm1, \pm2, \cdots\cdots$, where λ is the wave length, C_1 and C_2 become zero.

The time- and space-averaged electrical complex power, whose sign is defined to be negative when it is supplied to the converter, becomes

$$P_o = -\frac{1}{b+w}\frac{1}{\lambda}\int_0^{\lambda}\{1/2 J_0 E_z^*\}\,dx$$

$$= \frac{1}{2}\frac{\sigma_f V_s^2 B_{0m}^2}{(1+\varepsilon_2)}\left[P_1\{s+\varepsilon_1\varepsilon_2 - j(1+\varepsilon_2)/R_{mf}\} + P_2\left\{\frac{(1-n)s+n+\varepsilon_1\varepsilon_2}{(1-n)^2} - j\frac{1+\varepsilon_2}{R_{mf}}\right\} + P_3\left\{\frac{(1+n)s-n+\varepsilon_1\varepsilon_2}{(1+n)^2} - j\frac{1+\varepsilon_2}{R_{mf}}\right\}\right] \quad (3\text{-}29)$$

where

$$P_1 = (1-\gamma)^2 \left[1 + \left(\frac{R_{mf}}{1+\varepsilon_2} \right)^2 (s+\varepsilon_1\varepsilon_2)^2 \right]^{-1} \tag{3-30}$$

$$P_2 = \frac{\gamma^2}{4} \left[1 + \left(\frac{R_{mf}}{1+\varepsilon_2} \right)^2 \left\{ \frac{(1-n)s+n+\varepsilon_1\varepsilon_2}{(1-n)^2} \right\}^2 \right]^{-1} \tag{3-31}$$

$$P_3 = \frac{\gamma^2}{4} \left[1 + \left(\frac{R_{mf}}{1+\varepsilon_2} \right)^2 \left\{ \frac{(1+n)s-n+\varepsilon_1\varepsilon_2}{(1+n)^2} \right\}^2 \right]^{-1} \tag{3-32}$$

and the asterisk denotes the complex conjugate.

The electro-mechanical power per unit volume of generator, whose sign is defined to be positive when it is supplied to the external fluid system by the generator, becomes, in time- and space-average,

$$\begin{aligned} P_m &= -\frac{b}{b+w}\frac{V}{\lambda}\int_0^{\lambda} \mathcal{R}e\{1/2 J_f B_y^*\}\, dx \\ &= \frac{1}{2}\frac{\sigma_f V_s^2 B_{0m}^2}{1+\varepsilon_2}\left\{ P_1 s + P_2\left(s + \frac{n}{1-n} \right) + P_3\left(s - \frac{n}{1+n} \right) \right\}(1-s) \end{aligned} \tag{3-33}$$

where $\mathcal{R}e$ denotes the real part of the complex value.

The power dissipated in the fluid per unit volume of generator becomes, in time- and space-average,

$$\begin{aligned} P_{floss} &= \frac{b}{b+w}\frac{1}{\lambda}\int_0^{\lambda} \frac{1}{\lambda}\frac{J_f J_f^*}{\sigma_f}\, dx \\ &= \frac{1}{2}\frac{\sigma_f V_s^2 B_{0m}^2}{1+\varepsilon_2}\left\{ P_1 s^2 + P_2\left(s+\frac{n}{1-n} \right)^2 + P_3\left(s+\frac{n}{1+n} \right)^2 \right\} \end{aligned} \tag{3-34}$$

while the power dissipated in the channel wall per unit volume of generator is given, in time- and space-average by

$$P_{wloss} = \frac{w}{b+w}\frac{1}{\lambda}\int_0^{\lambda}\frac{1}{2}\frac{J_w J_w^*}{\sigma_w}\,dx$$

$$= \frac{1}{2}\frac{\sigma_f V_s^2 B_{0m}^2}{1+\varepsilon_2}\{P_1 + P_2(1-n)^{-2} + P_3(1+n)^{-2}\}\varepsilon_1\varepsilon_2 \qquad (3\text{-}35)$$

In the analysis mentioned above, the imposed magnetic field intensity B_0 is independent of the slip, and therefore, from Eq.(3-11), the amplitude of the electric current density in the exciting windings is always constant and the performance characteristics obtained correspond to these of the generator operated in constant current mode[3][5].

3-2-b Constant Voltage Mode

On the other hand, assuming that the total magnetic field intensity is independent of the slip and is expressed by

$$B_y(x,t)=B_m[(1-\gamma)+\gamma/2\{\exp(jn\kappa x)+\exp(-jn\kappa x)\}]\exp j(\omega t-\kappa x)\} \qquad (3\text{-}36)$$

where B_m is the amplitude of the total magnetic field intensity, the electric field intensity is given from Eq.(3-14):

$$E_z(x,t) = -V_s B_m\left[(1-\gamma) + \frac{\gamma}{2}\left\{\frac{1}{1-n}\exp(jn\kappa x)+\frac{1}{1+n}\exp(-jn\kappa x)\right\}\right]$$
$$\times\exp\{j(\omega t-\kappa x)\} \qquad (3\text{-}47)$$

and its amplitude is always constant. The performance characteristics of the generator analyzed under such an assumption correspond to those of a generator operated in constant voltage mode, which is the usual mode of operation of machines in conventional power systems.

The magnetic field induced by the electric currents both in the fluid and in the channel wall is given from Eqs.(3-6), (3-8), (3-36) and (3-37):

$$B_{yi}(x,t) = jB_m \frac{R_{mf}}{1+\varepsilon_2}\left[(\gamma-1)(s+\varepsilon_1\varepsilon_2)\right.$$
$$-\frac{\gamma}{2}\left\{\frac{1}{1-n}\left(s+\frac{n+\varepsilon_1\varepsilon_2}{1-n}\right)\exp(jn\kappa x)\right.$$
$$\left.\left.+\frac{1}{1-n}\left(s+\frac{\varepsilon_1\varepsilon_2-n}{1+n}\right)\exp(-jn\kappa x)\right\}\right]\exp\{j(\omega t-\kappa x)\} \tag{3-38}$$

Subtracting the induced magnetic field from the total magnetic field, the magnetic field imposed by the electric currents in the exciting windings is given by

$$B_0(x,t) = B_m\left[(1-\gamma)\left\{1+j\frac{R_{mf}}{1+\varepsilon_2}(s+\varepsilon_1\varepsilon_2)\right\}\right.$$
$$+\frac{\gamma}{2}\left\{\left(1+j\frac{R_{mf}}{1+\varepsilon_2}\frac{1}{1-n}\left(s+\frac{n+\varepsilon_1\varepsilon_2}{1-n}\right)\right)\exp(jn\kappa x)\right.$$
$$\left.\left.+\left(1+j\frac{R_{mf}}{1+\varepsilon_2}\frac{1}{1+n}\left(s+\frac{\varepsilon_1\varepsilon_2-n}{1+n}\right)\right)\exp(-jn\kappa x)\right\}\right]$$
$$\cdot\exp\{j(\omega t-\kappa x)\} \tag{3-39}$$

Its amplitude is dependent on the slip and compensates the induced magnetic field so that the total magnetic field is kept constant.

From Eqs.(3-6) and (3-39) the electric current density per unit length in the exciting current sheet becomes

$$J_0(x,t) = j\kappa B_m \frac{b+w}{\mu_0}\left[(\gamma-1)\left\{1+j\frac{R_{mf}}{1+\varepsilon_2}(s+\varepsilon_1\varepsilon_2)\right\}\right.$$

$$+\frac{\gamma}{2}\left\{(n-1)\left(1+j\frac{R_{mf}}{1+\varepsilon_2}\frac{1}{1-n}\left(s+\frac{n+\varepsilon_1\varepsilon_2}{1-n}\right)\right)\exp(jn\kappa x)\right.$$

$$\left.-(n+1)\left(1+j\frac{R_{mf}}{1+\varepsilon_2}\frac{1}{1+n}\left(s+\frac{\varepsilon_1\varepsilon_2-n}{1+n}\right)\right)\exp(-jn\kappa x)\right\}\Bigg]$$

$$\cdot\exp\{j(\omega t-\kappa x)\} \qquad (3\text{-}40)$$

The time- and space-averaged electrical complex power per unit volume of generator becomes, in the same manner as Eq.(3-29),

$$P_0=\frac{1}{2}\frac{\sigma_f V_s^2 B_m^2}{1+\varepsilon_2}\left[(1-\gamma)^2\left\{(s+\varepsilon_1\varepsilon_2)-j\frac{1+\varepsilon_2}{R_{mf}}\right\}\right.$$

$$+\frac{\gamma^2}{4}\left\{\frac{1}{1-n}\left(s+\frac{n+\varepsilon_1\varepsilon_2}{1-n}\right)-j\frac{1+\varepsilon_2}{R_{mf}}\right\}$$

$$\left.+\frac{\gamma^2}{4}\left\{\frac{1}{1+n}\left(s+\frac{\varepsilon_1\varepsilon_2-n}{1+n}\right)-j\frac{1+\varepsilon_2}{R_{mf}}\right\}\right] \qquad (3\text{-}41)$$

The electro-mechanical power per unit volume of generator becomes, in time- and space-average,

$$P_m=\frac{1}{2}\frac{\sigma_f V_s^2 B_m^2}{1+\varepsilon_2}\left[(1-\gamma)^2(1-s)s\right.$$

$$\left.+\frac{\gamma^2}{4}\left\{2s+\frac{n}{1-n}-\frac{n}{1+n}\right\}(1-s)\right] \qquad (3\text{-}42)$$

The power dissipated in the fluid and in the channel wall per unit volume of generator becomes, in time- and space-average, respectively

$$P_{floss}=\frac{1}{2}\frac{\sigma_f V_s^2 B_m^2}{1+\varepsilon_2}\left[(1-\gamma)^2 s^2\right.$$

$$\left.+\frac{\gamma^2}{4}\left\{\left(s+\frac{n}{1-n}\right)^2+\left(s-\frac{n}{1+n}\right)^2\right\}\right] \qquad (3\text{-}43)$$

$$P_{wloss} = \frac{1}{2}\frac{\sigma_f V_s B_m}{1+\varepsilon_2}\left[(1-\gamma)^2 + \frac{\gamma^2}{4}\left\{\frac{1}{(1-n)^2} + \frac{1}{(1+n)^2}\right\}\right]\varepsilon_1\varepsilon_2 \tag{3-44}$$

The power factor of generator is obtained in the form

$$\cos\Theta = \frac{\text{Real part of complex power}}{\{(\text{Real part of complex power})^2 + (\text{Imaginary part of complex power})^2\}^{1/2}} \tag{3-45}$$

where Θ is the phase difference between the electric field and the electric current in the exciter winding.

The generator efficiency becomes

$$\eta_g = \frac{\text{Real part of complex power}}{\text{Electro-mechanical power}} \tag{3-46}$$

The pump efficiency becomes

$$\eta_p = \frac{\text{Electro-mechanical powe}}{\text{Real part of complex power}} \tag{3-47}$$

Figure 3-3 shows the gross electrical power, i.e., the real part of the electrical complex power, and the electro-mechanical power per unit volume of the generator operated in a constant current mode, neglecting the ohmic loss in the channel wall.

The numerical results are shown for $\gamma=0.2$, $n=12$ and $B_t=1T$.

In this figure, the converter acts as a generator when the slip is negative, as a pump with the slip between zero and unity, and as a damper with slip above unity. The efficiency and the power factor of the converter in this case are shown in Fig.3-4, where the dot-dash-lines show the efficiency of an ideal converter which has neither the variation of the effective value

of magnetic field intensity nor the wall loss.

When the slip approaches zero, the ratio againist the gross electrical power indicated by the loss due to the variation of the effective value of magnetic field intensity increases, and the efficiency becomes much smaller than the ideal value.

When the converter is operated in constant voltage mode, the gross electrical power and the electro-mechanical power per unit volume of converter are as shown in Fig.3-5, and in this case the efficiency and the power factor become as shown in Fig.3-6 for the same conditions as in constant current mode.

It has been analyzed by Wang and Dudzinsky that the ideal converter should have the same efficiency whether operated in constant current mode or constant voltage mode[5].

In actuality, however, as is evident from Fig.3-4, the efficiency obtained with constant current mode decreases with increasing magnetic Reynolds number. This is due to currents being induced in the fluid by the variation of the effective value of magnetic field which create an additional standing wave magnetic field, and which does not contribute to the exchange of power between the fluid and the external power source or load, so that in constant current mode the total magnetic field is decreased by this additional magnetic field which increases with the magnetic Reynolds number, whereas in constant voltage mode it is kept constant. As for the power factor, the difference between those obtained in constant current mode and in constant voltage mode is very small, and it is almost the same as the ideal converter.

Figure 3-7 shows the efficiency of the converter operated in constant voltage mode calculated for n=12, ε_1=0.5, ε_2=0.5 and R_{mf}=2.0 and the efficiency of the ideal converter is given by the dot-dash-lines. As the γ-value increases, the range of slip in which the converter acts as pump becomes narrow, but the slip at which the converter begins to act as generator under self-excitation is not affected by the γ-value.

This is attributed to the following reason. The gross electrical power of the converter depends on both the ohmic loss in the channel wall perpendicular to the applied magnetic field and the variation of the effective value of the magnetic field as given by Eq.(3-41) and the latter is masked by the former, particularly at low generator efficiency.

The electro-mechanical power of the converter, on the other hand, depends only on the magnetic field variation as given by Eq.(3-42), and therefore the effect of differences in γ-value appears obviously even at low pump efficiency. Figure 3-8 shows the efficiency of the converter operated in constant voltage mode for three parameter values: n=3, 6 and 18, with γ=0.3, ε_1=0.5, ε_2=0.5 and R_{mf}=2.0. It is clear from this figure that the efficiency is improved slightly by increasing n.

In a practical generator excited by three phase current source, the concentrated winding corresponds to n=6 and then the distributed winding n>6.

In order to find the effects of eddy current induced in channel wall, the gross electrical power per unit volume and the power factor of the converter operated in constant voltage

mode are shown in Fig.3-9 with $\varepsilon_1\varepsilon_2$ as parameter, for γ=0.2, n=12 and R_{mf}=2.0, and the efficiency is then as shown in Fig.3-10. As $\varepsilon_1\varepsilon_2$ increases, the ratio of the ohmic loss in the channel wall per unit volume of converter increases, the efficiency decreases, and furthermore the slip at which the converter begins to act as generator under self-excitation increases its negative value as shown in Fig.3-10. The slip range in which the converter acts as pump, however, does not change with variation of the $\varepsilon_1\varepsilon_2$. The effect of change in $\varepsilon_1\varepsilon_2$ is deffe-rent from that in γ, for the same reason as mentioned in relation to Fig.3-7.

3-2-c Validity of Slit-Channel Approximation (Skin Effect and Leakage of Magnetic Flux)

In the analysis mentioned above, the author assumes that the magnetic field is constant in the air gap in the direction parallel to the y-coordinate axis but has no decrease due to the leakage and to the skin effect in the fluid.

If this decrease of magnetic field toward the center of the air gap is taken into account, the ratio δ of the gross electrical power and the electro-mechanical power per unit volume of converter to the corresponding values of the ideal converter is obtained from the results analyzed by Wang and Dudzinsky:

$$\delta = \frac{2}{b}\int_0^{b/2} \frac{|\cosh \alpha y|^2}{|\cosh \alpha b/2|^2}\, dy \qquad (3\text{-}48)$$

where $\alpha^2=\kappa^2(1+jsR_{mf})$ (3-49)

Figure 3-11-a shows δ as function of the ratio between travel-

ing magnetic wave length and the air gap of the magnet as parameter of sR_{mf}. Figure 3-11-b shows δ whose function is interchange with the parameter in Fig.3-11-a.

The dependence of the leakage on the δ-value is determined by λ/b and the dependence of the skin effect on the δ-value by sR_{mf}.

As is evident from Figure 3-11, when the wave length is fifteen or more times as long as the air gap unless sR_{mf} is less than 10, the δ-value becomes 0.97 or more, and hence the loss in power due to the leakage of magnetic flux and skin effect does not appear to be a serious problem.

3-3 Experimental Apparatus

The author has performed experiments at room temperature, using NaK-78 (conductivity=$2.5\times10^{6}/\Omega m$) as the electrically conducting fluid.

Figure 3-12 shows the flow diagram of the experimental apparatus, in which the thick lines denote the piping for NaK and thin lines those for N_2 gas. The NaK is transfused into the pressure tank by compressed N_2 gas and the high velocity flow of NaK through the generator channel is provided by the pressure tank whose pressure is automatically kept constant during the run by the pressure regulator R-1, and hence the fluid velocity measured by the electro-magnetic flow meter is kept constant during the run. The system contains 230 l of NaK of which 180 l is transferred to the dump tank through the NaK filter before every operation to trap impurities included in

the NaK. The excitation system for the induction generator and the measuring system are shown in Fig.3-13. Figure 3-14 shows the stator and the fluid channel geometry. The channel walls are made of INCONEL alloy X-750*, whose conductivity is 8.2×10^5 /Ωm, and copper side-bars, 5×15×600 mm, were fixed to the channel wall in the later runs of the experiment. A value of 20 was chosen for the aspect ratio (length-to-width) of the channel under the traveling magnetic field in order to reduce the end loss[6]. The stators were made with 0.35 mm iron laminations with one slot per pole per phase, and the wave length of traveling wave was 0.2 m. The three phase windings are concentrated, with 180 turns/coil. These windings were 6-Δ connected in parallel with a 90 KVA synchronous generator, driven by an induction motor through a variable-speed coupling to provide frequencies from 40 to 250 Hz. The measured winding resistance per phase was 0.094, 0.096 and 0.095 Ω for the three phase.

Figure 3-15 shows the variation of the effective value of traveling magnetic field intensity measured at the center of the air gap by scanning with a Hall-effect type probe in the direction of fluid flow. The γ-value of our experimental generator was found from Fig.3-15 to be 0.31.

The maximum velocity of NaK obtained was 45 m/sec under a pressure difference of 30 kg/cm^2 between the pressure tank and the dump tank.

The accuracy of the NaK velocity measurement is considered to be within a few percent. The duration of the run was 33sec at 45 m/sec of NaK velocity.

3-4 Experimental Results and Discussions

The electrical power and the electro-mechanical power obtained in our experimental converter without copper side bars are shown in Figs.3-16 and -17. The power experimentally determined was normalized to a unit volume of converter and a square of the effective value of magnetic field intensity measured with a search coil. The purpose of this was to eliminate the error in setting the magnetic field intensity.

The converter was operated in constant voltage mode at each frequency, and the theoretical values given from Eqs.(3-41) and (3-42) are indicated by solid lines in the figures. As is evident from Fig.3-16, the gradients of the experimental plots of electrical power are less steep than those of the theoretical curves, and hence the electrical interaction between the converter windings and the fluid is considered to be weak.

On the other hand, as shown in Fig.3-17, the converter decelerated the fluid at a slip between zero and unity, where the ideal converter acts as pump, except for the case of the slip of 0.7 at 160 Hz. Besides, the fluid supplied much more electro-mechanical power to the converter than the theoretical value at negative slip, where the ideal converter acts as a generator.

It is assumed from the analysis that the electric currents in both fluid and channel wall flow in the direction of the current loop (1) shown in Fig.3-18 and therefore the induced magnetic field formed by them has only the y-component. Some parts of electric currents induced within our experimental converter, however, flow in the direction of the current loop (2) since

the side wall of the converter channel has finite conductivity instead of being a perfect conductor assumed in the analysis, and hence the induced magnetic field formed by them has an x-component, which has no interaction with the windings.

In addition to the low electrical interaction, the induced electric currents in the direction of current loop (2) creates additional ohmic losses in both the fluid and the channel wall, and this causes the converter to decelerate the fluid.

It would even appear that the electric currents induced in our experimental converter flow more in the direction of the current loop (2) than loop (1). In order to diminish the induced currents in the current loop (2), the author fixed copper bars onto the channel side wall, as shown in Fig.3-14. Figure 3-19 and -21 show the electrical power and the electro-mechanical power of the experimental converter with copper side bars with the theoretical values in constant voltage mode indicated by solid lines. As is evident from Fig.3-19, the gradient of the electrical power agrees with the theoretical value at each frequency, but the ohmic losses in both the side walls of channel and the copper side bars in addition to that in the channel walls perpendicular to the applied magnetic field have shifted the plots of the experimentally obtained electrical power toward the negative side of the slip compared with the theoretical curves. In the experiment, this is caused, for the most part, by the ohmic loss due to the eddy currents induced in the copper side bars, a portion of which bars protrudes into the applied magnetic field. (See Fig.3-14)

This ohmic loss was measured by empty channel tests, with results as shown in Fig.3-20, which presents the power losses dissipated in the converter with and without the copper side bars. The theoretical curve calculated from Eq.(3-44) is indicated by the solid line.

The converter with copper side bars accelerated the fluid almost in the full range of slip between zero and unity, as shown in Fig.3-21, which has brought the experimentally obtained electro-mechanical power quite close to the theoretical values.

The currents induced in the direction of the current loop (2) have decreased somewhat in the converter with copper side bars, though they were fixed outside the channel wall.

In my experiment the Hartmann number was about 50 and the flow was turbulent judging from the Reynolds number which was of the oder of 10^5, so that the effect of the velocity profile of the flow can be neglected[7].

3-5 Concluding Remarks

Analysis by Wang and Dudzinsky has indicated that the efficiency of an ideal converter operated in constant current mode would be the same as when operated in constant voltage mode[5].

The present analysis taking into account the variation of the effective value of the magnetic field has revealed, however, that, as the magnetic Reynolds number of fluid becomes larger, the efficiency of a converter operated in constant current mode becomes lower than in constant voltage mode. This is due to the fact that variation of the magnetic field creates an addi-

tional standing wave magnetic field, which does not contribute to the exchange of power between the fluid and the external power source or load, and which increases with the magnetic Reynolds number, and decreases the total magnetic field when operating in constant current mode, whereas in constant voltage mode the total magnetic field is kept constant.

The electro-mechanical power of the converter operated in constant voltage mode is dependent on the magnetic field variation and independent of the ohmic loss due to the eddy current induced in the channel wall perpendicular to the applied magnetic field, and therefore the range of slip in which the converter acts as pump is affected only by the magnetic field variation, and becomes narrow as the γ-value increases.

On the other hand, the gross electrical power of the converter operated in constant voltage mode is dependent on both the magnetic field variation and the ohmic loss in the wall perpendicular to the applied magnetic field, and the former is masked by the latter especially at low efficiency, and hence the slip at which the converter begins to act as generator under self-excitation is determined, for the most part, by the ohmic loss in the wall and increases its negative value as the ohmic loss in wall, i.e., $\varepsilon_1\varepsilon_2$, becomes larger.

The efficiency of a converter, with the value of γ left constant, is improved only slightly by increasing n, i.e., the number of teeth per wave length, but in an actual converter, the γ-value appears to have a tendency to diminish with increasing n, and thus the increase of n should contribute effectively

to improvement of the efficiency. Increasing the n, however, is limited by the accompanying increase in the difficulty of practically constructing the stator, in which the poly-phase windings are installed, and hence it is necessary to find a shape of tooth such as to produce a low γ-value without inconveniently increasing n.

The electrical power obtained with converter when equipped with copper side bars fixed to the side wall of the channel in order to decrease the electric currents in the direction of the current loop (2) in Fig.3-18, agreed with the analytical solution treated here, though the curves shifted to the negative side of the slip due to the additional ohmic losses in both the side wall of channel and the copper side bars, of which a part protrudes into the applied magnetic field.

The induced electric currents within my experimental converter without copper side bars would appear to have flowed in the direction of the current loop (2) rather than in loop (1) and thus the converter must have interacted so some extent with the fluid electrically and decelerated the fluid even at values of slip between 0 and 0.7 where the converter had to act as pump. For a converter with annular channel, there should be no electric current flow corresponding to that in the current loop (2).

References

1) Wang, T.C., Dudzinsky, S.J.: AIAA J. 5[1], 107-112 (1967).

2) Pierson, E.S., Jackson, W.D.: ANL-7148, (Mar. 1966).

3) Dudzinsky, S.J., Wang, T.C.: Proc. IEEE, 56[7],1420-1431 (1968).

4) Sutton, G.W.: "Engneering Magnetohydrodynamics", 484-487 (1965), McGraw-Hill.

5) Wang, T.C., Dudzinsky, S.J.: AIAA J., 5[11], 2059-2060 (1967).

6) Cerini, D.J., Elliott, D.G.: ibid., 6[3], 503-510 (1968).

7) Tanatugu, N., Fujii-e, Y., Suita, T.: J. Nucl. Sci. Technol., 8[10], 588-596 (1971).

The contents of this chapter are presented in Journal of Nuclear Science and Technology, Vol. 9, No. 4, pp. 213～223, April 1972.

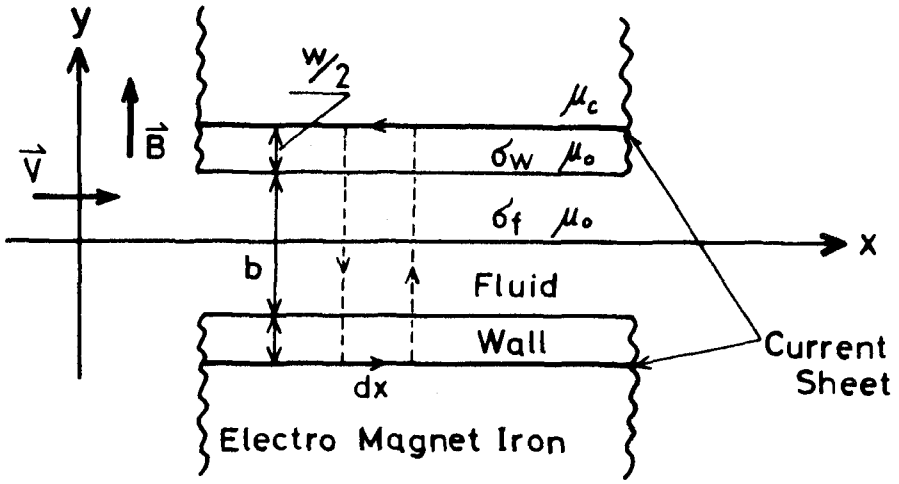

Fig. 3-1 Configuration of MHD induction converter

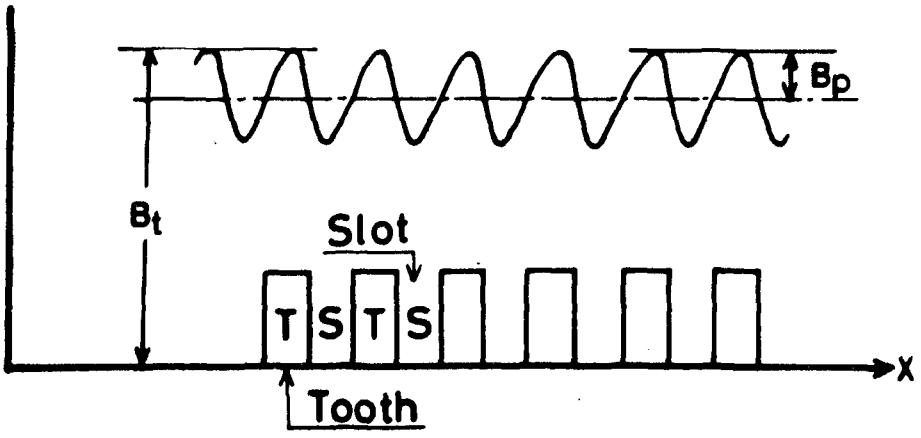

Fig. 3-2 Variation of effective value of magnetic field intensity

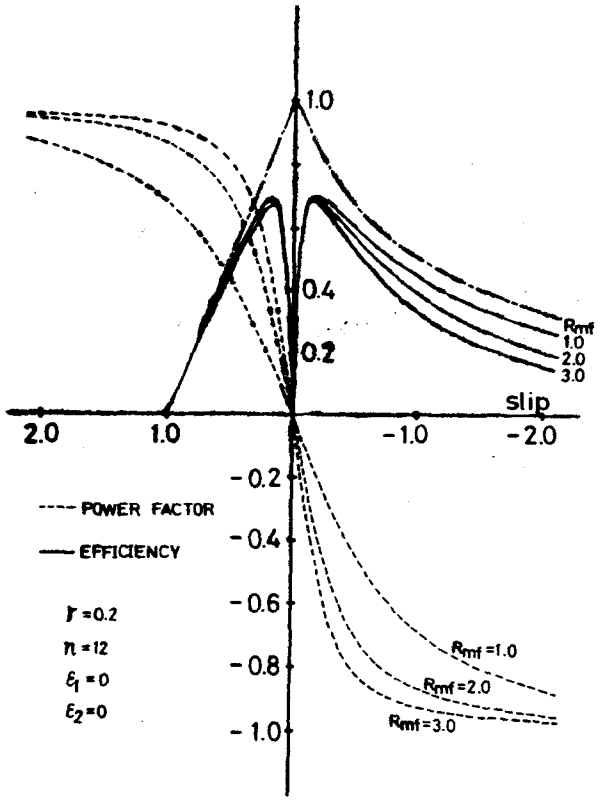

Fig. 3-4 Efficiency and power factor of converter operated in constant current mode

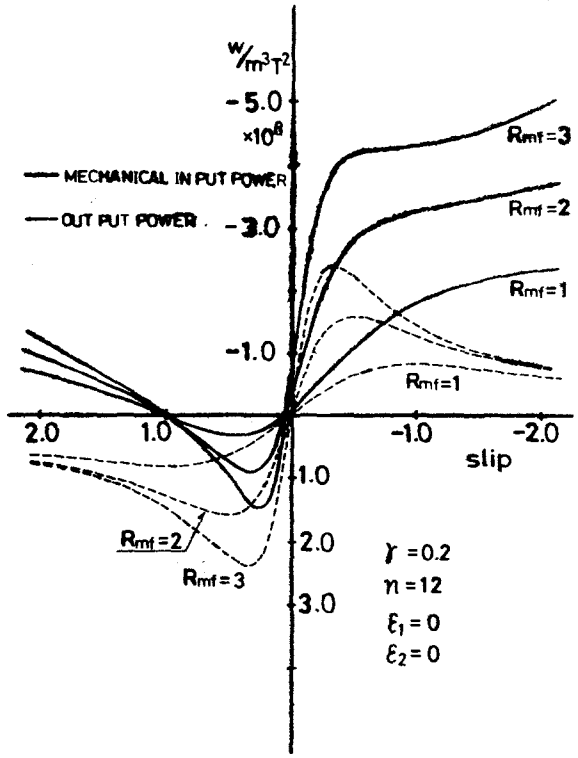

Fig. 3-3 Gross electrical power and electromechanical power per unit volume of converter operated in constant current mode

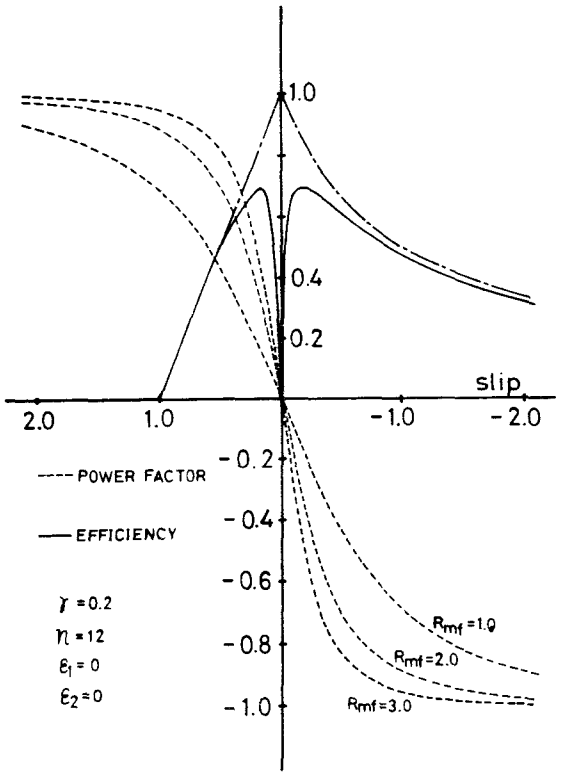

Fig. 3-6 Efficiency and power factor of converter operated in constant voltage mode

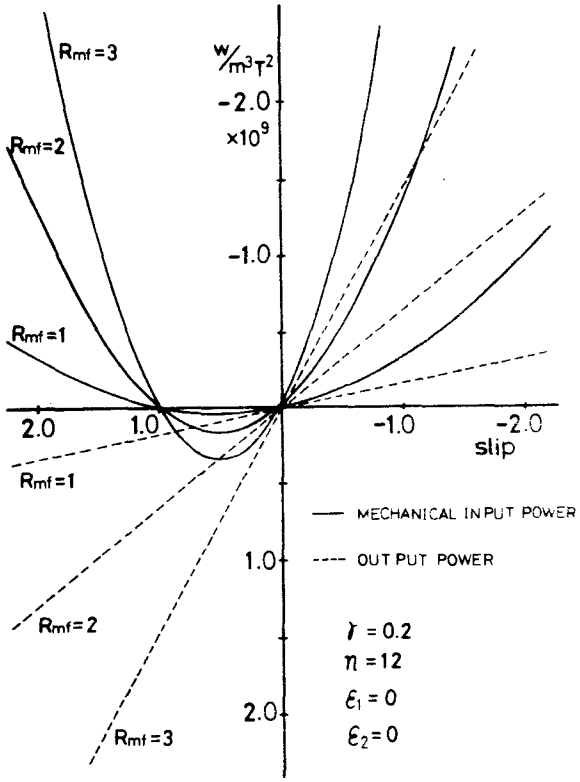

Fig. 3-5 Gross electrical power and electromechanical power per unit volume of converter operated in constant voltage mode

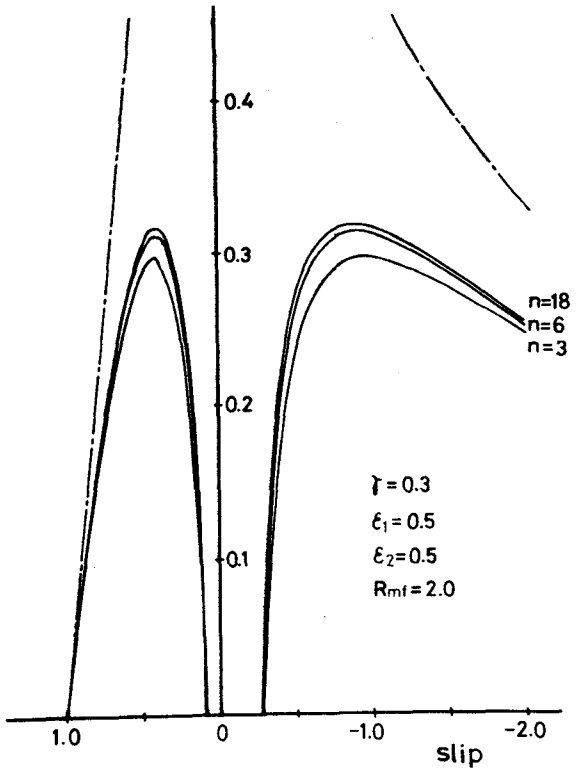

Fig. 3-8 Efficiency of converter operated in constant voltage mode

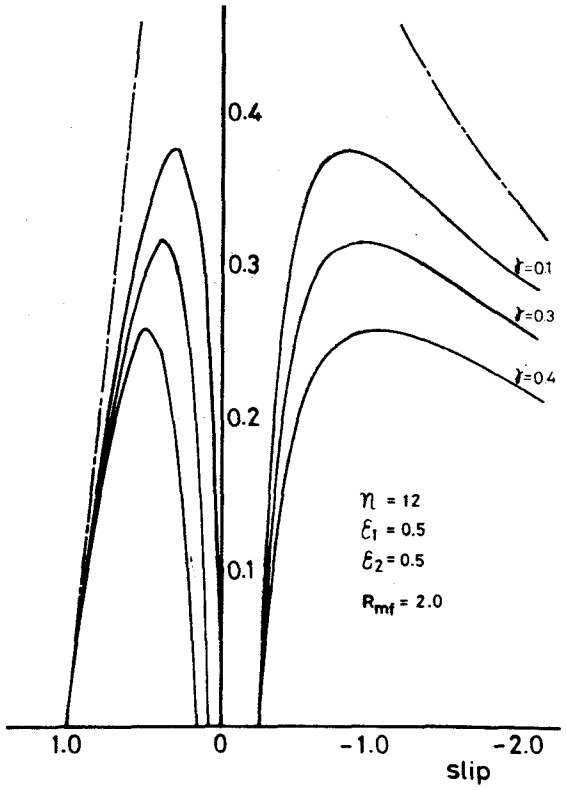

Fig. 3-7 Efficiency of converter operated in constant voltage mode

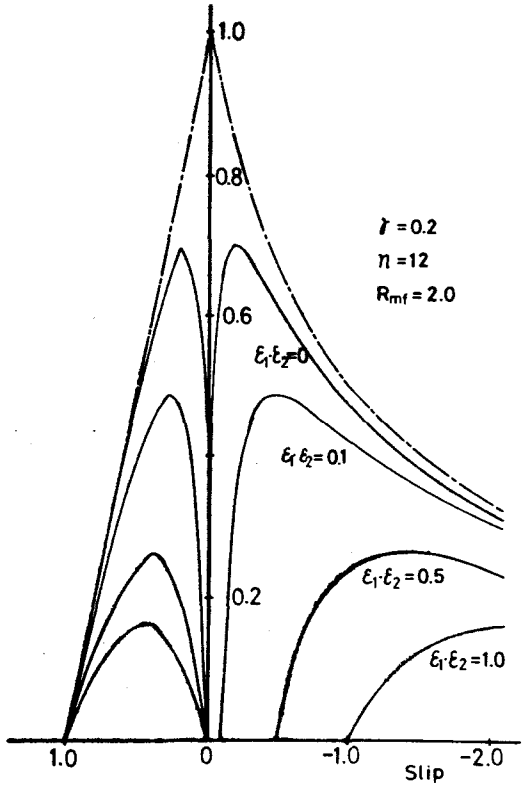

Fig. 3-10 Efficiency of converter operated in constant voltage mode

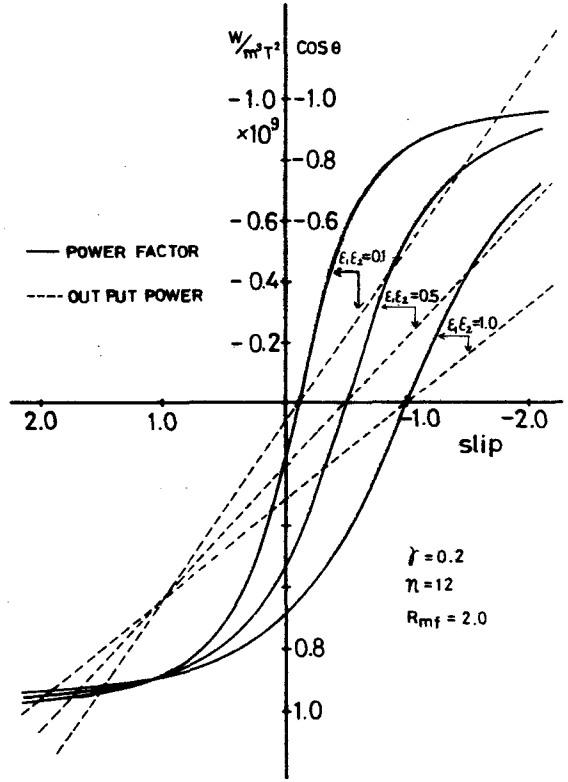

Fig. 3-9 Power factor and gross electrical power per unit volume of converter operated in constant voltage mode

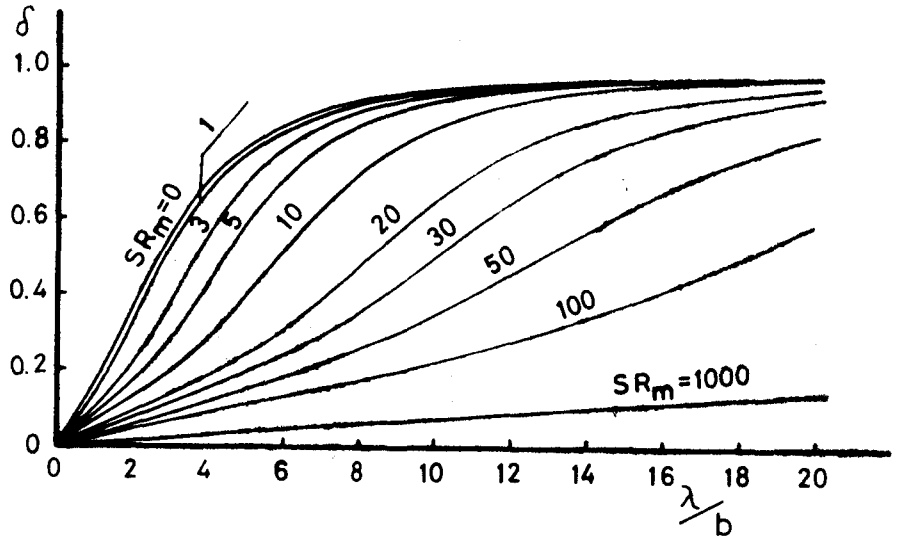

Fig. 3-11-a δ-value given from Eq.(48)

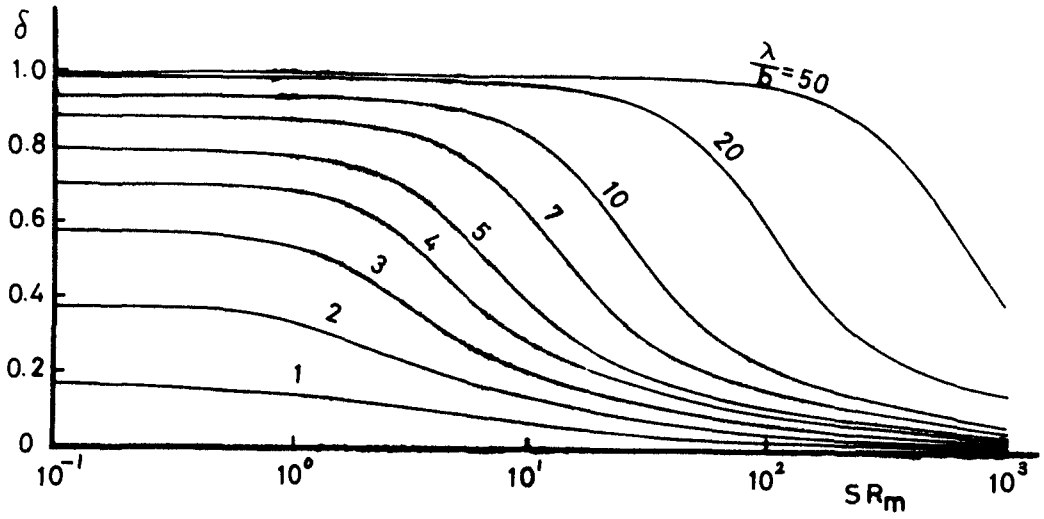

Fig. 3-11-b δ-value given from Eq.(48)

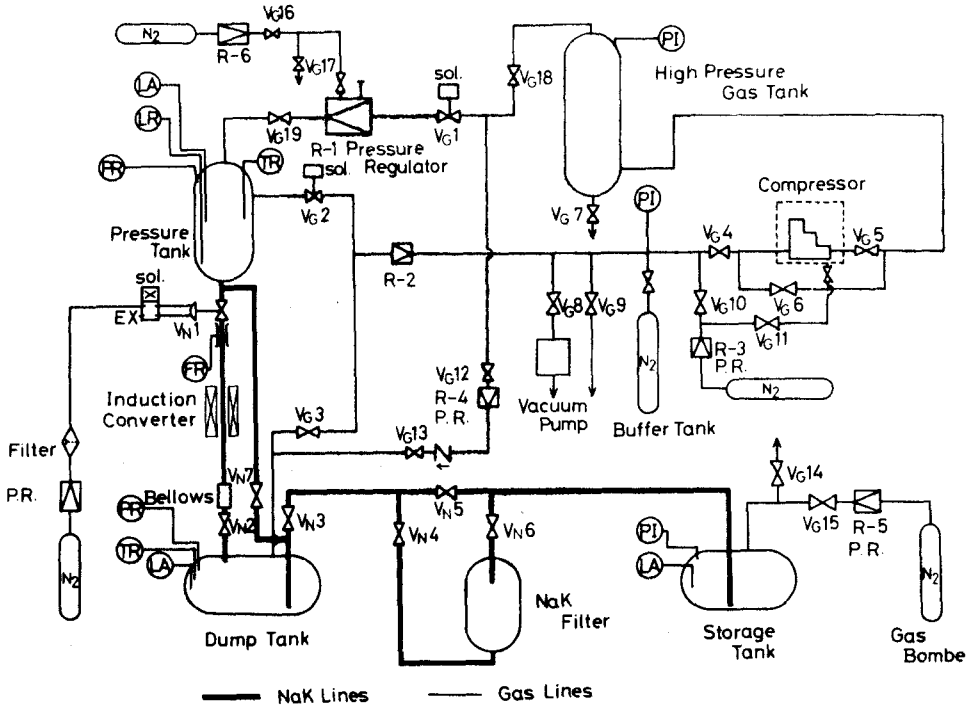

Fig. 3-12 Flow diagram of experimental apparatus

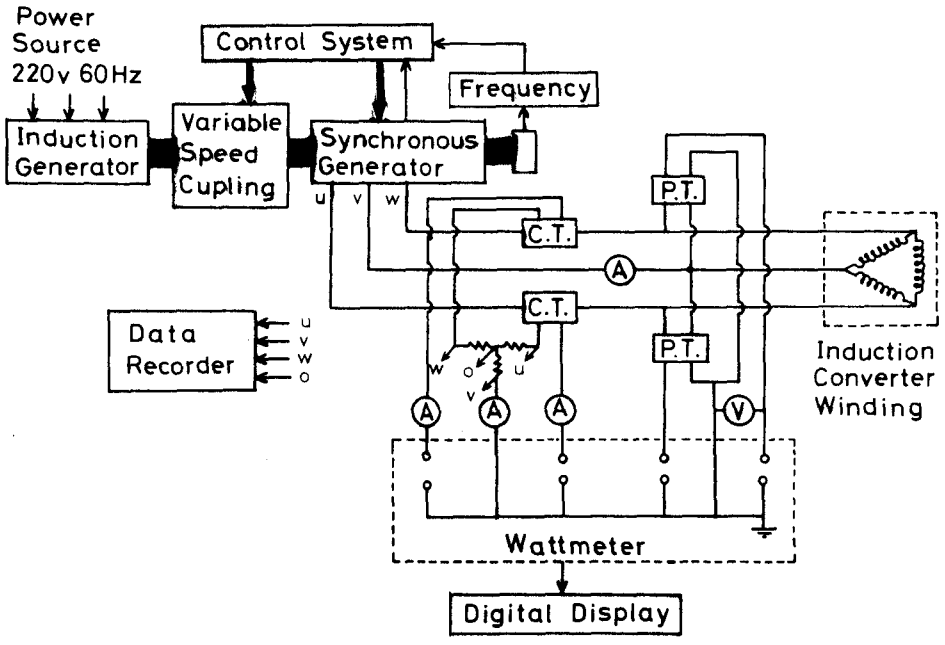

Fig. 3-13 Excitation system for induction converter and electrical measurement system

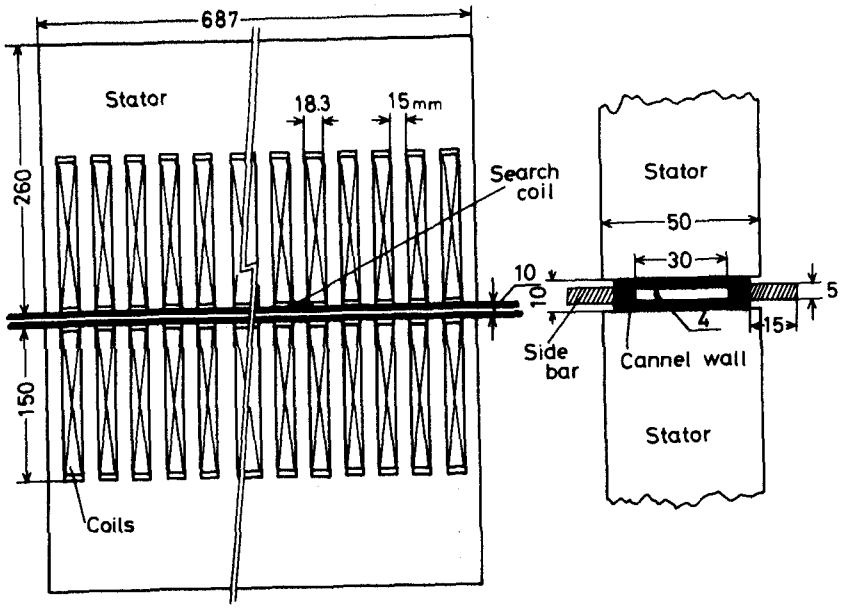

Fig. 3-14 Stators and fluid channel geometry

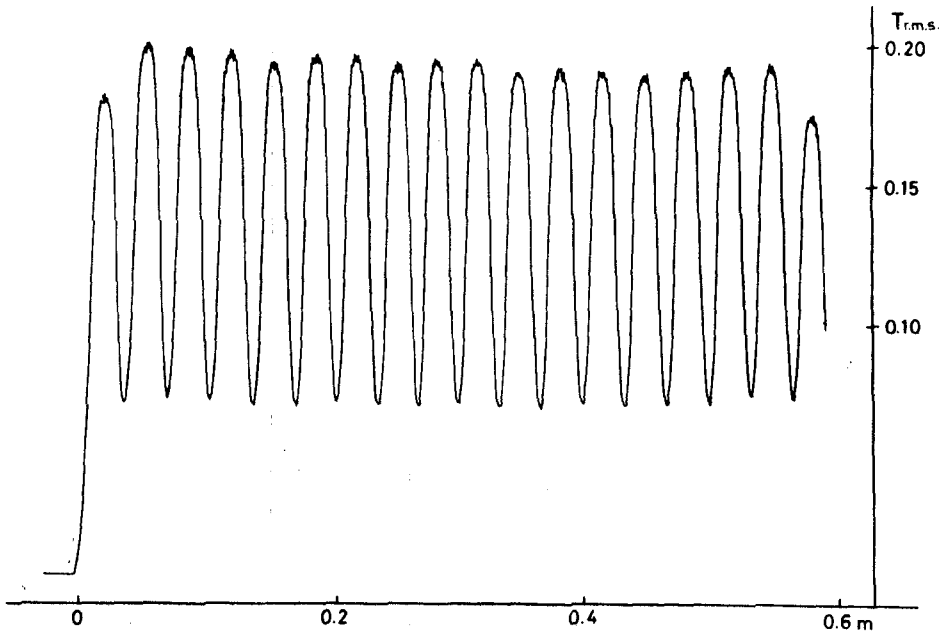

Fig. 3-15 Variation of effective value of traveling magnetic field intensity measured with a Hall-effect type probe

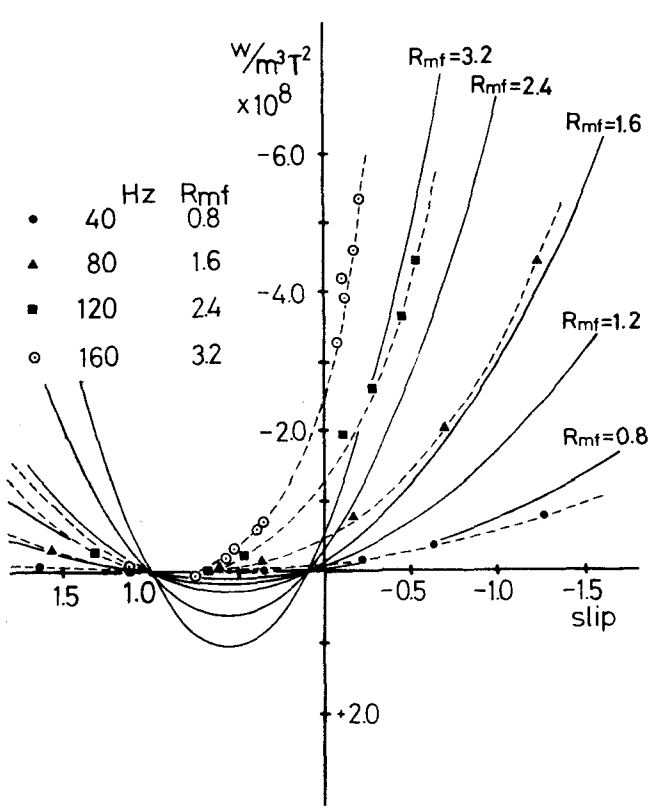

Fig. 3-17 Electromechanical power obtained in experimental converter without copper side bars

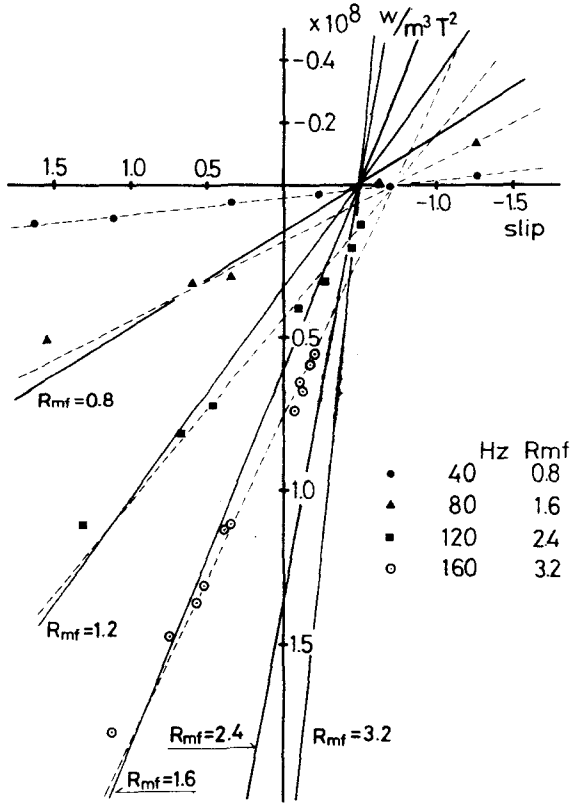

Fig. 3-16 Electrical power obtained in experimental converter without copper side bars

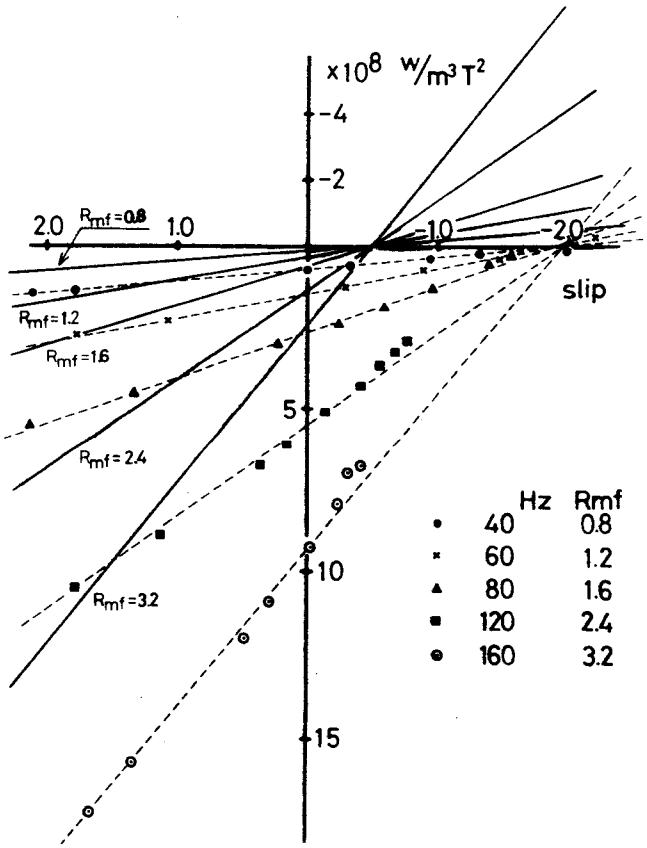

Fig. 3-19 Electrical power obtained in experimental converter with copper side bars

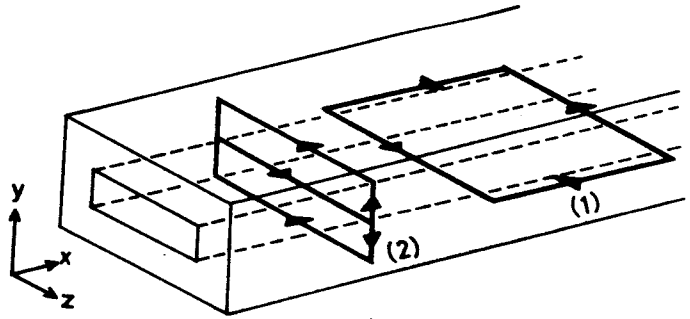

Fig. 3-18 Induced electric current loops within converter channel

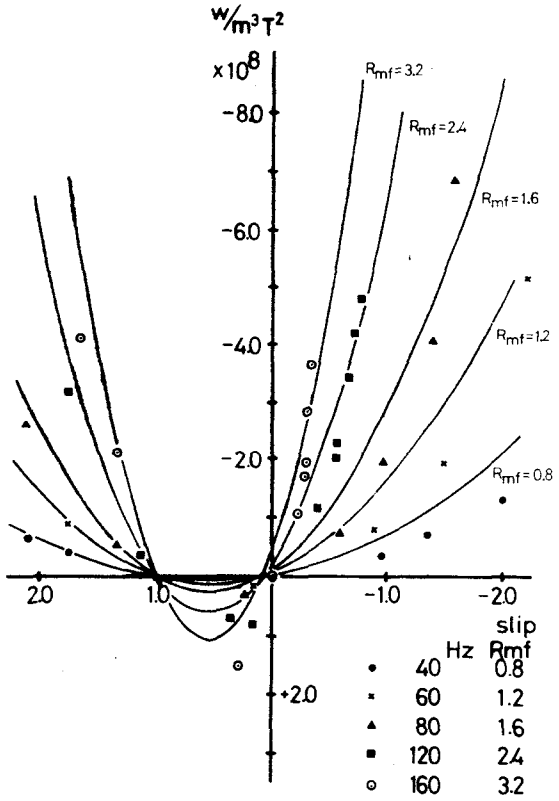

Fig. 3-21 Electromechanical power obtained in experimental converter with copper side bars

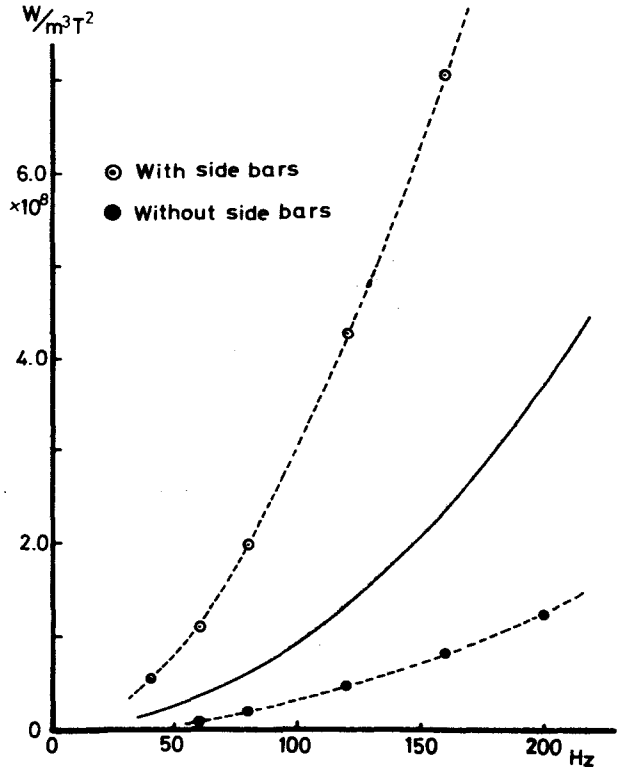

Fig. 3-20 Power losses of converter in empty channel test

Part II

Power Generation Using the Two-Phase Flow as the Working Fluid

Introduction

In the cycle, e.g. Separator and Injector-condenser cycles, in which the liquid metal single-phase working fluid flows through the generator channel, a two-step conversion is required for the conversion of thermal to electrical energy.

That is the conversion of thermal energy of vapor or gas to kinetic energy of liquid metal alone in such conversion unit as separator or injector-condenser and the conversion of kinetic energy of liquid metal to electric energy in the generator.

It has become evident from the analytical and experimental studies that the conversion of thermal of vapor or gas to kinetic energy of liquid alone was difficult to perform efficiently due to the large losses, e.g. friction and especially shock losses, in the separator and injector units.

In order to improve the low conversion efficiency, the Emulsion and Slug flow cycles were proposed in which the intermediate separation and condensation step were eliminated and therefore the accelerated two-phase mixture (homogeneous in the Emulsion and alternating in the Slug flow cycle) passes directly through the generator channel. That is, both the conversion of thermal to kinetic energy and the conversion of kinetic to electrical energy are accomplished simultaneously in the

generator channel.

Thereby the mechanism of energy conversion in the generator becomes very intricate.

Some experiments have been carried out up to date with respect to the correlation of conductivity versus void fraction but a few informetions about other phenomena in the generator using two-phase flow have been obtained.

It is Elliott and Cerini's group alone who operated the induction generator in which the two-phase mixture flowed.

However, the two-phase mixture in their experimental induction generator was produced against their purpose due to the incomplete separation of gas from liquid in the separator.

Slug flow cycle, in which the electrical power can be obtained using a synchronous generator, was proposed recently and experimental work remains to be initiated.

In this part, the liquid metal-gas two-phase flow in bubbly and slug flow regime is treated experimentally using NaK-N_2 two-phase flow system in the flat liner channel.

The frictional pressure drop in two-phase flow is discussed in Chapter 4, the apparent electrical conductivity of two-phase flow in Chapter 5 and the performance characteristics of the induction generator using two-phase flow in Chapter 6.

Chapter 4

Frictional Pressure Drop for NaK-N_2 Two-Phase Flow in Rectangular Cross Section Channel of Large Aspect Ratio

4-1 Introduction

The frictional pressure drop in two-phase flow has in the past been studied analytically and experimentally by many workers with various two-phase mixtures, e.g. air-water, steam-water and different oil-gas combinations. Since the time of Martinelli, the frictional pressure drop in two-phase flow has been discussed in comparison with either the superficial single-phase pressure, obtained by assuming that only one of the two phases is flowing in the channel[1][2][3][4][5][6], or with the actual single-phase pressure drop, obtained by assuming that the total flow is passing through the channel as a single-phase[7].

Such comparison of the frictional pressure drop in a two-phase flow with that in single-phase flow is based on the equivalence of mass flow rate transported in pipes, and thus it is adopted to the estimation of the frictional pressure drop in such two-phase flow systems as liquid-vapor mixtures in boiler tubes and in various refrigeration systems, which are governed by the mass flow rate.

On the other hand, the frictional pressure drop in such two-phase flow systems as liquid metal-vapor or gas mixtures in LM-MHD generator channels, which are governed by the velocity of the liquid, are more appropriately considered in reference to a flow

constituted of the liquid alone flowing with the same velocity as that of the liquid in the two-phase mixture.

In this chapter, the author treats semiempirically the frictional pressure drop in the NaK-N_2 two-phase medium flowing in a rectangular channel with large width-to-height ratio (15:1).

The results obtained are described in reference to the frictional pressure drop in the case of liquid flowing alone with the same velocity as that of the liquid component of the two-phase mixture, and also in reference to similar single-phase flow but with corresponding mass flow rate. Comparison is further made with typical results obtained by other authors.

Data were taken over the following parameter range: NaK velocity, 5 to 30 m/sec; void fraction, 0 to 70 %; density ratio, 0.006 to 0.013; quality, 0.07 to 1.10 %.

4-2 Frictional Pressure Drop in Two-Phase Flow

The frictional pressure drop per unit length of fluid in a rectangular channel, of height a and width b, is given by

$$\frac{\Delta P_f}{\Delta L} = \frac{2(a+b)}{ab} \tau_w , \tag{4-1}$$

where the wall shear stress τ_w is expressed by

$$\tau_w = \frac{1}{2} \zeta \rho u^2, \tag{4-2}$$

using the friction factor ζ know empirically to be related to the Reynolds number by the expression

$$\zeta = \frac{C}{Re^n} , \tag{4-3}$$

where C is a constant which depends only upon the dimensionless wall roughness.

4-2-a Treatment of Two-Phase Mixture as a Continuous Medium

Now the author considers the two-phase mixture as a continuous medium and then defines the density, velocity and viscosity of the two-phase mixture by

$$\rho_t = \alpha \rho_g + (1-\alpha) \rho_l , \tag{4-4}$$

$$u_t = \frac{\dot{M}_l + \dot{M}_g}{\rho_t} = \frac{1 - (1 - S_f \rho_g/\rho_l)\ \alpha}{1 - (1 - \rho_g/\rho_l)\ \alpha} u_l , \tag{4-5}$$

$$\mu_t = \mu_l (1 + K\alpha), \tag{4-6}$$

where the constant K becomes

$$K = \frac{2.5\ \mu_g + \mu_l}{\mu_g + \mu_l} , \tag{4-7}$$

as obtained by Taylor[8], who modified Einstein's expression[9], i.e. K=2.5, obtained by assuming that the gas bubbles behave like solid spheres, taking account of the currents set up inside the spheres.

4-2-b Expression of the Frictional Pressure Drop for Two-Phase Flow in Comparison with That for Single-Phase Flow

Utilizing these properties of the two-phase mixture, the ratio Ru of the frictional pressure drop per unit length between that in the two-phase flow and that in the liquid flowing alone with the same velocity as that of the liquid in the two-phase flow is given from Eqs.(4-1)~(4-3):

$$Ru = \frac{\left(\frac{\Delta P_f}{\Delta L}\right)_t}{\left(\frac{\Delta P_f}{\Delta L}\right)_l} = (1+K\alpha)^n \left\{1 - (1 - \frac{\rho_g}{\rho_l})\ \alpha\right\}^{-1} \left\{1 - (1 - S_f \frac{\rho_g}{\rho_l})\ \alpha\right\}^{2-n} . \quad (4-8)$$

On the other hand, the ratio R_m of the frictional pressure drop per unit length between that in the two-phase flow and that in the liquid flowing alone at the same mass flow rate as that of the liquid in the two-phase flow, which has been adopted to date by many investigators in order to predict the pressure drop in the two-phase flow, is also given from Eqs.(4-1)~(4-3):

$$R_m = \frac{\left(\frac{\Delta P_f}{\Delta L}\right)_t}{\left(\frac{\Delta P_f}{\Delta L}\right)_l} = (1+K\alpha)^n \left\{1 - (1 - \frac{\rho_g}{\rho_l})\ \alpha\right\}^{-1} \left\{1 + S_f \frac{\rho_g}{\rho_l} \frac{\alpha}{1-\alpha}\right\}^{2-n} . \quad (4-9)$$

Figure 4-1 shows the pressure drop ratio Ru as a function of void fraction with both slip S_f and density ratio ρ_g/ρ_l as parameters, using K=1.036 for NaK-N_2 mixture and n=0.228 obtained experimentally for the NaK-N_2 two-phase flow at Reynolds number 10^4~10^5. In this figure is also presented the pressure drop ratio Ru derived from both Martinelli and Nelson's empirical analysis and Bankoff's variable density single-fluid model, which are given in the appendix.

From Fig.4-1, it is seen that the pressure drop ratio Ru can be smaller than unity when the slip and density ratio is smaller, and therefore the frictional pressure drop in the two-phase flow appears to be smaller than that due to the liquid flowing alone with the same velocity as that of the liquid in the two-phase

flow. A similar is also derived from Bankoff's model, which is not the case with the Martinelli and Nelson's analysis. This is due to the fact that Martinelli and Nelson's correlation was originally derived for an annular flow through pipe of circular section, and subsequently was given by the ratio between the pipe diameter and the hydraulic diameter for liquid flow, as described in the appendix.

However, the contribution provided by the gas phase to the frictional pressure drop in the two-phase flow increases with the slip and density ratio, and in particular at large values of slip the frictional pressure drop in the two-phase flow can become several times that due to the liquid flowing alone with the same velocity as that of the liquid in the two-phase flow.

Figure 4-2 shows the pressure drop ratio R_m calculated from Eq. (4-9), together with Martinelli and Nelson's correlation. The present results for R_m can be considered close to Martinelli and Nelson's correlation, when it is considered that their correlation includes the increase of the slip with increasing void fraction.

It should be noted that, in an actual two-phase flow, the relation between slip and the void fraction is radically affected by the flow pattern and flow condition, while the present results are presented as a direct function of the void fraction with the slip as parameter, this being for the purpose of comparison with other properties of the two-phase mixture related to the void fraction, e.g. electrical conductivity of the two-phase mixture in an LM-MHD generator channel.

4-3 Experimental Apparatus

In order to produce the two-phase flow (NaK-N_2), both the test section and the mixing section including the gas injection line belonging to it were installed in the NaK-blow down apparatus described in Chapter 3.

Details of the test section and the mixing section are shown in Fig.4-3. The test section consists of a constant-area, rectangular cross section channel installed between stators, which generate the traveling magnetic field, and which are connected to the mixing section on the upper end through a channel of the same dimension and on the lower end to the circulating loop by a gradually expanding section. The test channel is built up from epoxy resin plates supported by glass wool, with inside dimensions of 4×60 mm^2. The mixing section consists of a perforated channel of rectangular cross section enveloped in a stainless steel tube and which has the same cross section as the test section. In this mixing section, nitrogen gas is introduced into the vertically-flowing NaK (78 w/o potassium, 22 w/o sodium) stream through 120 holes of 0.3 mm diameter spaced uniformly in the rectangular cross section channel wall.

The flow rate of NaK and nitrogen gas were measured by means of an electro-magnetic flow meter installed upstream of the mixing section and an orifice flow meter in the gas injection line respectively. The pressure at the entrance, exit and center of test section were measured by semiconductor pressure transducers. One of these at the center, however, ceased to function properly during the operation.

The void fraction at the entrance and exit of the test section was determined by the gamma-ray attenuation technique[10], the arrangement for which is as shown in Fig.4-3. The gamma ray source was 30 mCi of americium-241 which has a half-life of 458 years, and produces an energy spectrum with a peak at 0.06 Mev.

The gamma beam was applied to the narrow side of channel through the stainless steel tube guide and was collimated by a circular window of 4 mm diameter which was cut in the 2-mm-thick lead shield provided on each side of the channel.

The test section including stators, pressure transducers and all the accessories were enveloped by a stainless steel container, the space left in this container being filled with epoxy resin in order to avoid all NaK-leakage.

4-4 Experimental Results and Discussions

4-4-a Pressure Drop due to the Momentum Change

The pressure drop of a vertical two-phase flow, as shown in Eq. (4-10), consists of four components, i.e. the frictional pressure drop, the elevation pressure drop arising from the effect of the gra-itational force field, the difference between the in and out momentum fluxes, and an unsteady term.

$$\Delta P = \Delta P_f + \frac{1}{A}\iiint \rho g \, dv + \frac{1}{A}\left(\iint \rho u^2 \, dA\right)_1^2 - \frac{1}{A}\frac{\delta}{\delta t}\iiint \rho u \, dv \qquad (4\text{-}10)$$

Both the frictional pressure drop and the pressure drop due to the momentum change become dominant in the present experiment, where the fluid has considerably high velocity and appreciably large momentum change due to the void increase arising from the

large pressure drop.

It is, therefore, necessary to estimate the momentum change in order to obtain the improved data for the frictional pressure drop. Figure 4-4 shows the ratio β of the momentum flux $\rho_t u_t^2$ calculated with Eqs.(4-4) and (4-5) to the measured momentum flux as a function of void fraction. The momentum flux was measured by the equipment shown in Fig.4-5.

It is seen from Fig.4-4 that the ratio β becomes unity below 20 percent void fraction and then decreases suddenly near 20 percent void. This tendency can be seen in the electrical conductivity of two-phase flow to be mentioned in the next chapter and seems to be caused by the transition of flow pattern.

In obtaining the frictional pressure drop in NaK-N_2 two-phase flow, account was taken of the pressure decrease due to the difference between the momentum fluxes at the entrance and exit of the test channel which was calculated with the correlation shown in Fig.4-4.

4-4-b Friction Factor for NaK-N_2 Two-Phase Flow

The friction factor was obtained experimentally on both NaK and NaK-N_2 flow, in the range of velocity of 5$\sim$30 m/sec.

The result is presented in Fig.4-6 as function of the Reynolds number Re based on the height of the channel, and defined with the properties given by Eqs.(4-4), (4-5) and (4-6) for the NaK-N_2 two-phase mixture.

The following empirical expression was obtained for the friction factor

$$\zeta = 0.129\ Re^{-0.228}, \qquad (4\text{-}11)$$

which is shown by the dot-dash-line in Fig.4-6.

Martinelli had used a value of 0.2 for the exponent n in his analysis of the turbulent flow in a range of Reynolds number from 5×10^3 to 2×10^5[1][3], later Bankoff proposed n=0.25 for turbulent flow of the Reynolds number up to 10^5 by Blasius[7].

In the range of void fraction below 20 percent, the coefficient C of the friction factor obtained for the NaK-N_2 two-phase flow showed a tendency to be larger than that of the NaK flow alone, while above 20 percent void, the coefficient became smaller. It means that, below 20 percent void, the channel wall becomes virtually rougher for the two-phase flow than for NaK flow alone, and vice versa.

This change of the friction factor near the void fraction of 20 percent seems to have its origin in the transition from bubbly flow to slug flow, which was verified from a comparison of the measured electrical conductivity of NaK-N_2 two-phase flow with that of Hg-H_2O mixture in a transparent rectangular channel to permit visual observation (see Chapter 5). Further detailed experiments, however, are required in order to deal with this phenomenon qualitatively.

It should be noted that the friction factor in the presence of a transeverse magnetic field increases with the ratio between Hartmann and Reynolds numbers. In particular, in the transition from turbulent to laminar flow occasioned by magnetically induced force, the friction factor increases in propotion with 2(Ha/Re)[11][12].

The Ha/Re ratio for this transition was reported to be 1/225 by Brouillette and Lykoudis[11][12] and about 1/1000 by Michiyoshi and Nakura[13] for single-phase mercury flow.

4-4-c Empirical Correlation of Frictional Pressure Drop in NaK-N_2 Two-Phase Flow

The ratio of frictional pressure drop between that in NaK-N_2 two-phase flow and that in NaK flowing alone at the same velocity as that of the NaK in the two-phase flow is shown in Fig.4-7 as function of void fraction averaged along the test channel.

In this figure, both the theoretical value derived from Bankoff's model and the predicted value derived from Martinelli and Nelson's empirical results are shown together with the predicted value given by Eq.(4-8), where a value of 0.01 is taken for the density ratio and 1.0 for the slip. The basis for adopting these values in the present experiment is that the density ratio was in the range of 0.006～0.013 and the slip in the range of 0.9 1.3, as shown in Fig.4-8, in which the solid lines represent the slip ratios of 0.9, 1.0, 1.5 and 2.0, as determined from the conservation of mass relation

$$S_f = \frac{\chi}{1-\chi}\,\frac{1-\alpha}{\alpha}\,\frac{\rho_l}{\rho_g} . \qquad (4\text{-}12)$$

Figure 4-9 shows the ratio of frictional pressure drop between that in NaK-N_2 two-phase flow and that in NaK flowing alone at the same mass flow rate as that of NaK in the two-phase flow.

In this figure the theoretical results given by Bankoff[7] and

Levy and Marchaterre[4][5] for the homogeneous two-phase flow and the empirical results given by Martinelli and Nelson[1][2] and Inoue and Aoki[6] for the annular two-phase flow are shown together with the predicted value given by Eq.(4-9).

It is of interest to note that the results obtained in the past for the two-phase flow in pipe agree approximately with the present results, which pertain to high velocity liquid metal two-phase flow in a rectangular channel with large width-to-height ratio. Above 50 percent void fraction, however, the experimental results fall below the predicted values except those by Levy and Marchaterre.

4-5 Concluding Remarks

In a two-phase system composed of liquid metal mixed with vapor or with gas in a liquid metal MHD generator channel, which is affected significantly by the velocity of the liquid, the frictional pressure drop in the two-phase flow should be considered in reference to that of the liquid flowing alone at the same velocity and not at the same mass flow rate as that of the liquid in the two-phase flow, in order to clarify the difference in performance characteristics between that in the liquid flow alone and that in the two-phase flow system.

Based on semiempirical analysis assuming the two-phase mixture to be a continuous medium, the author has determined the friction factor as a function of Reynolds number with NaK-N_2 two-phase flow in the rectangular channel. The resulting coefficient of friction factor was found to be larger than single-phase NaK flow in

the case of bubbly flow and smaller in the case of slug flow.

Measurement of electrical conductivity in the NaK-N_2 two-phase flow revealed that the transition from bubbly flow to slug flow took place near the void fraction of 20 percent.

From the present semiempirical analysis, the frictional pressure drop in the two-phase flow appears to be smaller than that in a corresponding single-phase flow of the same velocity as that of the liquid in the two-phase flow in the range of small slip and small density ratio, where the contribution of the gas to the frictional pressure drop is not dominant.

The frictional pressure drop for NaK-N_2 two-phase flow obtained in comparison with that for a corresponding single-phase NaK flow of the same mass flow rate as that of the NaK in the two-phase flow agreed approximately with the results obtained by Martinelli and Nelson, Bankoff, Levy and Marchaterre, and Inoue and Aoki.

This agreement is rather unexpected, when it is considered that the present experiment was performed with a high-velocity liquid metal-gas two-phase flow in a rectangular channel with large width-to-height ratio (15:1).

Nomenclature

ρ : Density of fluid

μ : Viscosity of fluid

α : Void fraction

χ : Quality = $\dot{M}_g/(\dot{M}_g + \dot{M}_l)$

u : Velocity of fluid

$\dot{M}$: Mass flow rate per unit area

Re : Reynolds number

Ha : Hartmann number

L : Length in the direction of fluid flow

S_f : Slip = u_g/u_l

Subscripts

g : Gas phase

l : Liquid phase

t : Two-phase

Appendix

The Ratio of Frictional Pressure Drop between That in Two-Phase Flow and That in a Single-Phase Liquid Flow of the Same Velocity as That of the Liquid in the Two-Phase Flow

[1] Derivation from Martinelli's empirical analysis[1][2]

The two-phase frictional pressure drop is given by

$$\left(\frac{\Delta P_f}{\Delta L}\right)_t = C_1\left(\frac{\mu_1}{\rho_1 D_1 u_1}\right)^n \frac{\rho_1}{D_1}\frac{u_1^2}{2}$$

$$= C_1\left[\frac{\mu_1^n}{2\,\rho_1^{n-1}}\frac{u_1^{2-n}}{D_p^{1+n}}\right]\left(\frac{D_p}{D_1}\right)^{1+n}$$

$$= \left(\frac{\Delta P_f}{\Delta L}\right)_1\left(\frac{D_p}{D_1}\right)^{1+n} \qquad \text{(A1)}$$

The first term in Eq.(A1) represents the pressure drop for the liquid phase flowing alone with the liquid velocity u_1, in a pipe of diameter D_p. The ratio between the pipe diameter and the hydraulic diameter D_1 for liquid flow is given by

$$\left(\frac{D_p}{D_1}\right)=\left[\left(\frac{\rho_g}{\rho_1}\right)^{\frac{2}{n-5}}\left(\frac{\mu_1}{\mu_g}\right)^{\frac{2n}{n-5}}\left(\frac{\dot{M}_g}{\dot{M}_1}\right)^{\frac{2(n-2)}{n-5}}\alpha^{*\,\frac{2(n-5)}{n-5}} + \alpha^*\right]^{1/2} \qquad \text{(A2)}$$

For a turbulent flow of liquid-gas two-phase flow, n=0.2 is utilized, and α^* is determined as an empirical function of $\sqrt{\chi_{tt}}$ as given by Martinelli.

The resulting expression for Ru is

$$Ru = \left[\left(\frac{\alpha^*}{X_{tt}}\right)^{0.75} + \alpha^*\right]^{0.6} , \tag{A3}$$

where

$$X_{tt} = \left(\frac{\mu_l}{\mu_g}\right)^{0.111} \left(\frac{\rho_g}{\rho_l}\right)^{0.555} \left(\frac{\dot{M}_l}{\dot{M}_g}\right) . \tag{A4}$$

[2] Derivation from Bankoff's variable density single-fluid model[7]

The ratio of frictional pressure drop between that in two-phase flow and that in a single-phase liquid flow is given by

$$\frac{\left(\frac{\Delta P_f}{\Delta L}\right)_t}{\left(\frac{\Delta P_f}{\Delta L}\right)_l} = \left(\frac{\bar{\rho}}{\rho_l}\right)^{3/4} \left(\frac{\bar{u}}{\bar{u}_l}\right)^{7/4} \left(\frac{\bar{\mu}}{\mu_l}\right)^{1/4} \tag{A5}$$

where $\bar{\rho}/\rho_l = 1 - \bar{\alpha}(1 - \rho_g/\rho_l)$ and a value of unity has been taken for $\bar{\mu}/\mu_l$ by Bankoff and the superscript ($\bar{}$) denotes the average value

From the condition that the liquid velocity be equal in the two-phase and liquid-phase systems, it follows that

$$\frac{\bar{u}}{\bar{u}_l} = 1 + (S_f - 1)\,\bar{\alpha} . \tag{A6}$$

The resulting expression for Ru is

$$Ru = \left\{1 - \bar{\alpha}\,(1 - \rho_g/\rho_l)\right\}^{3/4} \left\{1 + (S_f - 1)\,\bar{\alpha}\right\}^{7/4} \tag{A7}$$

References

(1) Martinelli, R.C., et al. : Trans. ASME, 66, 139-151 (1944).

(2) Martinelli, R.C., Nelson, D.B. : ibid., 70, 695-702 (1948).

(3) Lockhart, R.W., Martinelli, R.C. : Chem. Eng. Prog., 45[1], 39-48 (1949).

(4) Levy, S. : Journal of Heat Transfer Trans. ASME, Series C, 82, 113-123 (1960).

(5) Marchaterre, J.F. : ibid., 83, 503-504 (1961).

(6) Inoue, A., Aoki, S. : Japan Soc. Mech. Eng., (in Japanese), 36[288], 1366-1373 (1970).

(7) Bankoff, S.G. : Journal of Heat Transfer Trans. ASME, Series C, 82, 265-272 (1960).

(8) Taylor, G.I. : Proc. Roy. Soc., A138, 41-48 (1932).

(9) Einstein, A. : Ann. Phys., 4[19], 289-306 (1906).

(10) Petrick, M., Swanson, B.S. : Rev. Sci. Instrum., 29[12], 1079-1084 (1958).

(11) Brouillette, E.C., Lykoudis, P.S. : Phys. Fluids, 10[5], 995-1001 (1967).

(12) Brouillette, E.C., Lykoudis, P.S. : ibid., 10[5], 1002-1007 (1967).

(13) Michiyoshi, I., Nakura, S. : J. Nucl. Sci. Technol., 9[8], 490-496 (1972).

The contents of this chapter are to be published in Journal of Nuclear Science and Technology, Vol. 10, No. 4, April 1973.

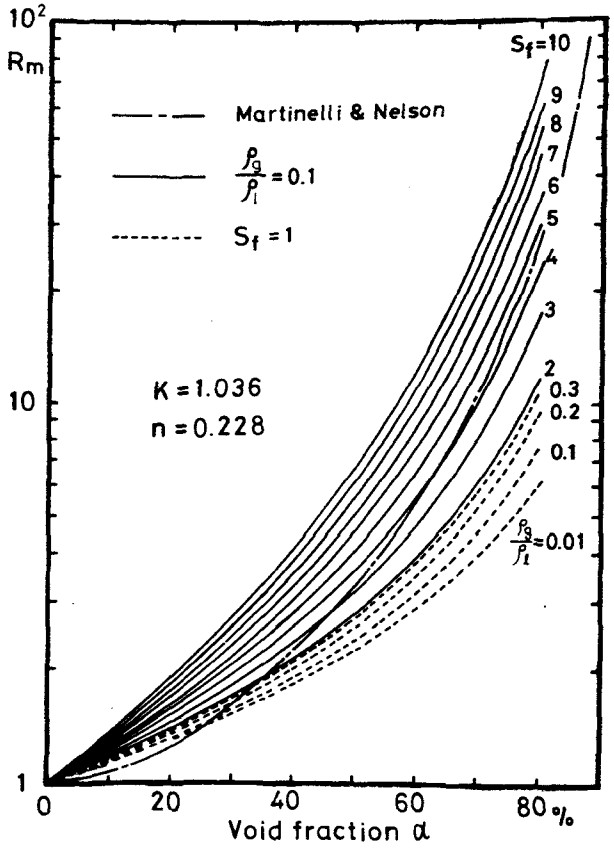

Fig. 4-2 Frictional pressure drop ratio Rm obtained from semiempirical analysis for NaK-N_2 two-phase flow

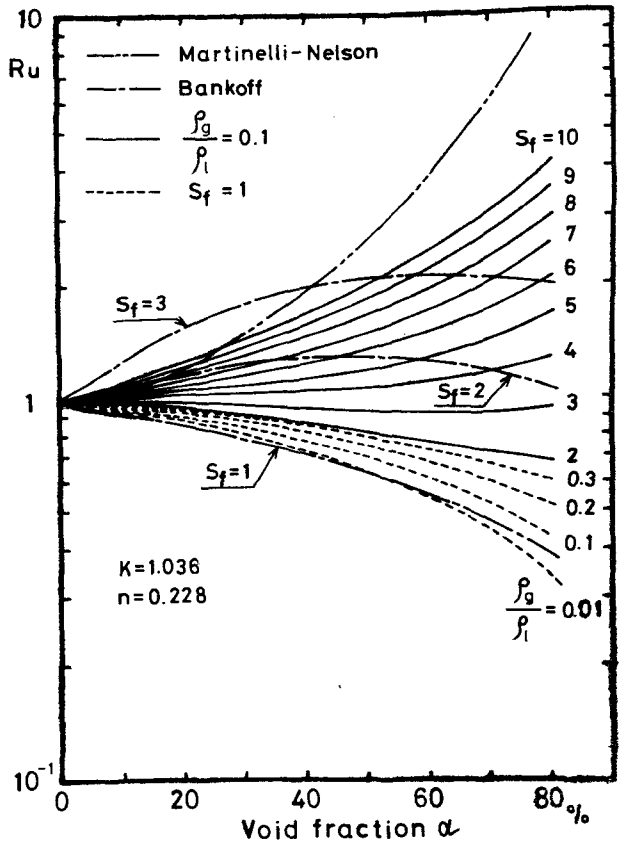

Fig. 4-1 Frictional pressure drop ratio Ru obtained from semiempirical analysis for NaK-N_2 two-phase flow

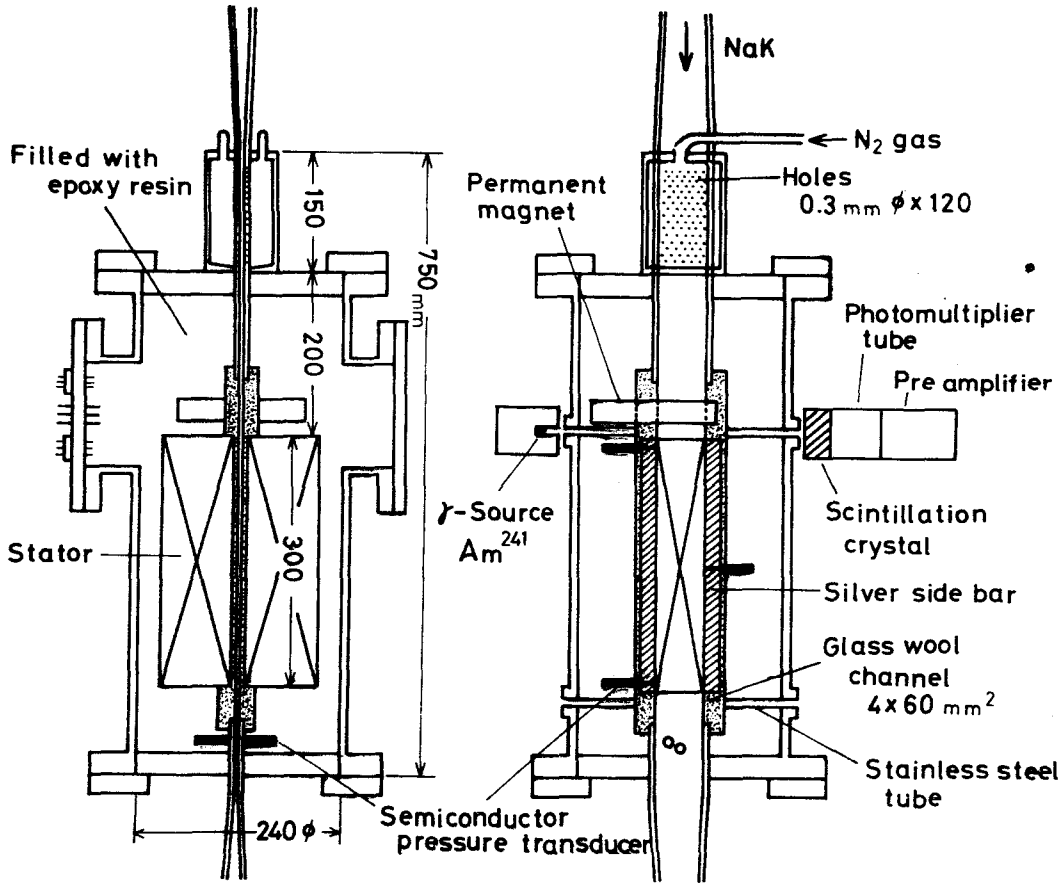

Fig. 4-3 Schematic diagram of test section and mixing section; setup for measurements

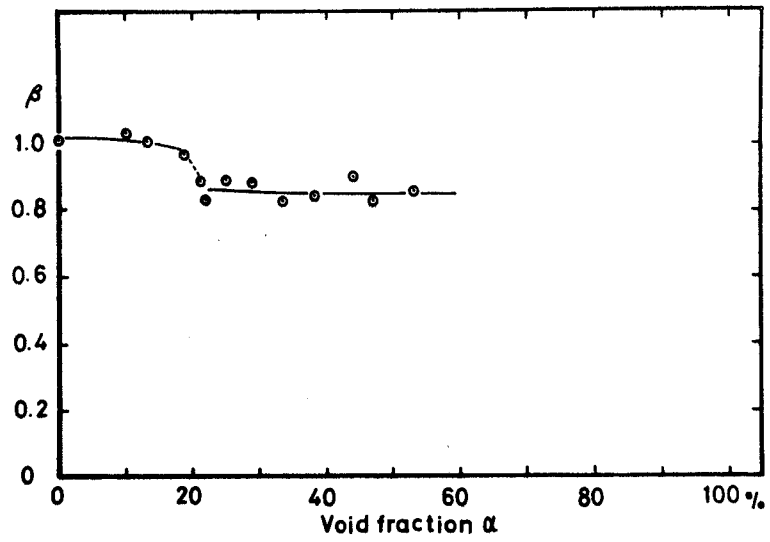

Fig. 4-4 β-value

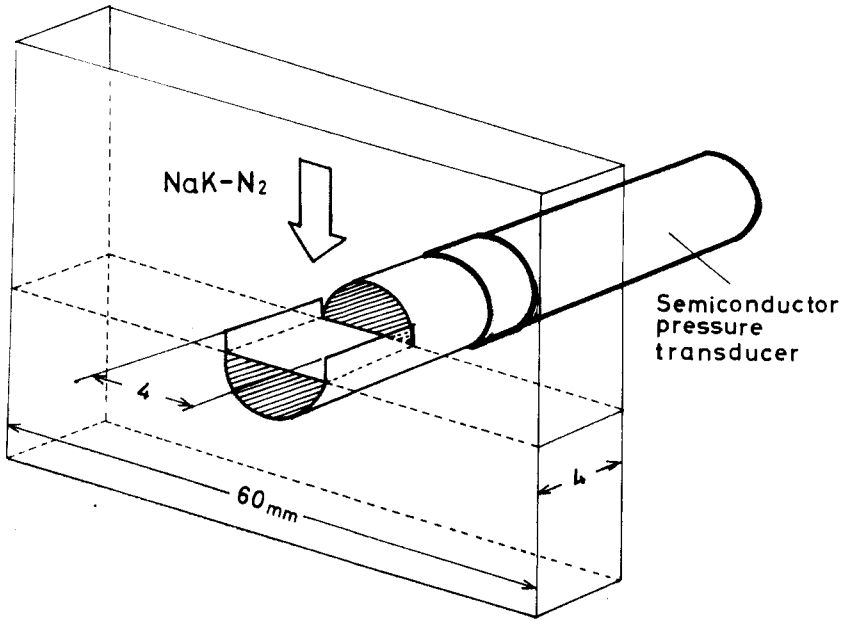

Fig. 4-5 Equipment for momentum flux measurement

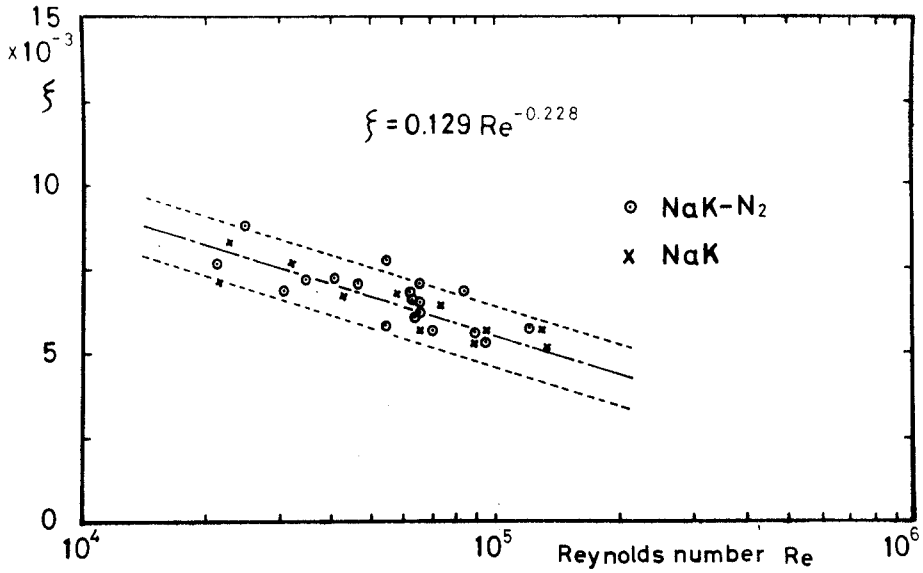

Fig. 4-6 Measured friction factor for NaK-N_2 two-phase flow and for NaK flow alone

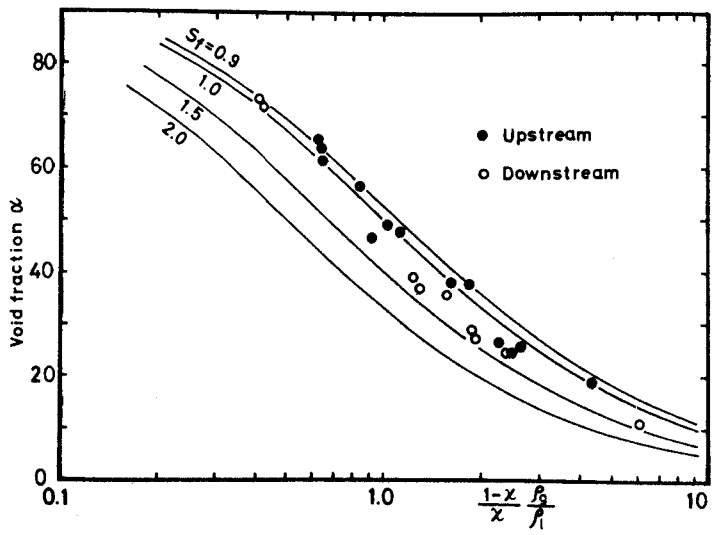

Fig. 4-8 Slip between velocity of nitrogen and NaK obtained from conservation of mass law, with void fraction, quality and density ratio obtained experimentally

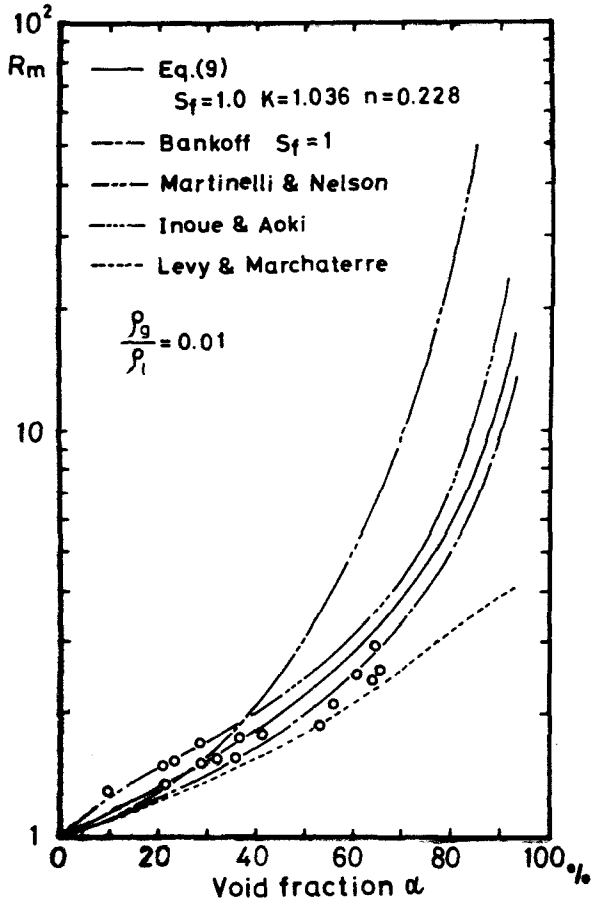

Fig. 4-9 Experimentally obtained frictional pressure drop ratio Rm

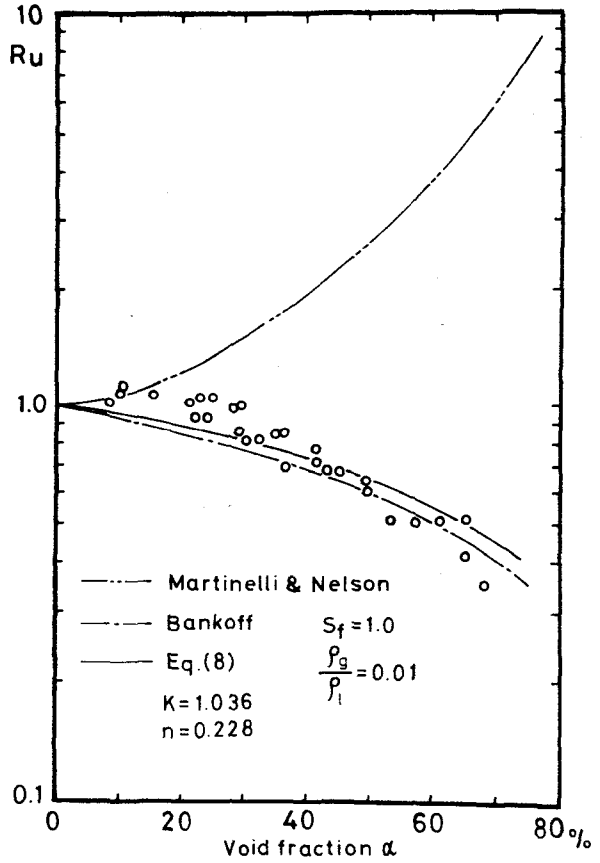

Fig. 4-7 Experimentally obtained frictional pressure drop ratio Ru

Chapter 5

Apparent Electrical Conductivity of Liquid Metal-Gas Two-Phase Mixture

5-1 Introduction

The performance characteristics of generator using liquid metal-vapor or gas two-phase flow as a working fluid depends significantly on the apparent electrical conductivity of the two-phase mixture, which decreases usually with increasing void fraction.

The correlation of electrical conductivity of two-phase mixture versus void fraction has been given theoretically by Maxwell[1] and Potter and Grossman[2], and also obtained experimentally by Petrick[3], Elliott[4] and other several workers. The results obtained by them do not, however, consist satisfactory with each other due to the difference in the fluid, the flow condition and the method of measurement.

In this chapter are treated the apparent electrical conductivity of a two-phase mixture determined experimentally in bubbly and slug flow regimes in its passage through a rectangular cross section channel of large width-to-height ratio (15:1), as is usual in LM-MHD generators.

The measurements were carried out with the water-nitrogen gas mixture in the static electric field, the NaK-nitrogen gas mixture in the static magnetic field and the NaK-nitrogen gas and the mercury-water mixtures in the traveling magnetic field.

5-2 Previous Results Obtained by Other Authors

Maxwell gives theoretically the following expression for the electrical conductivity of a compound medium

$$\sigma = \frac{2\sigma_2 + \sigma_1 - 2\alpha(\sigma_2 - \sigma_1)}{2\sigma_2 + \sigma_1 + \alpha(\sigma_2 - \sigma_1)} \sigma_2 \qquad (5\text{-}1)$$

Here, it is assumed that small spheres with conductivity σ_1 are dispersed in a medium of conductivity σ_2 at such distances from each other that their effect of disturbing the course of the current may be considered independent of each other[1], and therefore Eq.(5-1) is restricted to small values of void fraction. If the gas bubbles are assumed to be solid spheres with zero conductivity, we obtained from Maxwell's equation the ratio σ_t/σ_1 of electrical conductivity between that of a two-phase mixture and that of the liquid alone

$$\sigma_t/\sigma_1 = 2(1-\alpha)/(2+\alpha) \ . \qquad (5\text{-}2)$$

Potter and Grossman[2] solved the conductivity of the medium interrupted by voids, assuming that the medium occupies the volume of a right parallelepiped (rectangle) with a pair of opposite sides being ideal conductors and having an external voltage applied across them; the other sides being insulated.

The method of solution used in their work is to associate an abstract random walk with the physical process and then to use the standard techniques of stochastic processes to calculate the conductivity. In particular, if the voids are cubes (squares) with their sides parallel to the sides of the right parallelepiped (rectangle), and if the voids are uniformly

distributed in those directions that are perpendicular to the direction of conduction, then an approximate solution for the conductivity of the medium is derived:

$$\sigma_t/\sigma_1 = (1 - \alpha)^{6/5} \tag{5-3}$$

Petrick and Lee obtained the empirical expression[3]:

$$\sigma_t/\sigma_1 = \exp(-3.8\ \alpha), \tag{5-4}$$

which was obtained from their experiment on a NaK-N_2 mixture in a Faraday generator operated under both open and closed circuits.

Elliott obtained experimentally the expression for the conductivity of two-phase mixture:

$$\sigma_t/\sigma_1 = (1-\alpha)^{1.6} \tag{5-5}$$

which was obtained by passing DC current through a flowing NaK-N_2 mixture[4].

Lafferty and Hammitt have used the following expression for measuring local void fraction in air-water two-phase flow:

$$\sigma_t/\sigma_1 = 1-\alpha \tag{5-6}$$

which was obtained by assuming the electrical conductivity of the air-water mixture depends on the ion density of the mixture[5].

5-3 Experimental Procedure

The NaK-N_2 mixture flow was passed through an electrically non-conducting, rectangular cross section channel made from epoxy resin, at a velocity in the range of 5~30 m/sec.

The stationary Hg-H_2O mixture and flowing H_2O-N_2 mixture (velocity up to 10 m/sec) were observed in a transparent, rectangular cross section channel of lucite, which permitted visual obsevation of the flow pattern.

Both the static and the traveling magnetic field were applied to the wide side of channel wall (see Fig.4-3 of Chapter 4), and then the static electric field to the narrow side of channel wall.

The values correspond to the electric current in the two-phase mixture was measured in order to obtain the conductivity of two-phase mixture when the static electric and magnetic fields were applied, and then the output power when the traveling magnetic field was applied.

The void fraction α in both NaK-N_2 and H_2O-N_2 mixtures was determined with the γ-ray attenuation technique, and that in the Hg-H_2O mixture was estimated from the volume of mercury in the channel.

5-4 Experimental Results and Discussions

Figure 5-1 shows the conductivity ratio $\sigma t/\sigma_1$ as determined experimentally on the following mixtures;

(1) NaK-N_2 mixture in traveling magnetic field

(2) NaK-N_2 mixture in static magnetic field

(3) Hg-H_2O mixture in traveling magnetic field

(4) H_2O-N_2 mixture in static electric field

In this figure, the chain line represents Maxwell's theoretical value, the solid line Petrick and Lee's empirical expression and

the broken line (1-α) respectively.

It is seen from Fig.5-1 that the experimental values for the H_2O-N_2 mixture are higher than for the NaK-N_2 and Hg-H_2O mixtures, and fall slightly above the theoretical value given by Maxwell. A similar tendency is also seen in the experimental results for air-water mixture obtained by Petrick and Lee[6], who reported good agreement of their data with the Maxwell's theoretical value for void fractions up to 95%, despite the low void fraction applicable in Maxwell's theory.

This may be attributed to the difference in electric current conduction between liquid metal and water, which latter is a week electrolyte.

5-4-a Relation of the Electrical Conductivity to the Flow Pattern

The present experimental values for NaK-N_2 and Hg-H_2O mixtures are close to Maxwell's theoretical value below about 20% void fraction, beyond which point the conductivity decreases sharply.

It was verified from visual observation of the Hg-H_2O mixture that this sudden decrease was due to transition from bubbly to slug flow.

The experimental values for Hg-H_2O mixture appear to be lower than for NaK-N_2 mixture above 20% void fraction on account of a more complete establishment of the slug flow regime in the Hg-H_2O than in the NaK-N_2 mixture, judging from the difference of wetting ability between Hg and NaK-78.

Since the experiment on NaK-N_2 mixture performed by Petrick

and Lee lacks data under 20% void fraction, the sudden decrease of electrical conductivity due to the transition from bubbly to slug flow is not apparent. A spot value is, however, given for 15% void fraction, which appears to indicate this tendency to some extent.

5-5 Concluding Remarks

The electrical conductivity ratio of liquid metal-gas two-phase mixture agrees well with Maxwell's theoretical value in bubbly flow regime, and decreases suddenly upon transition from bubbly to slug flow regime.

The electrical conductivity ratio of a week electrolyte-gas two-phase mixture agrees well with Maxwell's theoretical value or $(1-\alpha)$ up to considerably higher void fractions, and differs from that for liquid metal-gas two-phase flow mixtures.

References

(1) Maxwell, J.C. : "A Treatise on Electricity and Magnetism", 435 441(1904), Oxford Univ. Press.

(2) Potter, W.E. and Grossman, L.M. : J. Appl. Mathe. Phys., 22[3], 621 629 (1971).

(3) Petrick, M. and Lee, K.Y. : Proc. 2nd Int. Symp. MHD Elect. Power Gen., Paris, Vol. 2, (1964).

(4) Elliott, D.G., Hays, L.G., Cerini, D.J. and Bogdanoff, D.W. Fifth Intersociety Energy Conversion Engineering Conference, September 1970, AIAA, New York.

(5) Lafferty, J.F. and Hammitt, F.G. : Nucl. Appl., 3[5], 317 323 (1967).

(6) Petrick, M. and Lee, K.Y. : ANL-6954, (1965).

The contents of this chapter are presented in Journal of Nuclear Science and Technology, Vol. 9, No. 12, pp. 753 755, December 1972.

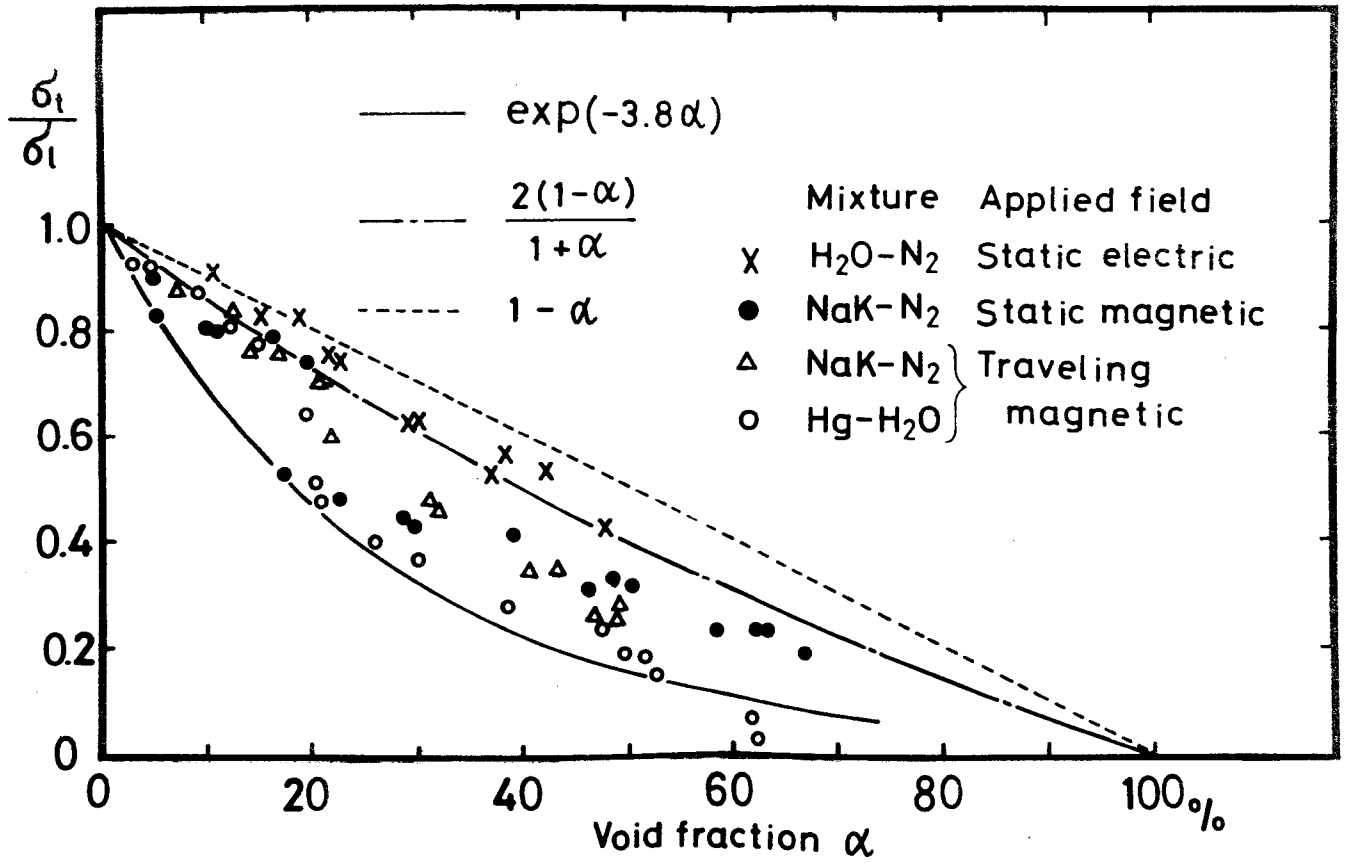

Fig. 5-1 Ratio of electrical conductivity of two-phase mixture to that of liquid alone

Chapter 6

Performance Characteristics of MHD Induction Generator Using The Two-Phase Flow

6-1 Introduction

In this chapter, the performance characteristics of the induction converter using the two-phase mixture flow are treated experimentally and analytically in comparison with those using the single-phase liquid flow as a working fluid.

The experiments have been performed with the flat-linear channel induction converter, through which NaK-N_2 two-phase mixture flowed at a velocity in the range of 5~30 m/sec.

The electrical output power of the experimental generator showed the sudden decrease near 20 percent void fraction due to the change of flow pattern, while the generator efficiency has not showed such tendency and decreased gradually with increasing the void fraction.

Coupling the electro-magnetic equations with the power law distribution for both velocity and void fraction proposed by Bankoff[1] and using the correlation of the electrical conductivity of two-phase mixture versus void fraction given by Maxwell (see Eq.(5-2) of Chapter 5), the author has solved numerically the performance characteristics of the induction converter using two-phase flow and explained well the results obtained experimentally.

6-2 Experiment

The author has performed experiments with an induction converter through which channel the NaK flowed in single-phase and also the NaK-N_2 mixture in two-phase at a velocity in the range of 5～30 m/sec. In Fig.4-3 of Chapter 4 are shown the experimental apparatus and the arrangement for the measurement of void fraction by the gamma-ray attenuation technique.

The converter channel has the rectangular cross section with inside dimensions of 4×60 mm^2 and is built up from electrically non-conducting epoxy resin plates supported by glass wool.

Figure 6-1 shows the stators to generate the traveling magnetic field and the fluid channel geometry.

The excitation system for the induction converter and the measuring system are shown in Fig.3-13 of Chapter 3.

The stators were made with 0.35 mm thick iron laminations with one slot per pole per phase, and the wave length of traveling wave 0.1 m. The three phase windings are concentrated, with 28 turns/tooth/phase. The maximum magnetic field intensity is 0.13 tesla in r.m.s. at the center of air gap.

Data were taken over the following parameter range: void fraction, 0 to 55 %; quality, 0 to 1.0 %.

6-3 Experimental Results

6-3-a Performance Characteristics of the Experimental Converter Operated with NaK Flow in Single-Phase as Working Fluid

The electrical power and the electro-mechanical power versus slip ratio (defined from Eq.(3-21) of Chapter 3) obtained experi-

mentally are shown in Fig.6-2, together with the theoretical values given from Eqs.(3-41) and (3-42) which are indicated by solid lines. The applied magnetic field is 0.1 tesla in r.m.s. and the stator windings are excited at 120 Hz which corresponds to the wave velocity of 12 m/sec in the present converter. As is evident from Fig.6-2, both powers obtained experimentally are lower than the theoretical values.

One of the reason for which is the eddy current loss induced in the silver side bars which was equipped in the each side of channel in order to establish the electric current loop in the fluid.

Figure 6-3 shows the generator efficiency obtained experimentally and the ideal one given from $\eta_{gl}=(1-s)^{-1}$ which is indicated by solid line.

It is seen from Figs.6-2 and -3 that the converter does not act as generator at values of slip between 0 and -0.4 due to the loss mensioned above.

6-3-b Performance Characteristics of The Experimental Converter Operated with NaK-N_2 Two-Phase Flow in Comparison with That with NaK Single-Phase Flow

In Fig.6-4, the ratio between the electrical power obtained with NaK-N_2 mixture and that with NaK flow alone are plotted as a function of bulk void fraction. In order to improve the accuracy of experiment, the author adopted the data for the average slip $\bar{s} = (\bar{u}_1 - u_w)/u_w$ below -1.0.

The experimental data were taken when the converter was

operated as both generator and damper.

In the damper where the magnetic wave travels in opposite direction to the fluid flow, both the electrical power given from the external excitation system and the electro-mechanical power supplied from the external fluid system are lost to become the ohmic loss in the working fluid and consequently the fluid is decelerated.

As is evident from Fig.6-4, the data obtained for generator decrease suddenly near 20 percent void fraction, while those for damper have never such tendency.

This sudden decrease is revealed in Chapter 5 to be caused by the change of flow pattern occasioned near 20 percent void.

Figure 6-5 shows the ratio between the generator efficiency obtained with NaK-N_2 mixture flow and that with NaK flow alone as a function of bulk void fraction.

It is seen from Fig.6-5 that the efficiency of experimental generator operated with NaK-N_2 mixture decreases gradually up to about 30 percent void fraction and sequently beyond this point it decreases more rapidly.

As is evident from the comparison between Figs.6-4 and -5, the efficiency shows the different tendency from the electrical power with respect to the void fraction.

In order to estimate the fluid slip S_f which is defined by the ratio of gas to liquid velocity in the two-phase mixture, the relation between void fraction α and $X = (1-\chi)/\chi \cdot \rho_g/\rho_l$ determined experimentally is shown in Fig.6-6. In this figure, the two solid lines represent the fluid slip S_f of 1.0 and 1.3, as

determined from the conservation of mass relation given from Eq.(4-12) of Chapter 4. The data were obtained with and without traveling magnetic field and all of them crowd in the narrow range between the fluid slip of 1.0 and 1.3.

However, the effect of the electro-magnetic force to the slip S_f has never been appeared due to the weak magnetic field intensity applied in the present experiment.

6-4 Analysis of Induction Converter with Two-Phase Mixture as Working Fluid

The configuration of the induction converter to be analyzed is shown in Fig.6-7. The working fluid flows in the x-direction with liquid velocity u_l, which has some distribution in the y-direction, between two parallel channel walls of infinite extent in the x- and z-directions spaced a distance 2b apart.

The gas phase is assumed to distribute non-uniformly in the y-direction and consequently the electrical conductivity σ_t of two-phase mixture varies along the y-direction.

Furthermore, the fluid is assumed to be electrically neutral with permeability μ_0 which is the same as that of free space.

In the rationalized MKS system, neglecting the displacement current, Maxwell's equations are

$$\nabla \cdot \vec{B} = 0 \tag{6-1}$$

$$\nabla \times \vec{B} = \mu_0 \vec{J} \tag{6-2}$$

$$\nabla \times \vec{E} = -\partial \vec{B}/\partial t \tag{6-3}$$

$$\nabla \cdot \vec{E} = 0 \tag{6-4}$$

and Ohm's law

$$\vec{J} = \sigma_t \, (\vec{E} + \vec{u}_1 \times \vec{B}) \tag{6-5}$$

Assuming the magnetic field B, the electric field E and the current density J to be a time harmonic function, we have

$$B = \{ \vec{i}_x B_x(y) + \vec{i}_y B_y(y) \} \exp\{j(\omega t - \kappa x)\} \tag{6-6}$$

$$E = \vec{i}_z E(y) \exp\{j(\omega t - \kappa x)\} \tag{6-7}$$

$$J = \vec{i}_z J(y) \exp\{j(\omega t - \kappa x)\} \tag{6-8}$$

where $\omega = 2\pi f$, f is the frequency, $\kappa = 2\pi/\lambda$ is the wave number, and λ is the wavelength. The wave velocity is given by $u_w = \omega/\kappa$. $\vec{i}$ denotes the unit vector and the subscripts x, y and z the quantities for x-, y- and z-directions. j is $\sqrt{-1}$.

Substituting Eq.(6-6) into Eq.(6-1), Eqs.(6-6) and (6-7) into Eq.(6-3) and Eqs.(6-6), (6-7) and (6-8) into Eqs.(6-2) and (6-5) respectively, there result

$$\frac{dB_y}{dy} = j \kappa B_x \tag{6-9}$$

$$\frac{dE}{dy} = -j \omega B_x \tag{6-10}$$

$$E = -u_w B_y \tag{6-11}$$

$$\frac{dB_x}{dy} + j \kappa B_y = -\mu_0 \sigma_t \, (E + u_1 B_y) \tag{6-12}$$

From the arrangement of Eqs.(6-9), (6-10), (6-11) and (6-12), we have the second order non-liner differential equation in respect of the magnetic field intensity:

$$\frac{d^2 B_y}{dy^2} - \kappa^2 \, (1 + j \, s \, R_m) \, B_y = 0 \tag{6-13}$$

where

$$s = \frac{u_w - u_1}{u_w} \quad \text{(slip)} \tag{6-14}$$

$$R_m = \frac{\mu_0 u_w \sigma_t}{\kappa} \quad \text{(magnetic Reynolds number)} \tag{6-15}$$

both of which are dependent on y and therefore Eq.(6-13) becomes non-linear.

Then, using the electro-magnetic bundary conditions

$$B_y = B_m \ , \ B_x = 0 \left(= - \frac{j}{\kappa} \frac{dB_y}{dy} \right) \qquad \text{at } y=0 \tag{6-16}$$

where B_m is the amplitude of the traveling magnetic field at the center of fluid channel, Equation (6-13) can be numerically solved for B with geven distribution profiles of fluid velocity u_1 and electrical conductivity σ_t which depends significantly on the void distributed in the working fluid.

Using this solution, the time-averaged electro-mechanical power is determined as

$$P_e = 2aL \int_0^b u_1 \mathcal{R}e\{\tfrac{1}{2} J B_y^* \} \, dy \tag{6-17}$$

where $\mathcal{R}e$ denotes the real part of a complex quantity, an asterisk denotes the complex conjugate, and a and L are width and length of the converter.

The ohmic loss dissipated in the fluid becomes, in time-average,

$$P_f = 2aL \int_0^b \mathcal{R}e\{\tfrac{1}{2} J J^*/\sigma_t\} \, dy \tag{6-18}$$

The gross electrical power output is the difference between P_e and P_f, namely,

$$P_g = P_e - P_f \tag{6-19}$$

The generator efficiency is given by

$$\eta_g = \frac{P_g}{P_e} \tag{6-20}$$

6-4-a Power Law Distribution for Both Velocity and Void Fraction Proposed by Bankoff

In the variable density single-fluid model proposed by Bankoff, it is conceived that the two-phase mixture flows as a suspension of bubbles in the liquid, where gradients exist in the concentration of bubbles. The bubble concentration is maximum at the center of the channel, decreases monotonically in a y-direction, and vanishes at the channel wall.

An impotant concept which has been introduced is that the gas and liquid have the same velocity at any position, the relative velocity of the bubbles with respect to the surrounding liquid being considered to be negligible compared to the gas velocity.

The average velocity of the gaseous phase is greater than that of the liquid phase only because the gas is concentrated in the regions of higher velocity.

Bankoff has assumed a power law distribution for both the velocity and the void fraction:

$$u_t = u_l = u_g = u_m \left(1 - \frac{y}{b}\right)^{1/m} \tag{6-21}$$

$$\alpha = \alpha_m \left(1 - \frac{y}{b}\right)^{1/n} \tag{6-22}$$

where u_m and α_m are velocity and void fraction at the center of the channel, and m and n are positive constants.

The averege velocity $\bar{u}_t$ and void fraction $\bar{\alpha}$ across the cross section are given by

$$\bar{u}_t = \frac{1}{b}\int_0^b u_t \, dy$$

$$= \frac{m}{m+1} u_m \tag{6-23}$$

$$\bar{\alpha} = \frac{1}{b}\int_0^b \alpha \, dy$$

$$= \frac{n}{n+1} \alpha_m \tag{6-24}$$

Using Eqs.(21) and (22), the liquid and gas mass-flow rates are given by

$$\dot{M}_l = 2a \int_0^b \rho_l \, u_t \, (1 - \alpha) \, dy$$

$$= 2ab \, \rho_l \, \bar{u}_t \, (1 - \bar{\alpha}/K) \tag{6-25}$$

$$\dot{M}_g = 2a \int_0^b \rho_g \, u_t \, \alpha \, dy$$

$$= 2ab \, \rho_g \, \bar{u}_t \, \bar{\alpha}/K \tag{6-26}$$

where ρ_g and ρ_l are the density of gas and liquid, and the flow parameter K is

$$K = \frac{mn+m+n}{(m+1)(n+1)} \tag{6-27}$$

Finally, the bulk slip velocity ratio is defined from the conservation of mass relation

$$S_f = \frac{\chi}{1-\chi} \frac{1-\alpha}{\alpha} \frac{\rho_l}{\rho_g} \tag{6-28}$$

where the quality χ is defined as

$$\chi = \frac{\dot{M}_g}{\dot{M}_g + \dot{M}_l} \tag{6-29}$$

Substituting Eqs.(6-25) and (6-26) into Eq.(6-28), we obtain

$$S_f = \frac{1 - \bar{\alpha}}{K - \bar{\alpha}} \tag{6-30}$$

6-4-b Performance Characteristics of Induction Converter Numerically Obtained with Power Law Distribution for Both Velocity and Void Fraction

Using the liquid velocity given by Eq.(6-21) and the electrical conductivity of two-phase mixture given by the Maxwell's correlation (see Eq.(5-2) of Chapter 5) into which Eq.(6-22) is substituted, Eqs.(6-13), (6-17) and (6-18) were integrated numerically with high speed digital computer.

It has become evident from the numerical survey that the generator efficiency depends only on the parameter m, that is, the velocity profile of liquid flow. According to this fact, the parameters m at each void fraction are determined from the experimental results shown in Fig. 5 respectively as follows:

α =	0	10	20	30	40	50 %
m =	7	6.5	5.5	3.5	2.5	2.0

where m = 7 corresponds to the velocity profile for turbulent flow. Four velocity profiles for the parameters m=2, 3, 6 and 7 are drawn in Fig.6-8 for reference.

On the other hand, the electrical output power of the experimental generator, as shown in Fig.6-4, decreases suddenly near 20 percent void fraction. This seems, as mentioned in Chapter 5, to be caused by the change of flow pattern occasioned near this void fraction. We can therefore consider that the gaseous phases distribute uniformly in the liquid phase except near the channel wall below about 20 percent void fraction and, beyond this void fraction, suddenly gather each other and sequently concentrate near the center of channel.

Then, taking the parameter n to be 7 below 20 percent void fraction and 2 above this value, the numerical computation was performed. The results obtained numerically are represented in Figs.6-4 and -5 with solid line for generator and broken line for damper.

The bulk slip S_f calculated with the parameters m and n used is in the range between 1.0 and 1.3 and similar to the values obtained experimentally (see Fig.6-6). The exact tendency for slip ratio S_f has not, however, been obtained due to the scatter of data.

6-5 Discussions and Concluding Remarks

Figure 6-9 shows the relation between the average void fraction with a power law distribution and the bulk void fraction determined experimentally by the gamma-ray attenuation technique, which is treated in Appendix.

As is evident from Fig.6-9, the difference between these void fractions is considered to be negligible below 50 percent void

fraction which is maximum in the present experiment.

Furthermore, the relation between the average velocity and the bulk velocity obtained experimentally from the liquid mass flow rate and bulk void fraction is shown in Fig.6-10 as a function of bulk void fraction, which is also treated in Appendix.

It is necessary to take into consideration the difference between these values, when both the parameters m and n are small.

As is evident from Fig.6-4, the results obtained numerically agree with those obtained experimentally, by assuming that the parameter m for velocity profile decreases gradually from 7 to 2 with increasing the bulk void fraction from 0 to 50 percent and then the parameter n for void distribution changes suddenly from 7 to 2 at 20 percent void fraction due to the change of flow pattern.

The sudden decrease in the electrical output power of generator can be explained as follows.

If the working fluid possesses some velocity distribution, the part of the working fluid with the velocity above that of the traveling magnetic wave is able to contribute to the output power and the other part dissipates a part of the output power to be accelerated.

Furthermore, if the gaseous phase gathers in the center of channel where the fluid has higher velocity, then the electrical conductivity of two-phase mixture becomes small value in the region with higher velocity and vice versa.

It becomes known from these facts that the contribution to output power decreases and the power dissipation increases due

to the change of flow pattern, i.e. the change of the parameter n from 7 to 2.

On the other hand, the electrical input power of damper does not decrease suddenly due to the change of flow pattern.

This is due to the fact that the electrical input power is always dissipated to be the ohmic loss in the entire region of working fluid because the magnetic wave travels in the opposite direction to the fluid flow, and then the difference between before and after the change of flow pattern does not appear clearly.

It is seen from Fig.6-4 that the electrical output power of the experimental generator becomes samewhat lower than that obtained numerically. This seems to be due to the fact that the analysis has utilized the Maxwell's correlation for the electrical conductivity of two-phase mixture, which is restricted to small values of void fraction as mentioned in Chapter 5. The actual electrical conductivity of two-phase mixture seems to be lower above 20 percent void fraction than the Maxwell's correlation.

Appendix

The Relation between The Average Void Fraction with A Power Law Distribution and The Bulk Void Fraction Determined Experimentally by The Gamma-Ray Attenuation Technique

Neglecting the attenuation of gamma-ray by the gaseous phase, the void fraction in the two-phase mixture with uniformly distributed gaseous phase is given by

$$\alpha = 1 - \frac{\ln\{I_t/I_e\}}{\ln\{I_f/I_e\}} \tag{A1}$$

where the intensity I_f of the gamma-ray passed across the channel which is completely filled with liquid is

$$I_f = I_e \exp\{-\mu_1 \rho_1 a\}, \tag{A2}$$

the intensity I_t of the gamma-ray passed across the channel in which the two-phase mixture flows

$$I_t = I_e \exp\{-\mu_1 \rho_1 a(1-\alpha)\}, \tag{A3}$$

I_e the intensity of the gamma-ray passed across the empty channel, μ_1 the density absorption coefficient, and ρ_1 the liquid density[2].

If the gaseous phase has a power law distribution, then the intensity of gamma-ray passed across the two-phase mixture is represented as

$$I_t^* = \frac{2I_e}{b}\int_0^b \exp\{-\mu_1 \rho_1 a(1-\alpha)\}\, dy \tag{A4}$$

where α is the local void fraction given by Eq.(6-22).

Using Eqs.(A1) and (A4), the relation between the average void fraction and the bulk void fraction determined by applying the gamma-beam to the entire height of channel is obtained as follows,

$$\alpha_B = 1 - \frac{\ln\{I_t^*/I_e\}}{\ln\{I_f/I_e\}} = 1 + \frac{\ln\left\{\frac{1}{b}\int_0^b \exp\{-\mu_1\rho_1 a(1-\alpha)\}dy\right\}}{\mu_1\rho_1 a} \quad (A5)$$

The Relation between The Average Velocity and The Bulk Velocity Obtained Experimentally from The Liquid Mass Flow Rate

The bulk velocity of liquid is determined, as Eq.(A6), from the liquid mass flow rate with the bulk void fraction:

$$u_B = \frac{\dot{M}_1}{2ab(1-\alpha_B)\rho_1} \quad (A6)$$

Using the liquid mass flow rate given by Eq.(6-25) in which the power law distribution is assumed for both the velocity and the void fraction, the relation between the average velocity and the bulk velocity is obtained as

$$u_B = \frac{1 - \bar{\alpha}/K}{1 - \alpha_B}\bar{u}_1 \quad (A7)$$

Reference

(1) Bankoff, S.G. : Journal of Heat Transfer Trans. ASME, Series C, 82, 265-272 (1960).

(2) Petrick, M. : Proc. Symp. Magnetohydrodynamic Electrical Power Generation, Salzburg, 1966, SM-74/196.

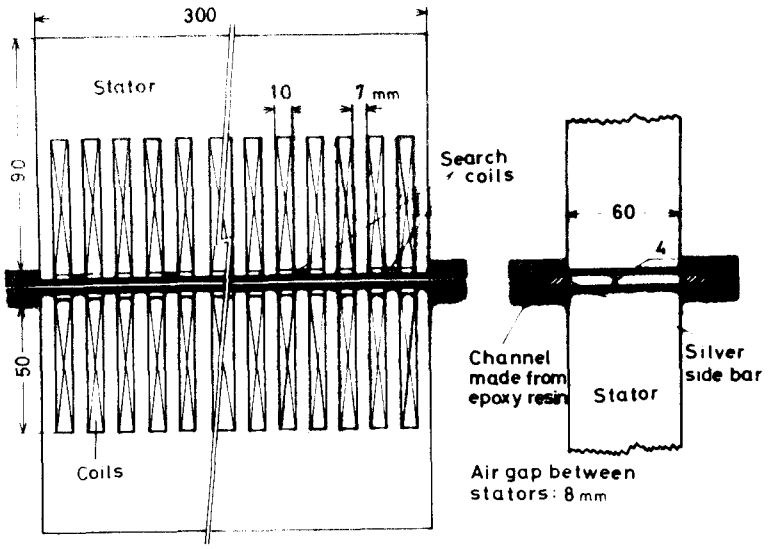

Fig. 6-1 Stators and fluid channel geometry

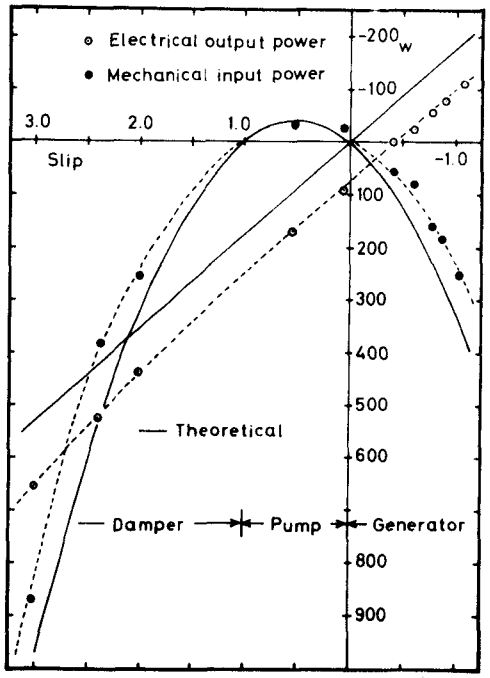

Fig. 6-2 Electrical power and electromechanical power obtained in experimental converter operated with NaK flow alone

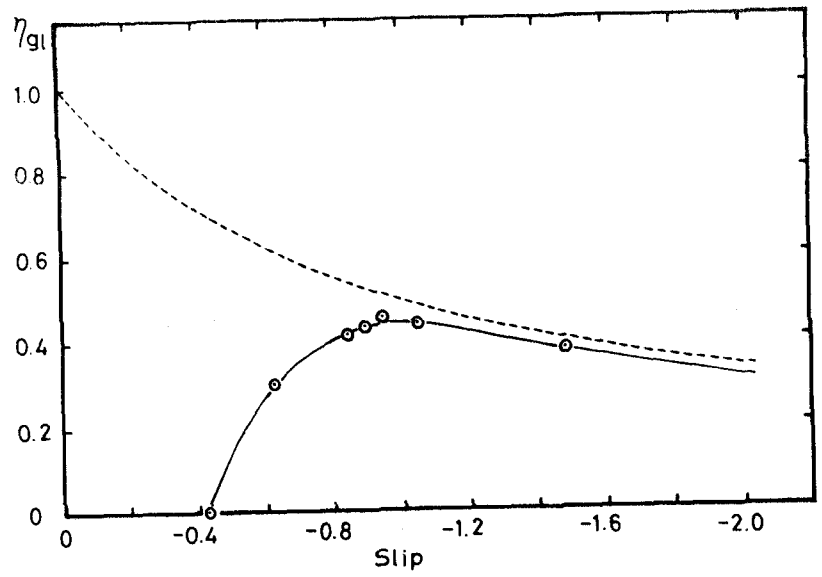

Fig. 6-3 Generator efficiency obtained in experimental converter operated with NaK flow alone

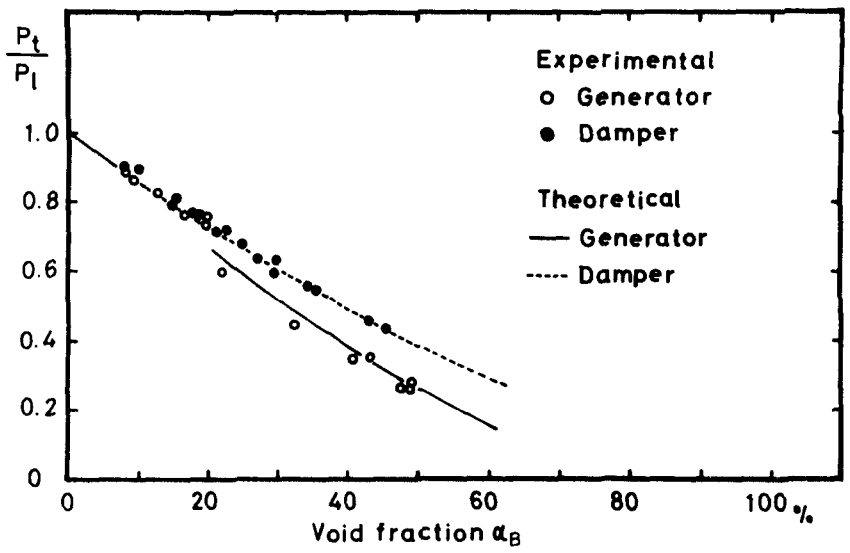

Fig. 6-4 Ratio between electrical power obtained with NaK-N_2 flow and that with NaK flow alone

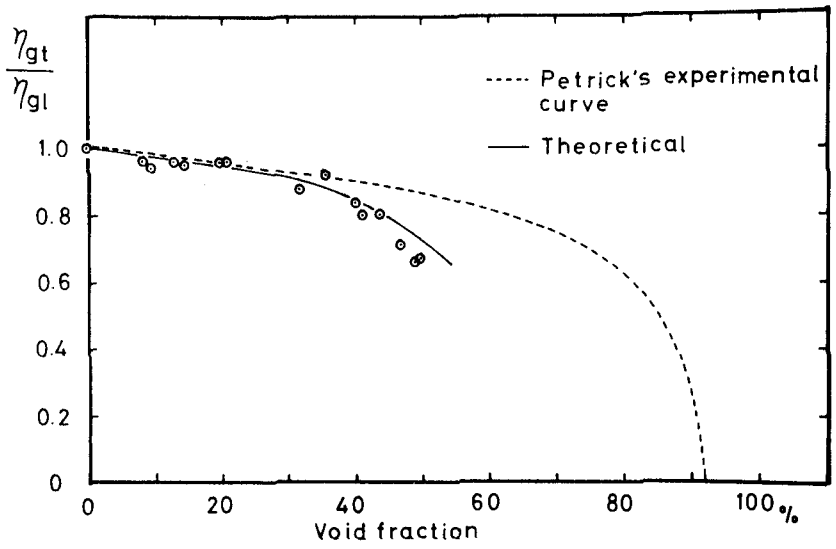

Fig. 6-5 Ratio between generator efficiency obtained with NaK-N_2 flow and that with NaK flow alone

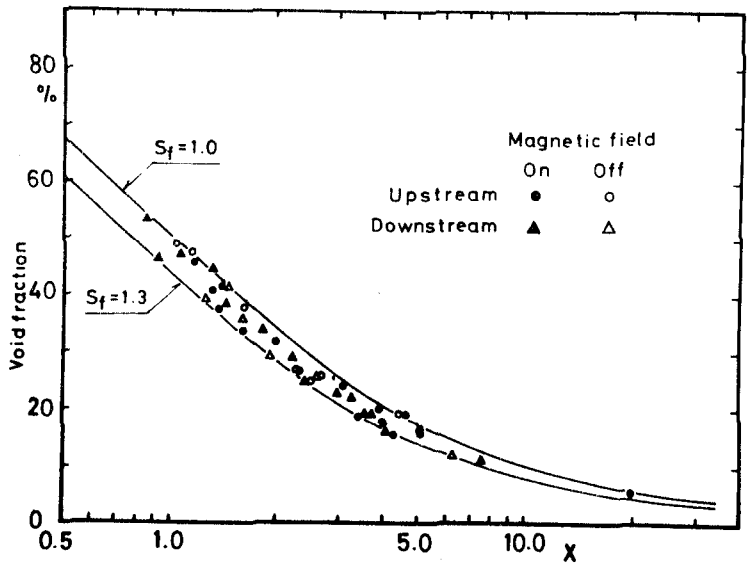

Fig. 6-6 Fluid slip ratio between velocity of nitrogen gas and that of NaK in NaK-N_2 two-phase flow

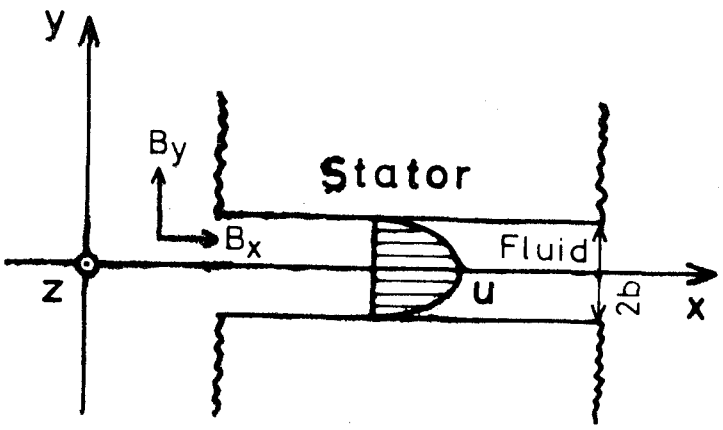

Fig. 6-7 Configuration of induction converter for analysis

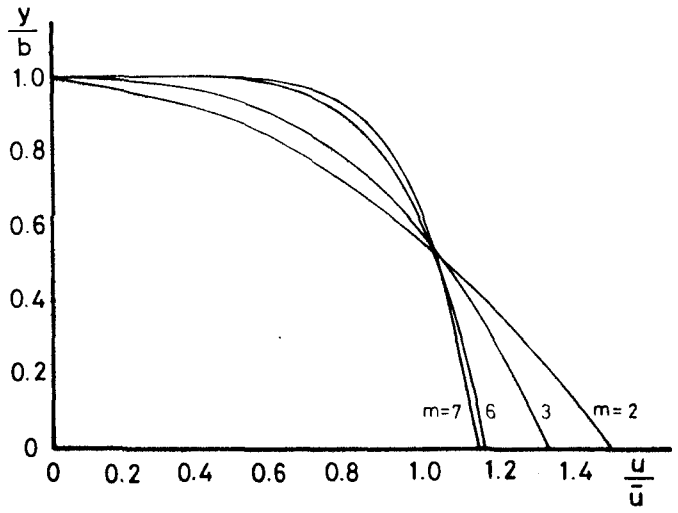

Fig. 6-8 Velocity profiles for parameters m=2, 3, 6 and 7

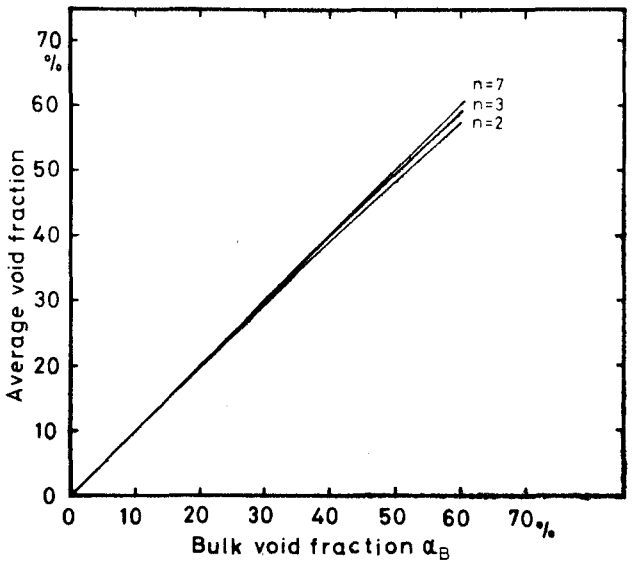

Fig. 6-9 Relation between average void fraction and bulk void fraction

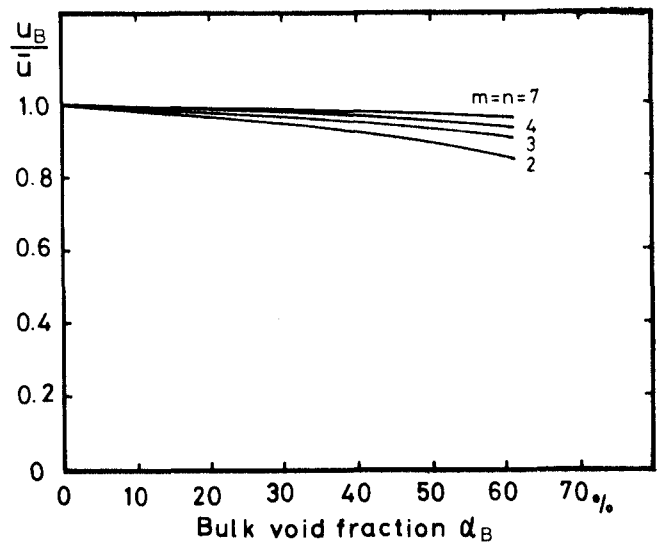

Fig. 6-10 Relation between average velocity and bulk velocity

Chapter 7

Summary

In the previous chapters are described the performance characteristics of the liquid metal MHD power generator using single- and two-phase flow as working fluid, which have been researched with the experimental generators operated using mercury, NaK (liquid metal eutectic consisted of 78 w/o potassium and 22 w/o sodium) and NaK-N_2 flows, and furthermore treated analytically and/or numerically in order to generalize the problems.

Concerning the liquid metal MHD power generation using single-phase flow as working fluid, in the present thesis were treated both the effects due to the finite conductivity of the electrode in the D.C. Faraday generator in comparison with the end loss and due to the variation of the traveling magnetic field intensity in the induction generator together with the ohmic loss induced in the metallic channel wall.

In the liquid metal MHD D.C. Faraday generator, the perfect conductor approximation can not always be applied to the electrode because the electrical conductivity of the electrode is so large as to be comparable with that of the working fluid, and therefore the distortion of the electric potential distribution has to be taken into consideration not only in the fluid but also in the electrode. According to the analytical solution of Laplacian field equation obtained here under some simplification, the performance characteristics of the generator are represented by multiplying that of the ideal generator by the factor λ_0 given from

Eq.(2-26) of Chapter 2.

The results obtained analytically have agreed very well with those obtained in the present experiments, where the generators were operated with mercury as working fluid and had the relatively large aspect ratio and magnetic field extensions for the purpose of reducing the end loss. However, the power density of the generator with the stainless steel electrodes had become lower than the analytical results due to the contact resistance between the electrode and the fluid, whereas, with copper electrode, the amalgamation could occur to reduce the contact resistance.

Superposing the electrode loss analytically obtained here by neglecting the end loss and the end loss analytically obtained by Sutton by assuming the perfect conductor for the electrode, the performance characteristics taken into consideration the two losses are expressed by Eq.(2-37) of Chapter 2. It cannot, however, be considered to represent accurately the losses incurred in an actual generator, where the two kinds of loss are interrelated and not independent of each other. For the purpose of treating simultaneously the two losses and predicting the more accurate performance characteristics, a numerical computation using high speed digital computor had been performed to solve the Laplacian field equation taking into consideration both the two losses.

The results obtained numerically are shown in Fig.2-4 of Chapter 2 comparing with λ_0.

The performance characteristics of liquid metal MHD induction generator have been analyzed by Wang & Dudzinsky and Pierson & Jackson, etc. by assuming the traveling magnetic field intensity

to be uniform in the direction of fluid flow. In an actual generator, the magnetic field intensity generated in the fluid channel, however, has certain variations according to differences in the disposition of the teeth and slots in the stators.

Taking into consideration the ohmic loss induced in the metallic channel wall in addition to this variation of the magnetic field intensity, the performance characteristics of liquid metal MHD induction generator have been obtained analytically in the present thesis by applying the slit channel approximation.

The results obtained for the generator operated in constant current made and in constant voltage mode are represented in Eqs.(3-29)~(3-35) and in Eqs.(3-41)~(3-44) of Chapter 3 respectively.

The following facts are revealed from this analytical results.

The electro-mechanical power of the converter operated in constant voltage mode is dependent on the magnetic field variation and independent of the ohmic loss due to the eddy current induced in the channel wall, and therefore the range of slip in which the converter acts as pump is affected only by the magnetic field variation, and becomes narrow as the dgree of this variation becomes large. On the other hand, the gross electrical power of the converter operated in constant voltage mode is dependent on both the magnetic field variation and the ohmic loss in the wall, and the former is masked by the latter especially at low efficiency, and hence the slip at which the converter begins to act as generator under self-excitation is determined, for the most part, by the ohmic loss in the wall and increases its negative value as the ohmic loss in wall becomes larger.

The electrical power obtained with the converter when equipped with copper side bars fixed to the side wall of the channel in order to decrease the electric currents in the direction of the current loop (2) in Fig.3-18 of Chapter 3, agreed with the analytical solution obtained here, though the curves shifted to the negative side of the slip due to the additional ohmic losses in both the side wall of channel and the copper side bars, of which a part protrudes into the applied magnetic field.

Concerning the liquid metal MHD power generation using two-phase mixture flow as working fluid, the frictional loss in the generator channel, the apparent electrical conductivity of two-phase mixture and the performance characteristics of induction generator with the two-phase flow were treated in the present thesis.

In a two-phase system composed of liquid metal mixed with vapor or with gas in a liquid metal MHD generator channel, which is affected significantly by the velocity of the liquid, the frictional pressure drop in the two-phase flow should be considered in reference to that of the liquid flowing alone at the same velocity and not at the same mass flow rate as that of the liquid in the two-phase flow, in order to clarify the difference in performance characteristics between that in the liquid flow alone and that in the two-phase flow system.

Based on semiempirical analysis assuming the two-phase mixture to be a continuous medium, the author has determined the friction factor as a function of Reynolds number with the NaK-N_2 two-phase flow in the rectangular channel, which is represented in Eq.(4-11) of Chapter 4.

From this semiempirical analysis, the frictional pressure drop in the two-phase flow appears to be smaller than that in a corresponding single-phase flow of the same velocity as that of the liquid in the two-phase flow in the range of small slip and small density ratio, where the contribution of the gas to the frictional pressure drop is not dominant.

The apparent electrical conductivity of the two-phase mixture obtained experimentally with Hg-H_2O and NaK-N_2 mixtures in the traveling magnetic field decreased suddenly near 20 % void fraction due to the transition of the flow pattern from bubbly to slug flow regime, and in the bubbly flow, agreed well with Maxwell's theoretical value, and in the slug flow falled between Maxwell's theoretical value and Petrick and Lee's experimental value according to the dgree of the establishment of the slug flow regime.

The results obtained with H_2O-N_2 mixture in the static electric field agreed well with Maxwell's theoretical value or $(1-\alpha)$ up to considerably higher void fractions. A similar tendency is also seen in the experimental results for air-water mixture obtained by Petrick and Lee. This may be attributed to the difference in electric current conduction between liquid metal and water, which latter is a weak electrolyte.

The electrical output power of the induction generator operated with NaK-N_2 two-phase flow decreased with increasing void fraction and furthermore had a sudden decrease near 20 % void fraction, while the electrical input power of the induction damper decreased gradually without having such sudden decrease.

On the other hand, the efficiency of the induction generator

operated with NaK-N_2 two-phase flow decreased slightly up to about 30 % void fraction and sequently beyond this void fraction decreased more rapidly.

This experimental results can be explained as follows by assuming both the liquid velocity and the void fraction have certain distributions and these distributions change due to the transition of flow pattern.

If the working fluid posseses certain distribution, the part of the working fluid with the velocity above that of the traveling magnetic wave is able to contribute to the output power and the other part dissipates a part of the output power to be accelerated.

Furthermore, if the gaseous phase gathers in the center of channel where the fluid has higher velocity, then the electrical conductivity of two-phase mixture becomes smaller value in the region with higher velocity and vice versa.

It becomes known from these facts that the contribution to the output power decreases and the dissipation of the output power increases due to the change of flow pattern, that is the consentration of void into the central region of the channel together with the acceleration of the liquid in the central region of the channel and the deceleration of the liquid near the channel wall.

On the other hand, the electrical input power supplied to the induction damper is always dissipated to be the ohmic loss in the entire region of working fluid because the magnetic wave travels in the opposite direction of the fluid flow, and then the difference between before and after the change of flow pattern does not appear clearly.

Coupling the electro-magnetic equations with the power law distribution for both velocity and void fraction proposed by Bankoff and using the correlation of the electrical conductivity of two-phase mixture versus void fraction given by Maxwell, the author has solved numerically the performance characteristics of the induction converter using two-phase flow and explained well the results obtained experimentally.

The slip ratios between the velocity of gaseous phase and that of liquid phase in the two-phase flow crowd in the narrow range between 1.0 and 1.3 in the present experiment whether the traveling magnetic field was applied or not, though the effect of the electro-magnetic force to the slip ratio has never been appeared due to the weak magnetic field intensity applied in the present experiment, where the frictional pressure gradient was dominant.

Concerning the slip ratio and the flow pattern of the liquid metal-gas or -vapor two-phase flow which affect significantly to the performance characteristics of liquid metal MHD power generator, more advanced researches are required.

Acknowledgments

The author would like to express his appreciation to Professor T. Suita for his continuing guidance and affectionate encouragement.

The author would like to express their sincere thanks to Professor M. Ogasawara, Professor T. Sano and Professor S. Nishimura.

In addition, the author wishes to thank Professor M. Shinagawa, Professor T. Sekiya and S. Imoto for their warm encouragements.

The author cannot find proper words to express his gratitude to Dr. Y. Fujii-e for his helpful advice and continuing encouragement, without which this work could never have been accomplished.

Thanks are due to Dr. K. Miyazaki and Mr. S. Inoue who contributed their experimental skill and sustained effort to the accomplishment of the experimental program.

The author is greateful to Mr. H. Yamamoto, Mr. T. Matsuda, Mr. T. Sano, Mr. F. Shimizu, Mr. O. Kuroki, Mr. M. Saito, Mr. S. Satho and Mr. N. Yamaoka for their technical assistance.

The rest of the members in Suita Laboratory also helped the author both implicitly and explicitly.

List of Papers by the Author

1) Decrease in Power Density due to Finite Electrode Conductivity in Liquid Metal MHD Generator
J. Nucl. Sci. Technol., 8[10], 588-596 (1971).

2) Energy Loss in Liquid Metal MHD Induction Converter due to Discrete Tooth-Slot Arrangements
J. Nucl. Sci. Technol., 9[4], 213-223 (1972).

3) Electrical Conductivity of Liquid Metal Two-Phase Mixture in Bubbly and Slug Flow Regime
J. Nucl. Sci. Technol., 9[12], 753-755 (1972).

4) Frictional Pressure Drop for NaK-N_2 Two-Phase Flow in Rectangular Cross Section Channel of Large Aspect Ratio
To be published in J. Nucl. Sci. Technol., 10[4], (1973).

5) Performence Characteristics of MHD Induction Generator Using The Two-Phase Flow
To be published

List of Lectures by the Author

1) Experiment of Liquid Metal MHD D.C. Faraday Generator Using Mercury Flow as a Working Fluid (1).
The 9th Annual Meeting of the Atomic Energy Society of Japan, 1969. B7.

2) Experiment of Liquid Metal MHD D.C. Faraday Generator Using Mercury Flow as a Working Fluid (II).
The 10th Annual Meeting of the Atomic Energy Society of Japan, 1970. E53.

3) Experiment of Liquid Metal MHD D.C. Faraday Generator Using Mercury Flow as a Working Fluid (III).
The Autumnal Sectional Meeting of the Atomic Energy Society of Japan, 1970. D14.

4) Experiment of Liquid Metal MHD Induction Generator Using NaK Flow as a Working Fluid (I).
The Autumnal Sectional Meeting of the Atomic Energy Society of Japan, 1970. D15.

5) Experiment of Liquid Metal MHD Induction Generator Using NaK Flow as a Working Fluid (II).
The 11th Annual Meeting of the Atomic Energy Society of Japan, 1971. G50.

6) Measurement of Electrical Conductivity of Hg-N_2 Two-Phase Flow
The 11th Annual Meeting of the Atomic Energy Society of Japan, 1971. G51.

7) Experiment of Liquid Metal MHD Induction Generator Using NaK Flow as a Working Fluid (III).
The Autumnal Sectional Meeting of the Atomic Energy Society of Japan, 1971. C18.

8) Liquid Metal MHD Power Generation
Symposium of Magnetohydrodynamics held in Institute of Space and Aeronautical Science, University of Tokyo, 1972

9) Experiment of Liquid Metal MHD Induction Generator Using NaK as a Working Fluid (IV).
The 12th Annual Meeting of the Atomic Energy Society of Japan, 1972. A10.

10) Experiment of Liquid Metal MHD Induction Generator Using NaK as a Working Fluid (V).
-Frictional Pressure Drop and Electrical Conductivity of NaK-N_2 Two-Phase Flow-
The Autumnal Sectional Meeting of the Atomic Energy Society of Japan, 1972. A10.

11) Experiment of Liquid Metal MHD Induction Generator Using NaK as a Working Fluid (VI).
-Measurement of Dynamic Pressure of NaK-N_2 Two-Phase Flow-
The Autumnal Sectional Meeting of the Atomic Energy Society of Japan, 1972. A11.

12) Experiment of Liquid Metal MHD Induction Generator Using NaK as a Working Fluid (VII).
-Performance Characteristics of MHD Induction Generator Using NaK-N_2 Two-Phase Flow as a Working Fluid-
The 13th Annual Meeting of the Atomic Energy Society of Japan, 1973.